DYNAMICS OF NANOPARTICLES AND BUBBLES IN CREEPING FLOWS OF VISCOUS FLUIDS

A Thesis submitted by

Hassan Kiream Hassan, BSc, M Eng

For the award of

Doctor of Philosophy

2018

Abstract

This research deals with the study of dynamics of nanoparticles and bubbles in creeping flows of viscous fluids. The study was based on theoretical approaches and numerical methods. To conduct numerical simulations, the original FORTRAN codes were developed and realised on a desktop computer. To process the obtained results the Mathcad software was actively used.

Firstly, the dynamics of two unlike and like charged particles in viscous fluid in the creeping flow approximation was studied. Two types and different models of viscous drag forces were taken into consideration. The particles' trajectories under the influence of all these forces were studied and compared with those immersed in inviscid fluid.

Next, the complex dynamics of small rigid particles under the influence of acoustic radiation force were considered. Our analysis was based on a more advanced model in comparison with those used in the earlier works (Sarvazyan & Ostrovsky, 2009; Ostrovsky, 2015). In addition to the Stokes drag force, the model used in this study included particle inertia, added mass effect, and the Boussinesq–Basset drag force, the effects of these were ignored in the cited papers. It has been shown through numerical solutions that all of these additional effects can be important at some stages of particle motion, whereas in other stages they can be neglected. The particle motion was considered both for the plane and cylindrical geometries. An interesting and prospective method of particle control in a fluid was studied by periodic switching of the acoustic modes in a resonator.

In the last Chapter there is an analysis of the influence of memory integral drag forces on the resonance characteristics of oscillating solid particles and gaseous bubbles in a viscous fluid under the influence of an external sinusoidal force. It has been shown that the memory integral drag forces lead to the widening of resonance curves and the reduction of resonance peaks, so that the effective quality of oscillator significantly decreases in comparison with the similar oscillator with only Stokes drag force.

List of publications

The following papers were published during the period of study:

1. Hassan, H. K., & Stepanyants, Y. A. (2015). Dynamics of two charged particles in a creeping flow. *Journal of Physical Mathematics*, v. 6, n. 2, 7 p.
2. Hassan, H. K., Ostrovsky, L. A., & Stepanyants, Y. A. (2017). Particle dynamics in a viscous fluid under the action of acoustic radiation force. *Interdisciplinary Journal of Discontinuity, Nonlinearity, and Complexity*, v. 6, n. 3, 317–327.
3. Hassan, H. K., & Stepanyants, Y. A. (2017). Resonance properties of forced oscillations of particles and gaseous bubbles in a viscous fluid at small Reynolds numbers. *Physics of Fluids*, v. 29, n. 10, 101703, 5 p.

Certification of the Thesis

The work contained in this Thesis has not been previously submitted to meet the requirements for an award at this or any other higher educational institution. To the best of my knowledge and belief, the Thesis contains no material previously published or written by another person except where due reference is made.

Candidate: Hassan Kiream Hassan

Signed:

Date:

ENDORSEMENT

Principal Supervisor: Professor Yury Stepanyants

Signed:

Date:

Associate Supervisor: Dr Trevor Langlands

Signed:

Date:

Acknowledgement

I would like to express my deepest gratitude to my principal supervisor, Professor Yury Stepanyants for his unwavering support, collegiality and mentorship throughout this project.

I would also like to express my sincere gratitude and appreciation to my associate supervisor Dr Trevor Langlands, for his support, valuable advice, and suggestions.

I am also very thankful to all staff of the University of Southern Queensland for their cooperation and hospitality and Special thanks go to Libby Collett to her proofread an editing on my Thesis.

Last but not least, I would like to thank my family: to my loving, supportive, and encouraging wife Roa'a whose faithful support during all stages of this Ph-D-project is very much appreciated, and my three wonderful children, Zahraa, Ali and Mohammed, who provide unending inspiration. Words cannot express how grateful I am to my mother, father, my mother-in-law, and father-in-law for all of the sacrifices that they've made on my behalf. Their prayer for me was what sustained me thus far. Last, but not least, I send big thanks to all my friends, who always support me, give me good advice and make my life colorful!

Contents

List of Figures

List of Tables

Chapter 1: Introduction and literature review

In the late 20th century, the dynamics of nanoparticles and bubbles in creeping flows of viscous fluids have been under a focus of many research groups because this field of research plays an important role in various biotechnological, pharmacological and pure technological applications. Nanoparticles are important elements in the medical field (Murthy, 2007) as they can be used as the carriers for vaccines and anticancer drugs (Madhav & Kala, 2011). It was discovered that by using an external force (for example, the acoustic force (Zhu & Trung Nguyen, 2010; Ostrovsky & Stepanyants, 2017), magnetic force (Zhu & Trung Nguyen, 2010), electric force (Zhu & Trung Nguyen, 2010), laser-generated electromagnetic (light) force (Hidai et al. 2010), etc), one can control particle motion and, in particular, move particles from one place to another without touching them. As a result, the nanoparticles can be used as drug carriers which are capable to deliver medicines to any organ in a human body.

Another benefit of ultrasound in medical fields is to non-invasively and temporarily disrupt the blood-brain barrier to reach brain tumors. This method has many advantages: firstly, to break through the blood-brain barrier without any surgery or risky of surgery. Secondly, to make microbubbles move and to move any objects (for examples, red cells, drugs, fatty plaques, etc) surrounding them in the blood across the blood-brain barrier. As has been shown in Refs. (Hynynen, 2008; Timbie et al., 2015), this is an efficient and safe method to deliver drugs crossing the blood-brain barrier. Figure 1.1 illustrates the mechanism of focused ultrasound mediated blood-brain barrier disruption. Circulating microbubbles oscillate in the ultrasonic field, producing forces that act on the vessel wall to generate three bioeffects that permit transport across the blood-brain barrier: disruption of tight junctions, sonoporation of the vascular endothelial cells and upregulation of transcytosis. Chapter 3 of this Thesis provides theoretical basis for the particle and bubble control by ultrasound.

In industrial applications, the nanoparticles also play an important role as they are principal elements in microfluidics. Zhu & Trung Nguyen (2010) have mentioned in their research many useful applications of nanoparticles in microfluidics and listed some methods of particle sorting. One of these methods is connected to the application of an acoustic force. For example, when there is a big

sample of particles which we need to sort, i.e., to separate particles of small and big sizes or smaller and greater density, we can apply an acoustic field of a certain frequency and play with the resonance properties of particles. Some of the particles will oscillate in the acoustic field because they are in resonance, and others will remain almost at rest because they are not in the resonance. There is a simple technology which allows us to collect highly oscillating resonance particles; other, non-oscillating particles or particles oscillating with small amplitude, can be then separated. Then the frequency of the acoustic field can be changed and further particle sorting and separation can be undertaken. The theoretical basis of this technology will be considered in chapter four of this Thesis.

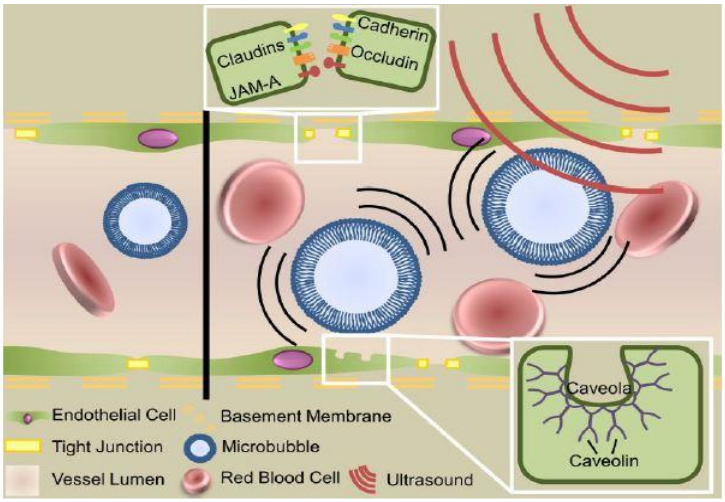

Figure 1.1: (From (Timbie, Mead & Price, 2015)). Mechanism of focused ultrasound mediated blood-brain barrier disruption.

Manipulation with nanoparticles by acoustic fields can be used for another practical application namely for the protection of wooden goods. The structure of wooden materials consists of very small and thin canals as shown in Figure 1.2. One of the options to protect the wood against deterioration by insects or atmospheric effects is to deliver special chemical solutions or particles to the canals which will preserve the wood against deterioration. Using the acoustical method, one can control delivery of small particles deeper into the wood to protect it in such a way.

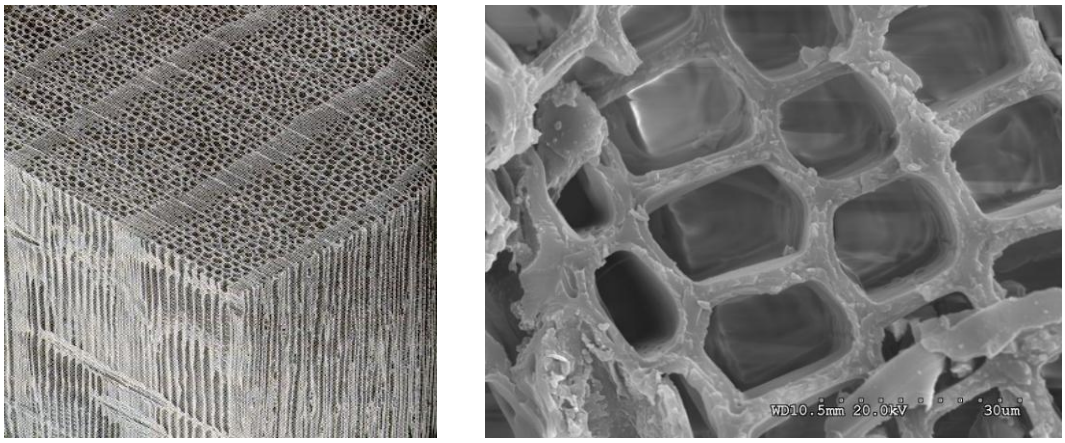

Figure 1.2: A cross-section of wooden materials at a microscopic view. (From the website: http://www.rationalskepticism.org/creationism/flood-geology-goes-up-in-flames-t51371.html).

As mentioned above, particle control can be implemented not only by an acoustic field but also by other external fields, for example, by an electric field. However, when conducting charged particles move in a viscous fluid they experience the action of distributed electric forces from other particles and viscous forces which are modified due to the presence of other particles. The importance of such effects has not studied thus far. In the meantime, Saranin (1999) has demonstrated that the electrostatic force acting between two charged conductive particles differs from the classic Coulomb force $F \sim 1/r2$, where r is the distance between the particle centers, due to the redistribution of electric charges within each particle (the modified formula for the electric force will be presented further in the next Chapter). This redistribution within two spherical conductive particles is illustrated by Figure 1.3.

In his first paper, Saranin (1999) derived a theoretical formula for the modified Coulomb law. Later Saranin & Mayer (2010) undertook experimental validation of the derived formula and presented the results of experimental data on interaction of two conducting charged particles in comparison with the theoretical finding.

Figure 1.3: (from (Hassan & Stepanyants, 2015)). Electric charge redistribution within two conducting unlikely charged spheres (a) and two unlikely charged spheres with uniformly distributed charges (b).

Figure 1.4 shows the results obtained which are in a very good agreement with Saranin's theory. As one can see from this figure, Coulomb's law is valid when the distance between the particles is large enough, $r > 10d$, where d is the diameter of the spherical particle (see the data in the left lower corner of the figure in comparison with line 1 when $1/x^2 < 0.15$). However, for the small distances ($1/x^2 > 0.15$) experimental data are in a very good agreement with the theoretical data by Saranin (1999) – see line 2 and experimental data by Saranin & Mayer (2010) shown by different symbols.

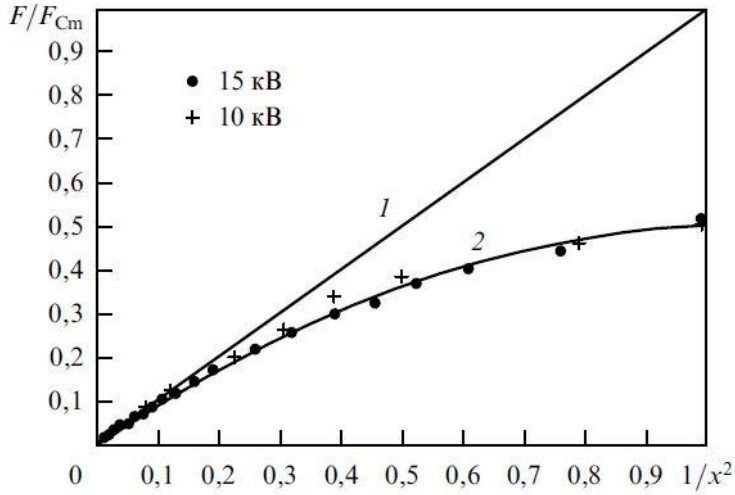

Figure 1.4: (From (Saranin & Mayer, 2010)). The normalised electric force acting between two conductive particles as a function of the inverse distance between the particles. Line 1 corresponds to the classic Coulomb law, and line 2 corresponds to improved Coulomb law. Symbols reflect experimental data.

Since that time (2010), no other experiments were conducted in this area, but the results obtained are quite convincing. The modified Coulomb law will be used in the next chapter of the Thesis to study the motion of charged conducting particle in a viscous fluid.

Despite the fact that the study of particle dynamics in a viscous fluid has a long history, many important problems still remain unsolved (Shoji, 2004). This pertains not only to the collective behaviour of big particle ensembles but even to interactions of two particles in a complex environment of shear flows or in the presence of solid obstacles, walls or free surfaces. Much research efforts have been undertaken over the years to elucidate the particle dynamics in various situations.

One of the intriguing problems that have not been solved so far is the dynamics of two interacting charged particles in a viscous fluid. In recent years a great deal of interest has been observed in micro- and nano-particles due to their potential applications in modern biotechnologies and other micro-fluid technologies. Quantitative descriptions of such systems represent a certain challenge not only from the practical but also from the academic point of view. In the next chapter, the elementary acts of the interaction of two charged particles moving in a viscous fluid are considered. Two cases of particle interaction are studied and compared: (1) when non-conducting charged particles with uniformly distributed electric charge interacting in a viscous fluid and (2) when conducting spherical particles interact. It is assumed that, in both cases, the particles can freely move in the fluid either one after another or side by side, and their electric interaction is controlled by the modified Coulomb force (Saranin, 1999). The equations of motion are studied analytically where possible and also numerically. The particle dynamics is considered in the creeping flow approximation, that is under the assumption that the Reynolds number is very small, $\mathrm{Re} \equiv ua/\nu << 1$, where u is the particle velocity relative to the fluid, a is the particle radius, and ν is the fluid kinematic viscosity. For simplicity, we assume that the particles are solid and have a spherical shape. Even in such relatively simple case the viscous force acting on each particle differs from the case when the particles are isolated or very far from each other; the force instead depends on the distance between the particles and their configuration in a space. The total viscous force consists the Stokes drag force and the memory

integral drag force, which is known as the Boussinesq–Basset drag force in the case of solid particles.

Another area of applications of theoretical study of motion of charged entities (particles, droplets, or bubbles) in a viscous fluid is related to the recent breakthrough experiments on microbubble dynamics. Recently, it was discovered (see Ref. (Bunkin & Bunkin, 2016)), that a small bubble in a liquid can be charged because it is usually surrounded by ions of impurities dissolved in a liquid. Such bubbles surrounded by ions deposited on the bubble surfaces were called ***bubstons*** in the cited paper. The ions make micro-bubbles stable in liquids, so that they play a role of nucleus in the processes of vaporization and cavitation. The bubstones carrying ions can be positively or negatively charged, or remain neutral. However, according to the experimental data mentioned in the review (Bunkin & Bunkin, 2016), in the majority of cases bubstones are charged either positively or negatively. In such cases, it is important to investigate the character of bubston motion and their interaction with each other in viscous fluids. Using external fields, for example, acoustic or electro-magnetic fields, one can undertake bubble control, suppressing bubble growth or removing bubbles from the liquid. This can be very important to prevent onset of cavitation in liquids and their negative impact on solid surfaces.

As well-known, cavitation is caused by microbubble nuclear which grow and then collapse in a fluid producing very high pressure in a small volume. When bubbles contact metallic surfaces (for example, fast rotating propellers in a fluid), they affect surfaces with a very high pressure in the process of a collapse. It is impossible to purify completely water from microbubbles even in a laboratory to avoid the onset of cavitation. However, the development of methods of bubble control in fluids can provide an effective protection against material destruction due to cavitation if, for example, charged microbubbles (the bubstons) can be repelled from metallic surfaces by electric forces. Therefore, there is a great interest to the dynamics of bubstons and methods of their control by external electric and acoustic fields.

The electric charge on the surface of bubstons can be distributed in accordance with the external electric forces. In particular, when two bubstons approach each other, the ions on their surfaces experience redistribution like within charged

conducting particles described above; this is shown schematically in Figure 1.5. This situation is very similar to what was considered by Saranin (1999) in his seminal papers. Due to the charge redistribution, the interaction of charged bubstons is described by Saranin's formula, rather than by Coulomb's formula. Therefore, motions of bubstons in the viscous fluid should be described by taking into account the combination of modified electric forces, buoyancy (Archimedean) forces and viscous drag forces, which include both the Stokes drag force and memory integral drag force.

(a) (b)

Figure 1.5: Bubbles (bubstons) surrounded by liquid molecules (a) and ions (b): (a) – neutral bubstons, (b) charged bubstons with redistributed ions on the surfaces.

The concept of bubstons and their role in fluid mechanics presented in the review paper by Bunkin & Bunkin (2016) and supported by recent experiments reflected in the review is relatively new. This concept opens an opportunity for the study of ensembles of interacting bubstons in fluids taking into account both electric and hydrodynamic forces acting on them. As a first step, the simple case of the elementary act of interaction of two bubstons should be studied. This study is currently underway as the development of the results presented in Chapter 2 for two conducting charged particles in water, but they are still incomplete and therefore are not included in this Thesis.

Two limiting cases of dynamics of solid particles and gaseous bubbles in liquids can be further generalised for droplets (liquid particles) moving in a liquid of different properties (for example, oil droplets in a water). The droplets can preserve their shapes due to surface tension on the interface between different liquids. In their recent paper, Charalampous & Hardalupas (2017) studied the interaction between droplets and demonstrated experimentally that droplet dynamics can be fairly

complicated. Figure 1.6 from their paper illustrates different regimes of droplet-droplet collisions.

The droplets can be both neutral and electrically charged. Therefore, further development of methods of description of their motion and interaction is topical and has a good perspective for application in engineering technology. It is of a special interest to develop methods of droplet control by acoustic fields. The results obtained in Chapter 3 of this Thesis shed light to the droplet dynamics under the action of acoustic fields, but needs further development.

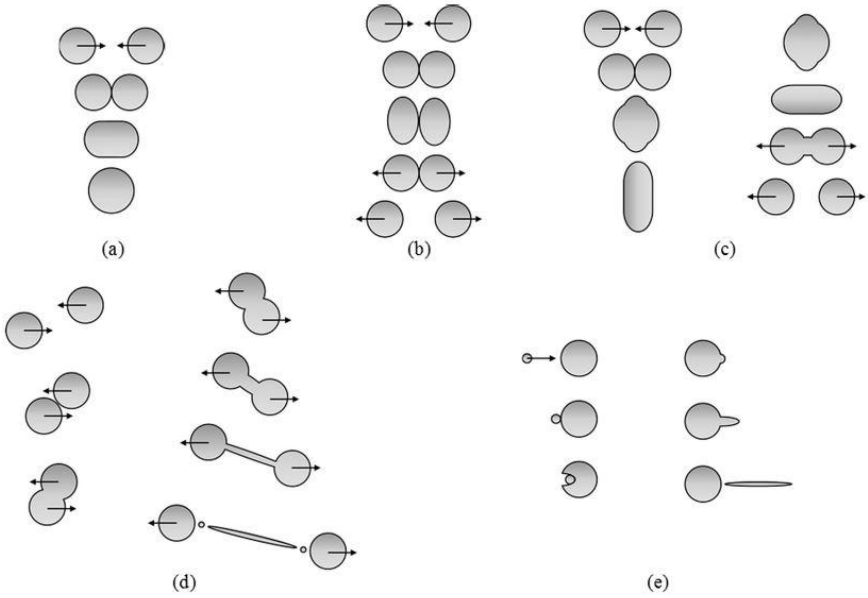

Figure 1.6: (From (Charalampous & Hardalupas, 2017))). Regimes of droplet-droplet collision: (a) coalescence, (b) bouncing, (c) reflexive separation, (d) stretching separation, and (e) penetration.

One of the interesting phenomena which has not been studied well so far is the possibility to force droplet and bubbles to oscillate under the action of external acoustic field. Oscillating droplets and bubbles produce a hydrodynamic force known as the Bjerknes force (Lamb, 1932; Pelekasis & Tsamopoulos, 1993). The structure of such force is very similar to the structure of the Coulomb electric force; it decreases with the distance from oscillating bubble as r^{-2}, and it can be of either attractive, if two bubbles oscillate in the same phase, or repulsive, if they oscillate in antiphase (the situation can be even more complicated, if they oscillate at the arbitrary phase shift between 0 and π). The expression for the classical Bjerknes

force was generalized by Nemtsov (1983) who showed that, in a compressible fluid the acoustic signal generated by one oscillating bubble reaches another bubble not instantaneously, but after some delay. This can produce several interesting and important effects that have not been studied thus far. For example, two oscillating bubbles can move forward, experiencing reactive momentum due to the radiation of an acoustic wave. The first approach to bubble study in a compressible fluid was undertaken in the paper by Stepanyants & Yeoh (2008), but they considered bubble motion only in a perfect fluid. Even in this simplified case they obtained interesting results which show that two oscillating bubbles can demonstrate a behavior very similar to what is shown in Figure 1.6 for the droplets. The bubbles can coalesce, bounce, reflex, or separate. This study can be further developed and extended for droplets in viscous fluids. In general, interaction of two droplets or bubbles in a viscous fluid can be a subject of action of various forces including electric force with Saranin's modification, Bjerknes force with Nemtsov's modification, viscous forces with Stokes and memory integral drag forces. Some of these effects are studied in the present Thesis, others will be studied later.

One of the topical problems is the manipulation of particle motion in a fluid medium by external forces. This can be done with the help of an electric or a magnetic force, if a particle is charged, or by an acoustic force, if the particle is uncharged. The period-averaged action of sound on small particles can cause complex motions due to the action of the acoustic radiation force (ARF). This problem has been studied since the mid-1900s (Yosioka & Kawasima, 1955, Gor'kov, 1962). In the last two decades, ARF effects have been widely used in microfluidics, biological acoustics, and medicine. Among the promising areas of application are the manipulation, concentration and stirring of particles and bubbles in ultrasonic resonators of different configurations. The theoretical consideration of some of these effects was undertaken in Sarvazyan & Ostrovsky, (2009). However, in that work, only two extreme cases were studied, namely, the hard, non-deformable particles, and gaseous bubbles. This is not directly applicable to many practical cases, such as in the case of the biological cells which are typically only slightly different in density from the ambient fluid. One example of the latter case was analysed by Ostrovsky (2015) who considered the rate of change of such a "particle" concentration in a cylindrical resonator.

It is of significant theoretical and practical interests to study the particle motion under the action of ARF taking into account the two main parameters of a particle, its density and the sound speed in the particle material. It is known that even the direction of particle drift in a standing acoustic wave can be different depending on its mechanical parameters (Sarvazyan & Ostrovsky, 2009). Another potentially important extension of existing models is to incorporate the effects of the Boussinesq–Basset drag (BBD) force (see, e.g., (Lovalenti & Brady, 1993; Stepanyants & Yeoh, 2009) and references therein) and mass inertia, in addition to the viscous Stokes drag force which generally dominates at small Reynolds numbers, but with some noticeable exceptions as will be discussed below.

It is well known (Lovalenti & Brady, 1993), that a small fluid drop moving in a viscous fluid at a small Reynolds number experiences an influence of at least two drag forces, one of them is the traditional Stokes drag force and another is the memory-integral drag (MID) force. In the past decade, a vast number of papers devoted to the role of the MID force in the dynamics of solid particles, gaseous bubbles and other liquid drops in viscous fluids have been published (see, e.g., Refs. (Candelier, Angilella, & Souhar, 2004; Candelier, Angilella & Souhar, 2005; Kobayashi & Coimbra, 2005; Stepanyants & Yeoh, 2009; Visitskii, Petrov & Shunderyuk, 2009; Aksenov, Petrov & Shunderyuk, 2011; Xie & Vanneste, 2014 and Hassan, Ostrovsky & Stepanyants, 2017) and references therein). The growing interest in this problem in recent years is associated with the development of the new field of microfluidics and the technology of using micro- and nano-particles. Such technology is already used in medicine (for the diagnostics and drug delivery to the specific organs), biology, food quality control, and chemistry, etc. (see the review by Ostrovsky & Stepanyants (2017) and references therein). Chapter 3 of this Thesis is devoted to studying the problem of micro-particle manipulation by ARF.

In many cases nanoparticles can experience an oscillatory motion around quasi-stationary positions under the action of external forces, for example, by an acoustic radiative force (Visitskii, Petrov & Shunderyuk, 2009; Aksenov, Petrov & Shunderyuk, 2011; Hassan, Ostrovsky & Stepanyants, 2017; Ostrovsky & Stepanyants, 2017). In such cases, it is important to know the resonance properties of nanoparticles, e.g., the shape of the resonance curve (the dependence of the amplitude of oscillation on the frequency of the external sinusoidal force), the width

and the amplitude of the resonance curve, and the quality of the effective oscillator. All these characteristics are well known for the classical linear oscillator and have been described in many text books and monographs (see, e.g., Siebert, (1986); Klepper & Kolenkow, (2014))). When the particle oscillates in a viscous fluid under the action of external force, then, as mentioned above, at least two viscous forces should be taken into account, the Stokes drag force and the MID force. If only the Stokes drag force is taken into consideration, and the MID force is ignored, then the corresponding equation of motion reduces to the equation for the classical linear oscillator with dissipation. However, to our best knowledge, the influence of the MID force on the resonant property of an oscillator has not been studied thus far by other authors. This problem was considered in our recent publication (Hassan & Stepanyants, 2017) and is described in Chapter 4 of this Thesis.

Because the Thesis is focused on the particle, drop, and bubble dynamics in a viscous fluid, it is reasonable to present and explain the basic equations of motion for these entities. This is done in the next subsection.

1.1. The equation of motion of a fluid particle in a viscous surrounding fluid

The equation of motion of one spherical particle with the added mass effect taken into account is (Batchelor, 1970; Landau & Lifshitz, 1988):

$$\left(r+\frac{1}{2}\right)\frac{d^2 r_1}{dt^2} = -(r-1)g + \frac{3}{4}\frac{F_s}{\pi R^3 \rho} - \frac{9\upsilon}{2R^2}\left[f\left(R, r_1, r_2, \frac{dr_2}{dt}\right)\frac{dr_1}{dt} + \frac{R}{\sqrt{\pi\upsilon}} F\left(R, r_1, r_2, \frac{dr_2}{dt}\right)\int_{-\infty}^{t} I(r_1)\,d\tau \right], \tag{1.1}$$

where g is the acceleration due to gravity, ρ is the particle density, and r is the particle-to-fluid density ratio. The added mass effect is taken into account through the coefficient 1/2 in the brackets on the left-hand side of the equation.

The first term in the right-hand-side describes the gravity/buoyancy force, the second term describes the electrostatic force and the third term describes the total drag force including the Stokes drag (SD) force (the first term in the square brackets) and the MID force (the second, integral, term in the square brackets). Function $F \equiv 1$, if the correction to the BBD force is ignored, or $F \equiv f$, if the

correction to the BBD force is the same as to the SD force.

The SD and MID forces have a long history. In 1845 Stokes derived the first formula for the SD force acting on a stationary moving a solid spherical particle in the limit of a creeping flow (when Reynolds number is very small). Hadamard, and separately Rybczynski, in 1911 obtained a generalised Stokes formula for stationary moving spherical liquid inclusions (drops). Then in 1956 Proudman & Pearson introduced a correction to the formula for the SD force by using Oseen's solution (Landau & Lifshitz, 1993). Recently, the general formulae for the drag force acting on drops or bubbles of any densities and viscosities were obtained (Gorodtsov, 1975). On the other hand, in 1885 Boussinesq and three years later Basset presented another force acting on a solid particle, which is currently known as the memory integral drag (MID) force or in their particular case called the Boussinesq–Basset drag (BBD) force. More details for the MID force, especially for the case of a solid particle moving in quiescent fluids, can be found in many textbooks (see, e.g., (Landau & Lifshitz, 1993)).

During this time, many corrections to SD and MID forces have been derived for many cases of particles moving in different fluids. For example, in 1922 Faxen derived a formula for the non-uniformity of moving particles in an external fluid flow. Saffman in 1965 derived a formula for the force appearing due to particle rotation in the course of motion and external shear flow (see (Legendre & Magnaudet, 1997)). The latest version of the equation of drop motion (including gaseous bubbles and solid particles) has been derived by Lovalenty and Brady in 1993 (Lovalenty & Brady, 1993). More details about the history of the SD and MID forces can be found in Stepanyants & Yeoh, (2009).

The study of particle, drop, and bubble motions in fluid media has numerous practical applications. Some of them will be described in the next sections.

1.2. Applications

The importance of particle dynamics in a creeping flow is backed by many practical applications to mixtures of fluids and drops (including solid particles and gaseous bubble) and suspensions. One of known examples is particle-liquid mixtures used for pharmaceutical purposes. Other important examples pertain to

the transport of particles in the atmosphere (dust) and oceans (suspensions, sand, etc.). One of the more intriguing problems that have not been solved so far is the dynamics of two interacting charged particles in a viscous fluid.

Particle motion in viscous fluid was studied in several papers in application to the cooling systems of nuclear reactors (see, for example, (Stepanyants & Yeoh, 2009; 2010) and references therein). Dust particles can penetrate into the open pool vessel as shown in Figure 1.7. In the density stratified fluid (due the temperature difference in the upper and lower layers) particle motion can be decelerated or even terminated at the sharp density interface, where they can be easily collected and removed.

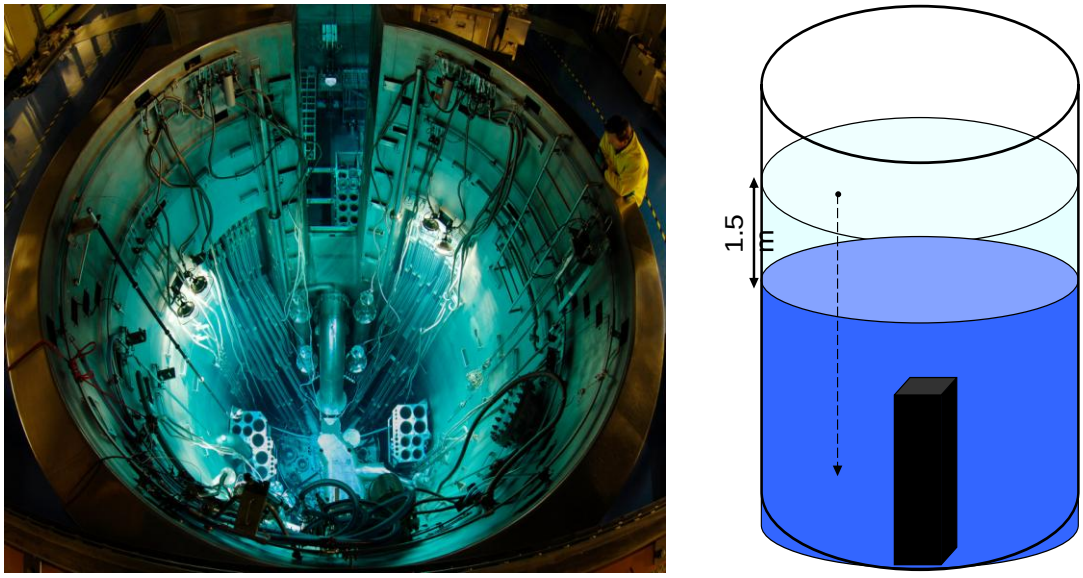

Figure 1.7: (From (Stepanyants & Yeoh, 2010)). Open pool Australian nuclear reactor (OPAL): (a) – photo; (b) – sketch of the cooling vessel containing two-layer fluid (tap water) of different density.

The particle motion under the action of the acoustic radiation force has a variety of potential applications. It can be used, in particular, for stirring and mixing of particles (Sarvazyan & Ostrovsky, 2009), as well as for their separation and collection at certain places, from where they can be subsequently removed to provide a cleaning of fluid. In particular, when there is an ensemble of particles of different properties (mass, radius, density) placed in the acoustic resonator, they can be collected in nodes and antinodes, as shown in Figure 1.8. This can be used as the method of particle separation in addition to that mentioned above.

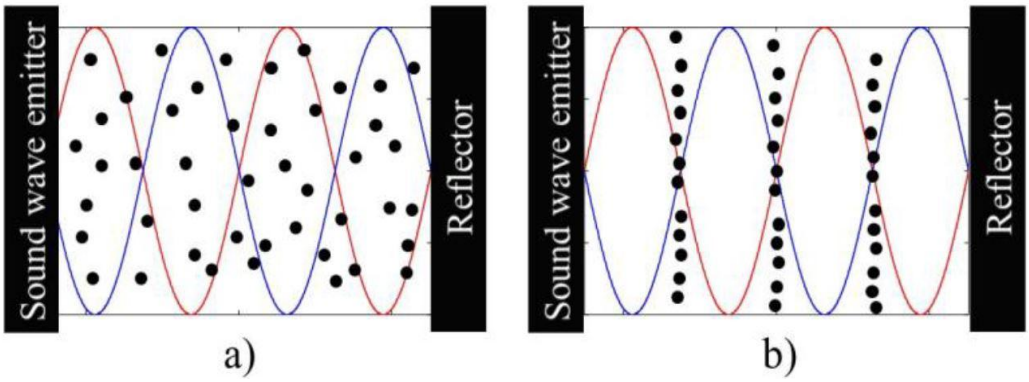

Figure 1.8: (From (Ostrovsky & Stepanyants, 2017)). Schematic illustration of particles gathering in the nodes of a standing acoustic wave in a plane resonator with initially randomly distributed particles (from panel a) to panel b). Lines show a standing acoustic wave in two instances of time when the wave phase differs on π.

Another possible application of particle motion under the action of the acoustic radiation force in industry is emulsion separation. Emulsion separation is an important method to many industry areas: for example, in petroleum industry (for isolation of crude oil at the oilfields), recycle system of valuable oils, recycle the wastewaters and much more. There are numerous ways to apply the emulsion separation: this can be done by means of physical methods, electrochemical methods, or by adding special chemicals. However, these methods are either not efficient (for example, the electrochemical methods are very costly) or are not as safe, for example, in the case of adding chemicals. In Ref. (Nii et al., 2009) it was proposed a new technique to apply emulsion separation by means of ultrasound. As the example, it has been shown that the method can be used to separate canola oil from water. This technique is safe and does not incur high operation cost.

Thévoz et al., (2010) studied how to separate particles by means of ultrasonic standing waves. The authors invented an acoustophoretic cell synchronization device shown in the Figure 1.9 below. As shown in frame (A), asynchronous mixture of cells and buffer volumetrically pumped into the device. Synchronization was achieved by fractionating the cells according to size such that larger cells (e.g., G_2) elute through the outlet A whereas smaller cells (e.g., G_1) elute through the outlet B. The photograph in frame (B) shows the device with the attached piezoactuator on its backside (scale bar is 5 mm). Frame (C) represents the fluorescence micrographs of the acoustophoretic cell synchronization device in operation. A binary mixture of green (5-μm-diameter) and red (2-μm-diameter)

polystyrene beads enters the inlet area (left) and are acoustophoretically separated to elute through the outlets A and B, respectively (right). Scale bars are 50 μm in both images. Frame (D) shows a two-dimensional numerical simulation of separation along the channel, showing buffer (gray) with bands of particle trajectories. Larger particles (green) are subject to a greater acoustic radiation force and thus converge faster to the nodal plane at the center of the channel (dashed line) and elute through the outlet A. Smaller particles (red) do not reach the nodal plane and elute through the outlet B. Thus, due to different response of large and small particles on the ultrasound standing waves, one can concentrate large particles in the center of a cylinder, while the small particles not affected by the acoustic force remain out of center. Therefore, it is possible to separate and collect the particles in different vessels.

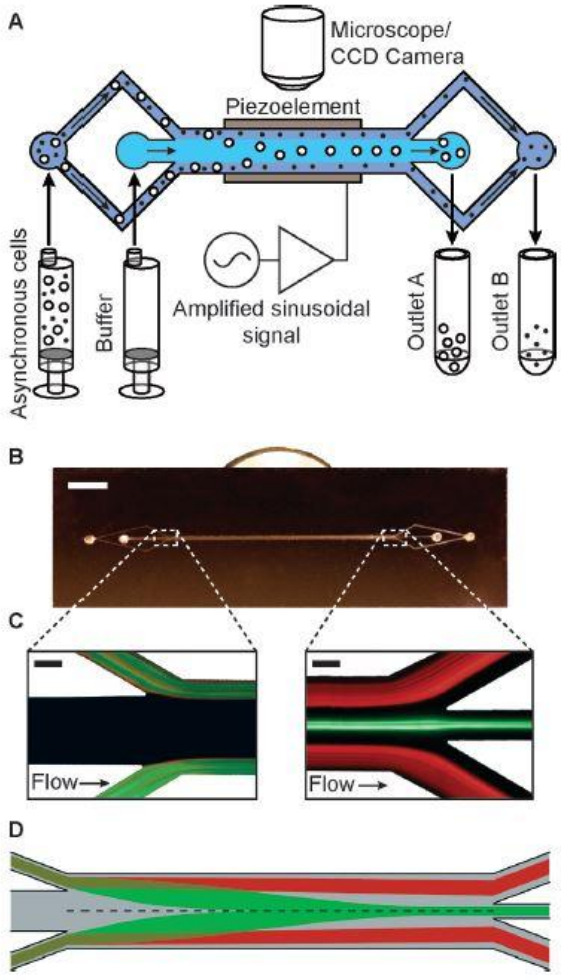

Figure 1.9: (From (Thévoz et al, 2010)). Acoustophoretic cell synchronization device and experimental setup as described in the text.

Similar technology is used for the separation of micro particles for example, fat globules and cells from milk (Priev et al., 2015), and alcohol from beverages (Priev & Barenholz, 2010). Figure 1.10 shows the separation of fat globules in milk by standing waves in the cylindrical pipe. Acoustic radiation force in resonators is also used for food and water quality control and monitoring (Priev & Sarvazyan, 2009; Priev & Barenholz, 2010; Ostrovsky et al., 2011).

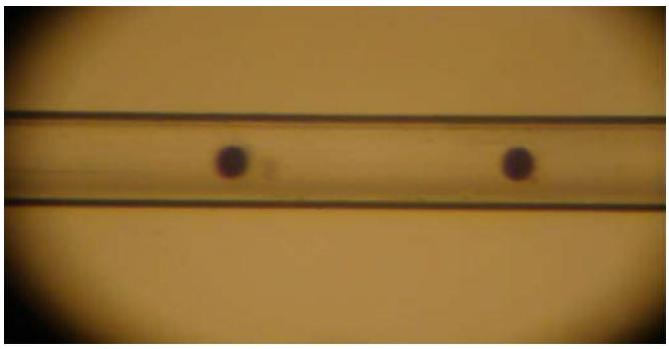

Figure 1.10: Separation of fat globules in milk (dark spots) by cylindrical standing waves in the pipe (from (Priev et al., 2015)).

Acoustic fields can be used for the micro-particle delivery to certain places within liquids, tissues, or other fluid materials. There are in particular devices, known as the “acoustic tweezers”, which allow researchers and engineers to manipulate with individual particles. Figure 1.11 shows an example of how particles can be controlled by an acoustic field. As one can see, it was possible to write even relatively complex texts by, manipulating number of isolated particles.

Further development of this technology is very topical in many applications and especially in medicine and food technology. With the help of acoustic tweezers, operating with the low-intensity sound waves, one can deliver drugs to the particular organs within a human body. This is a very promising field of research currently developing in many countries and requiring a strong support from theory. Results obtained within this Thesis contributes to this field of research and is presented in Chapter 3.

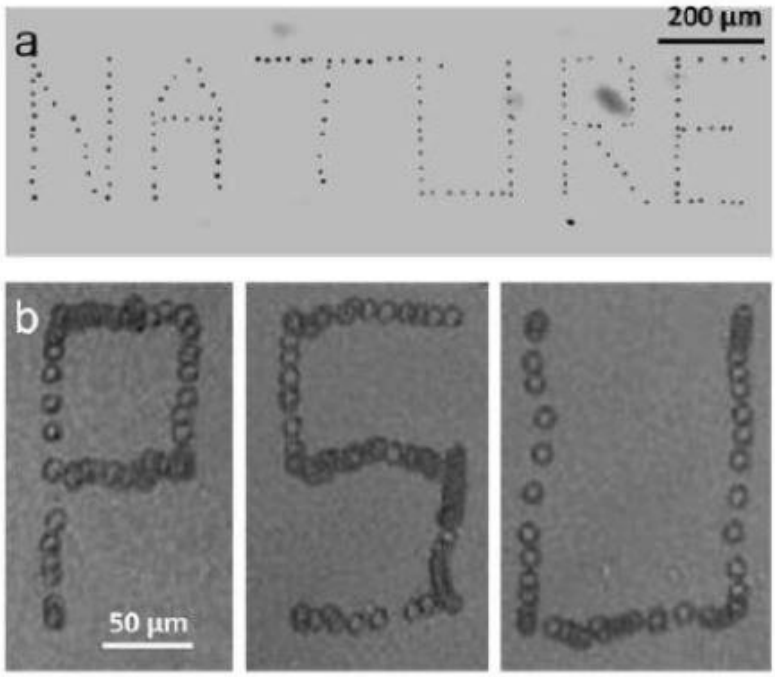

Figure 1.11: (From (Ding et al, 2012)). a) Stacked images demonstrating the particle motion control in *x* and *y* directions using 7-μm fluorescent polystyrene beads to write the word "NATURE". b) Stacked images showing dynamic control of bovine red blood cells to trace the letters "PSU" (the acronym for the Penn-State University).

If a droplet or a particle moves forth and back due to the action of external acoustic field, it can be eventually dissolved in the surrounding liquid. This idea was discussed in the paper by Schmid et al. (2016) who suggested to deliver nanoparticles containing a solvable drug to specific organs in a human body. An alternative method of particle manipulation suggested in the paper by Ashkin (1997) is based on the optical trapping of particles by a highly focused laser beam. But this method can be applied only to the transparent liquids, whereas the acoustic methods can be used even in the case of non-transparent liquids.

The growing interest in the resonance properties of forced oscillations of particles and gaseous bubbles in a viscous fluid at small Reynolds numbers in recent years is associated with the development of a new field of microfluidics and the technology of using micro- and nano-particles. Such a technology is already used in the medicine (for the diagnostics, drug delivery to specific organs), biology, food quality control, and chemistry, etc. (see the review in Ostrovsky & Stepanyants, (2017) and references therein).

Taking into account the importance of the study of particle dynamics in viscous fluids, the topicality of the theme of such research and numerous possible applications, we can formulate the objectives of this research Thesis.

1.3. Research Objectives

The objectives of the Thesis are threefold:

1) The first objective is to investigate the influence of disturbed electric charges within conducting solid particles on their dynamics in a viscous fluid. This will be done in the second chapter. Two types of viscous drag forces will be taken into consideration: the quasi-stationary Stokes drag force and the transient Boussinesq−Basset drag force. Different models of viscous drag forces will be analysed: when the viscosity coefficients are constants, like in the case of a single particle, and when they are modified due to the presence of a second particle. Comparison of particle trajectories under the influence of all these forces will be studied and compared with the case of particles in an inviscid fluid. Precise knowledge of the electric and hydrodynamic forces acting on the particles in a fluid will allow one to control the particle motion by external forces.

2) The second objective is to investigate the particle motion under the influence of an external acoustic force. This will be done in the third chapter. The influence of the MID force will be studied in application to particles of different properties (different densities and materials) in the acoustic resonators of different geometries (plane and cylindrical). The aim of this chapter is to demonstrate that particle motion in a viscous fluid can be effectively manipulated by an external acoustic field. Figure 1.12, in particular, illustrates that the ice particle can be moved by radiative acoustic force. As a result, this can be used in many applications, for example in medical applications, when a particle drifts to a specific place and then oscillates around that place; the particle could contain some medicine. In the process of oscillations, it will dissolve and it will deliver a special drug to the organ and then oscillate until fully dissolved in the organ (Ostrovsky & Stepanyants, 2017).

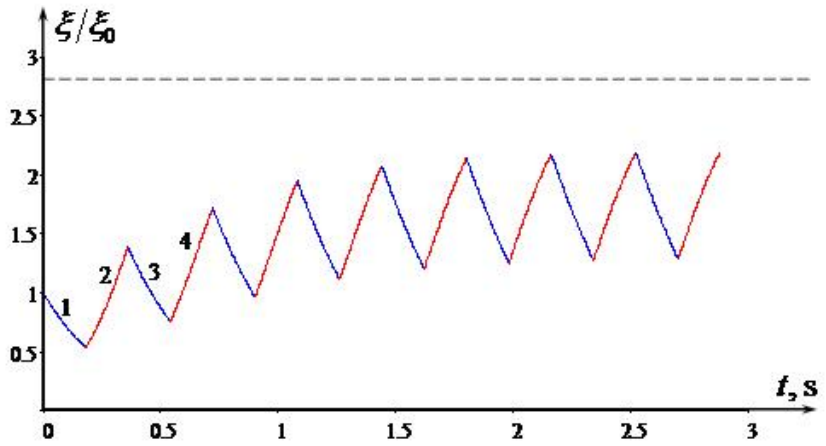

Figure 1.12: (from (Hassan et al., 2017)). Dependences of ice particle position on time when the acoustic field periodically switches from mode 3 to mode 4 and back. Odd decreasing lines (1, 3, …) pertain to mode 3, and even increasing lines (2, 4, …) pertain to mode 4. The dashed horizontal line shows an equilibrium position for a particle in the presence of fourth acoustic mode only.

3) The third objective is to study the resonance properties of oscillating particles and bubbles in a viscous fluid under the action of an external force. As one can see from Figure 1.12, under the action of external ARF, a particle experiences not only a drift motion but also oscillations. The amplitude of oscillations depends both on the intensity of external force and mainly on the frequency. Therefore it is important to know what will be the response of the particle due to the external force. The resonance properties of a linear oscillator with dissipation are very well known (Siebert, 1986 and Klepper & Kolenkow, 2014) for the case when only Stokes drag force is taken into account. However, in Chapter 4 it will be shown that the influence of MID forces can dramatically change the resonance properties both solid particles and gaseous bubbles. The qualities of corresponding oscillators are also significantly changed.

1.4. Content of research

The outline of the Thesis is as follows:

- In chapter 2 the influence of charge distribution on particles motion in viscous fluid will be investigated in detail. A motion of an individual uncharged particle in a viscous fluid at small Reynolds numbers in the creeping regime has been

studied in the paper by Stepanyants & Yeoh, (2009). It has been demonstrated, in the case of a transient flow, that the influence of Boussinesq−Basset drag (BBD) force (Gorodtsov, 1975, Lovalenti & Brady, 1993, and Kim & Karrila, 2005) is very important. It provides a different character of particle motions in comparison with the well-known Stokes drag (SD) force (Batchelor, 1970; Landau & Lifshitz, 1988). In chapter 2, a motion of two electrically charged particles in different setups will be considered taking into account a gravity/buoyancy forces, an electrostatic force, and a viscous drag force. The effect of viscosity will be taken into consideration through the SD force and BBD force which depends on the motion prehistory (Gorodtsov, 1975; Lovalenti & Brady, 1993; Kim & Karrila, 2005; Landau & Lifshitz, 1988). A reciprocal influence of particles on the drag force (Happel & Brenner, 1983) will be also studied for several particle configurations.

- In chapter 3 the influence of the external acoustic force on the dynamics of solid particles will be investigated. Complex dynamics of small particles under the action of acoustic radiation force will be studied. This work extends the previous studies of Ostrovsky & Sarvazyan (2009) and Ostrovsky (2015) in two aspects. Firstly, in this study in contrast to the previous works, the particle material can have an arbitrary compressibility and sound speed. Secondly, in addition to the viscosity effect described by the Stokes drag force, the Boussinesq–Basset drag force and the inertial force which includes added mass effect will be accounted for.
- Chapter 4 contains a study of resonance properties of forced oscillations of solid particles and gaseous bubbles in a viscous fluid at small Reynolds numbers taking into account both Stokes and integral memory drag forces. Small oscillations of micro-particles and gaseous bubbles in a viscous fluid around their equilibrium states will be considered under the action of a sinusoidal external force. Exact solutions to the governing integro-differential equations containing both Stokes and memory-integral drag forces will be obtained and analysed graphically. The main aim of this study is to clarify the influence of the memory-integral drag force on the resonance characteristics of oscillating particles or gaseous bubbles in a viscous fluid at small Reynolds numbers. The resonant curves (amplitude versus frequency of external force), as well as phase-frequency dependences, will be obtained for both these particle types and compared with the corresponding dependences of the traditional oscillator with the Stokes drag force only included.
- Chapter 5 contains the conclusion and discussions of results obtained in the

Thesis, as well as the perspectives of further research.

- In Appendix I present a Fortran code which was used for the numerical modelling of particle motion in a viscous fluid under the action of acoustic radiation force.

Chapter 2: Dynamics of charged particles in a creeping flow

2.1 Introduction

In this Chapter, the dynamics of charged and interacting solid particles in a viscous fluid will be studied. We consider a simple model of two particles moving either side-by-side or one after another along the same vertical line under the influence of the Archimedean (buoyancy) and gravity forces, the Coulomb electrostatic force (or its modification), and the viscous drag force. The drag force consists of two components: the quasi-stationary Stokes drag force and the Boussinesq–Basset drag force resulting from the unsteady motion. Solutions of the governing equations will be analysed analytically and numerically for the cases of a perfect fluid and for a viscous fluid. The results obtained for these two cases will be then compared.

2.2 Equations of motion and problem formulation

A motion of an individual uncharged particle in a viscous fluid at small Reynolds numbers in the creeping regime has been studied (Stepanyants & Yeoh, 2009). It has been demonstrated that in the case of a transient flow the influence of the Boussinesq−Basset drag (BBD) force (Gorodtsov, 1975; Lovalenti & Brady, 1993; Kim & Karrila, 2005) is very important. It provides a different character of particle motion in comparison with the well-known Stokes drag (SD) force (Batchelor, 1970; Landau & Lifshitz, 1988). We consider here the motion of two electrically charged particles in different setups taking into account all forces mentioned above. The specific feature of the BBD force is in its dependence on the motion prehistory, which results in the appearance of an integral term in the equation of motion. We also take into account a reciprocal influence of particles on the hydrodynamic drag force which depends on the particle configuration (Happel & Brenner, 1983). To the best of our knowledge, the combined effect of all these factors has not been studied thus far by other authors.

As a first step we consider two identical metallic particles with electric charges of the same absolute value (they can be either of like or unlike charges). As has

been shown, by Saranin, (1999), the electrostatic force acting on metallic particles deviates from the one predicted by the classical Coulomb law for point particles: at small distances the force is not inversely proportional to the square of the distance between the particle centres. This deviation is important at relatively small distances between the particles while at large distances the electrostatic force asymptotically approaches the classical Coulomb law. The exact expressions for the electrostatic force $\mathbf{F}_s$ as derived by Saranin (1999) and its asymptotic Coulomb approximation $\mathbf{F}_c$ are as follows,

$$\mathbf{F}_s\left(\mathbf{r}_1-\mathbf{r}_2\right)=-\frac{q^2}{8\pi\varepsilon}\frac{\mathbf{r}_1-\mathbf{r}_2}{\left|\mathbf{r}_1-\mathbf{r}_2\right|}\frac{S(\beta)}{a^2}, \tag{2.1}$$

$$\mathbf{F}_c\left(\mathbf{r}_1-\mathbf{r}_2\right)=-\frac{q^2}{4\pi\varepsilon}\frac{\mathbf{r}_1-\mathbf{r}_{22}}{\left|\mathbf{r}_1-\mathbf{r}_2\right|^3}, \tag{2.2}$$

where a is the particle radius, q is the value of the electric charge, ε is the permittivity of the medium,

$$S(\beta)=\sum_{n=1}^{\infty}\left\{(-1)^{\kappa_n}\frac{n\coth n\beta-\coth\beta}{\sinh n\beta}\left[\sinh\beta\sum_{n=1}^{\infty}\frac{(-1)^{\kappa_n}}{\sinh n\beta}\right]^{-2}\right\},$$

$$\beta=\ln\left(\frac{\left|\mathbf{r}_1-\mathbf{r}_2\right|}{2a}+\sqrt{\frac{\left|\mathbf{r}_1-\mathbf{r}_2\right|^2}{4a^2}-1}\right).$$

The parameter κ_n is taken as $\kappa_n=n+1$ for like charged particles and as $\kappa_n=0$ for unlike charged particles.

Figure 2.1 shows the dependences of the attractive and repulsive electrostatic forces (normalised by the factor $q^2/(16\pi\varepsilon a^2)$ as described by Equation (2.1) and the corresponding Coulomb forces under the same normalization as described by Equation (2.2). As one can see from this figure, corrections to the Coulomb forces become notable only when the distance between the particle centers is less than $4a$. The modified attractive force infinitely increases when the particles approach each other (see line1 in the Figure 2.1).

When a solid particle moves in a viscous fluid, it experiences an influence of a drag force (Batchelor, 1970; Landau & Lifshitz, 1988). In the presence of another particle, the drag force modifies and depends on many factors, including the

particle shape, the distance between them, their reciprocal orientation, and their velocities (Happel & Brenner, 1983). The correction to the quasi-stationary SD force acting on particle in the presence of another particle can be taken into account through the effective viscosity $\nu_{eff} = \nu\, f(a_1, a_2, \mathbf{r}_1, \mathbf{r}_2, d\mathbf{r}_1/dt)$, where ν is the coefficient of kinematic viscosity, and f is a rather complicated function of its arguments. This function gradually reduces to unity when the distance between the particles becomes much greater than their radii.

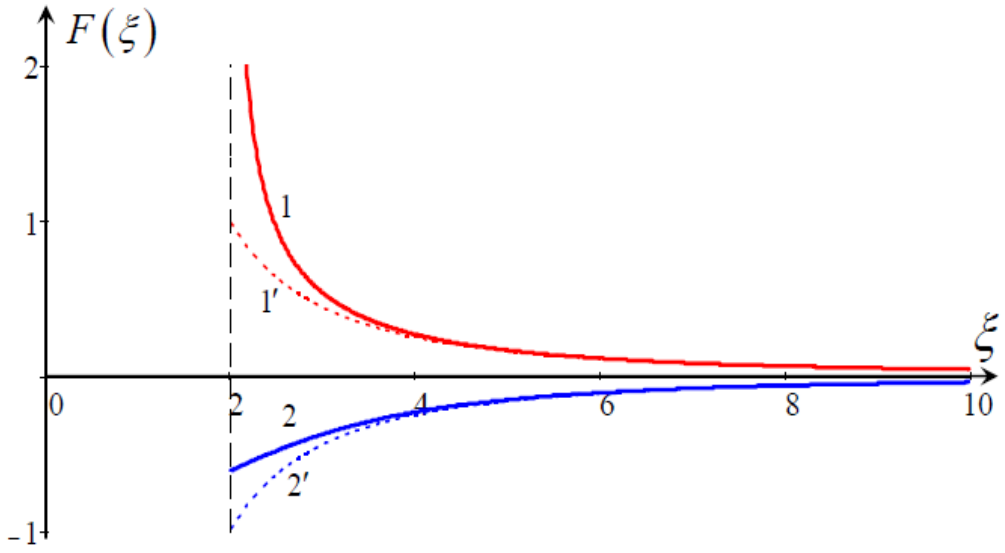

Figure 2.1: Normalised electrostatic force versus normalised distance, $\xi = x/a$, between two like (line 1) and unlike (line 2) charged particles as per Equation (2.1). Dashed lines show the Coulomb approximations as per Equation (2.2).

Description of particle motion in a viscous fluid has a long history, however until now only approximate equations describing viscous forces acting on a moving particle where obtained. Relatively good understanding of particle motion was obtained for small Reynolds numbers (Re << 1) for so-called creeping motions. As was shown in many papers (see, for example, (Lovalenty & Bready, 1993; Stepanyants & Yeoh, 2010), and references therein), there are two viscous forces, one of them is the Stokes drag force which acts even when a particle uniformly moves in a fluid, and another force, the memory integral drag force acts only when a particle moves non-uniformly. These results derived and experimentally validated for the individual particles should be modified when the motion of another particle

accompanies a particle motion (the same pertains to the bubble motions with a minor modification). Even for the motion of two particles or bubbles the viscous drag forces depend on the spatial configuration of particles or bubbles, for example, whether they move side-by-side or one-after-another (see Figure 2.2). The theoretical consideration of drag forces acting on a pair of particles has been described in the book by Happel & Brenner (1983), but details of particle motion were not studied. The results from this book will be used below in the study of particle motion in the viscous fluid taking into account the modified electric forces as per Saranin (1999) exerting on charged conducting particles.

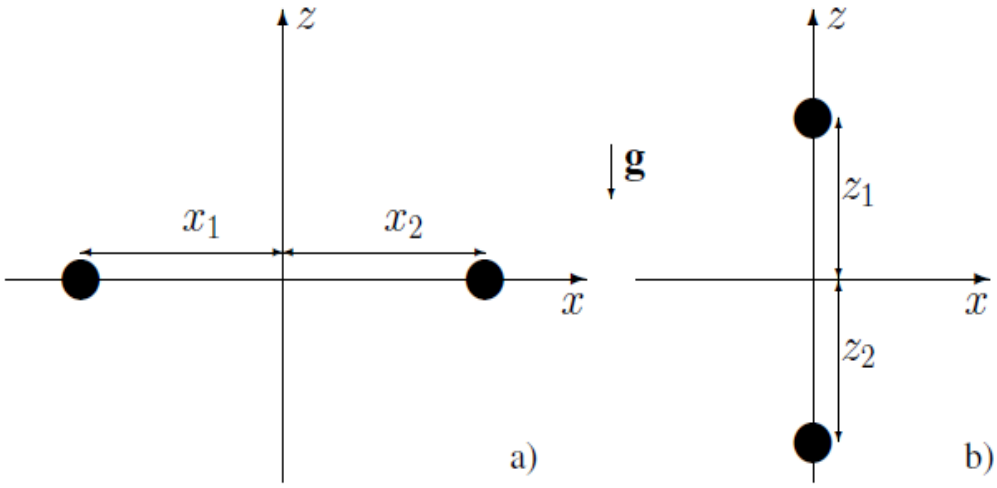

Figure 2.2: Two particles moving side-by-side in the direction normal to the line connecting their centres (a) and one after another along the line connecting their centres (b).

To the best of our knowledge, modifications of the transient BBD force exerting on a particle in the presence of another particle have not been studied yet. With this in mind, we can consider two notional possibilities: (a) there is no correction to the BBD force due to the presence of another particle, so that the BBD force remains the same as for a single particle; and (b) the correction to the BBD force is described by the same effective viscosity as the SD force. In what follows, both these possibilities will be explored and results will be compared.

Consider further two spherical particles moving in a viscous fluid in the creeping flow regime, where the Reynolds number is much less than one, Re << 1.

The equation of motion of one spherical particle with the added mass effect taken into account is (Batchelor, 1970; Landau & Lifshitz, 1988):

$$\left(r+\frac{1}{2}\right)\frac{d^2\mathbf{r}_1}{dt^2}=-(r-1)\mathbf{g}+\frac{3}{4}\frac{\mathbf{F}_s}{\pi a^3\rho}- \\ \frac{9\nu}{2a^2}\left[f\left(a,\mathbf{r}_1,\mathbf{r}_2,\frac{d\mathbf{r}_2}{dt}\right)\frac{d\mathbf{r}_1}{dt}+\frac{a}{\sqrt{\pi\nu}}F\left(a,\mathbf{r}_1,\mathbf{r}_2,\frac{d\mathbf{r}_2}{dt}\right)\int_{-\infty}^{t}\frac{d^2\mathbf{r}_1}{d\tau^2}\frac{d\tau}{\sqrt{t-\tau}}\right], \tag{2.3}$$

where **g** is the acceleration due to gravity, ρ is the particle density, r is the particle-to-fluid density ratio.

The added mass effect is taken into account through the coefficient 1/2 in the brackets on the left-hand side of the equation. The first term in the right-hand-side describes the gravity/buoyancy force, the second term describes the electrostatic force and the third term describes the total drag force including the SD force (the first term in the square brackets) and the BBD force (the second, integral, term in the square brackets). The function $F \equiv 1$ if the correction to the BBD force is ignored, or $F \equiv f$ if the correction to the BBD force is the same as to the SD force.

The same equation with the indices interchanged holds for the second particle. Subtracting and summing the equations for the individual particles, we obtain

$$\left(r+\frac{1}{2}\right)\frac{d^2\left(\mathbf{r}_2-\mathbf{r}_1\right)}{dt^2}=\frac{3}{4}\frac{\mathbf{F}_s}{\pi a^3\rho}-\mathbf{D}_1; \tag{2.4}$$

$$\left(r+\frac{1}{2}\right)\frac{d^2\left(\mathbf{r}_2+\mathbf{r}_1\right)}{dt^2}=-2(r-1)\mathbf{g}-\mathbf{D}_2; \tag{2.5}$$

where

$$\mathbf{D}_1=\frac{9\nu}{2a^2}\left\{f\left(a,\mathbf{r}_1,\mathbf{r}_2,\frac{d\mathbf{r}_1}{dt}\right)\frac{d\mathbf{r}_2}{dt}-f\left(a,\mathbf{r}_1,\mathbf{r}_2,\frac{d\mathbf{r}_2}{dt}\right)\frac{d\mathbf{r}_1}{dt}+ \\ \frac{a}{\sqrt{\pi\nu}}\left[F\left(a,\mathbf{r}_1,\mathbf{r}_2,\frac{d\mathbf{r}_1}{dt}\right)\int_{-\infty}^{t}\frac{d^2\mathbf{r}_2}{d\tau^2}\frac{d\tau}{\sqrt{t-\tau}}-F\left(a,\mathbf{r}_1,\mathbf{r}_2,\frac{d\mathbf{r}_2}{dt}\right)\int_{-\infty}^{t}\frac{d^2\mathbf{r}_1}{d\tau^2}\frac{d\tau}{\sqrt{t-\tau}}\right]\right\}, \tag{2.6}$$

and

$$\mathbf{D}_2 = \frac{9\nu}{2a^2}\left\{ f\left(a,\mathbf{r}_1,\mathbf{r}_2,\frac{d\mathbf{r}_1}{dt}\right)\frac{d\mathbf{r}_2}{dt} + f\left(a,\mathbf{r}_1,\mathbf{r}_2,\frac{d\mathbf{r}_2}{dt}\right)\frac{d\mathbf{r}_1}{dt} + \right.$$
$$\left. \frac{a}{\sqrt{\pi\nu}}\left[F\left(a,\mathbf{r}_1,\mathbf{r}_2,\frac{d\mathbf{r}_1}{dt}\right)\int_{-\infty}^{t}\frac{d^2\mathbf{r}_2}{d\tau^2}\frac{d\tau}{\sqrt{t-\tau}} + F\left(a,\mathbf{r}_1,\mathbf{r}_2,\frac{d\mathbf{r}_2}{dt}\right)\int_{-\infty}^{t}\frac{d^2\mathbf{r}_1}{d\tau^2}\frac{d\tau}{\sqrt{t-\tau}}\right]\right\}. \quad (2.7)$$

Below we consider two particular cases of particle configuration when they move (i) side-by-side as sketched in Figure 2.2a and (ii) one after another as shown in Figure 2.2b.

2.3 Two particles moving side-by-side

Considering the case of two particles moving side-by-side as shown in Figure 2.2a and assuming that the centre of masses of the system does not move in the horizontal direction, we write down the scalar projections of Equations (2.6) and (2.7) onto the horizontal, *x*, and vertical, *z*, axes

$$(2r+1)\frac{d^2\xi}{d\theta^2} = -\frac{E_{es}}{2}S_n - f_2(\xi)\frac{d\xi}{d\theta} - \frac{3}{\sqrt{\pi}}F_2(\xi)\int_{-\infty}^{\theta}\frac{d^2\xi}{d\eta^2}\frac{d\eta}{\sqrt{\theta-\eta}} \quad (2.8)$$

$$(2r+1)\frac{d^2\zeta}{d\theta^2} = -G(r-1) - f_3(\xi)\frac{d\zeta}{d\theta} - \frac{3}{\sqrt{\pi}}F_3(\xi)\int_{-\infty}^{\theta}\frac{d^2\zeta}{d\eta^2}\frac{d\eta}{\sqrt{\theta-\eta}} \quad (2.9)$$

where the normalised variables are:

$$\xi = \frac{x_2 - x_1}{a}, \qquad \zeta = \frac{z}{a}, \qquad \theta = \frac{9\nu}{a^2}t, \qquad E_{es} = \frac{1}{108\rho}\left(\frac{q}{\pi\nu a}\right)^2, \qquad G = \frac{2\mathbf{g}a^3}{81\nu^2}, \qquad \text{and}$$

$$S_n = \frac{\sum_{n=1}^{\infty}\left[(-1)^{\kappa_n}\frac{n\coth n\beta - \coth\beta}{\sinh n\beta}\right]}{\sinh^2\beta\left[\sum_{n=1}^{\infty}\frac{(-1)^{\kappa_n}}{\sinh n\beta}\right]^2}.$$

Functions $f_1(\xi)$, $f_2(\xi)$, and $f_3(\xi)$ as well as $F_1(\xi)$, $F_2(\xi)$ and $F_3(\xi)$ account for the reciprocal influence of particles on the drag forces exerted on them (Happel &Brenner, 1983). Functions f_1, f_2, and f_3 can be presented in terms of the variable $\xi_1 = 1/(2\xi)$ as follows.

- In the case when two particles move one after another with equal speeds in the same direction along the line connecting their centres:

$$f_1(\xi_1) \approx 1-3\xi_1+9\xi_1^2-19\xi_1^3+93\xi_1^4-387\xi_1^5+1197\xi_1^6-5331\xi_1^7+19821\xi_1^8- 76115\xi_1^9+\frac{2^{20}}{3}\frac{\xi_1^{10}}{1+4\xi_1}, \tag{2.10}$$

- In the case when two particles move with equal speeds on absolute value in the opposite directions along the line connecting their centres:

$$f_2(\xi_1) \approx 1+3\xi_1+9\xi_1^2+19\xi_1^3+93\xi_1^4+387\xi_1^5+1197\xi_1^6+5331\xi_1^7+19821\xi_1^8+ 76115\xi_1^9+\frac{2^{20}}{3}\frac{\xi_1^{10}}{1+4\xi_1}, \tag{2.11}$$

- In the case when two particles move with equal speed in the same direction side-by-side in the direction perpendicular to the line connecting their centres and can freely rotate:

$$f_3(\xi_1) \approx 1-\frac{3}{2}\xi_1+\frac{9}{4}\xi_1^2-\frac{59}{8}\xi_1^3+\frac{273}{16}\xi_1^4-\frac{1107}{32}\xi_1^5+\frac{64\xi_1^6}{1+2\xi_1}. \tag{2.12}$$

The graphs of $f_{1,2,3}(\xi)$ are shown in Figure 2.3.

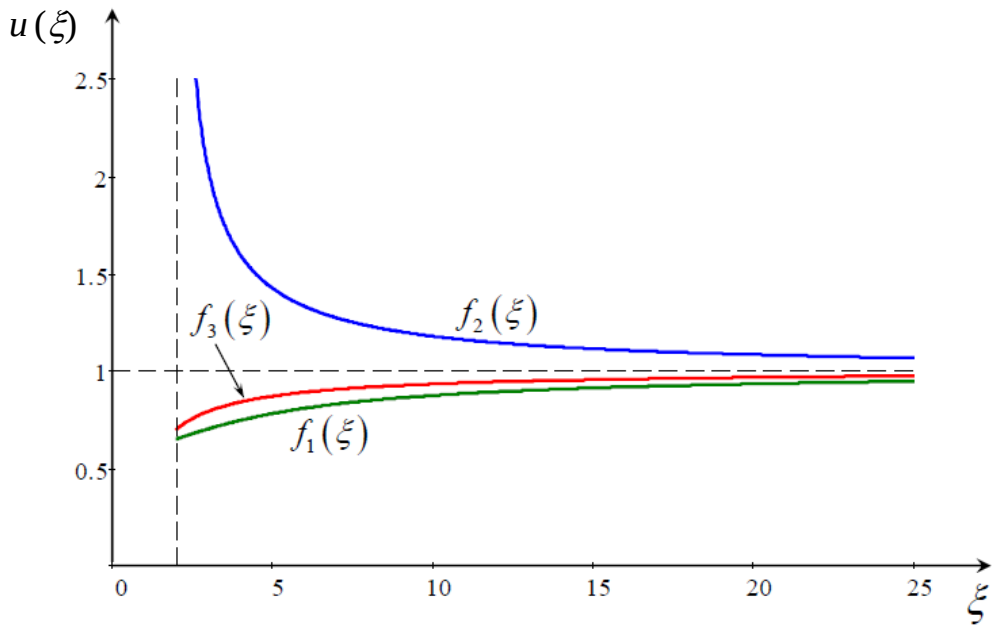

Figure 2.3: Functions $f_{1,2,3}(\xi)$ versus ξ. The horizontal dashed line shows the asymptotic value for all functions when the particles are far away from each other. The vertical dashed line shows the minimal distance between the particles, in the normalised variables $\xi_{min} = 2$.

As have been mentioned above, the expressions for the functions $F_{1,2,3}(\xi)$ are not known thus far, therefore we will consider two cases, when $F_{1,2,3}(\xi) \equiv 1$ and when $F_{1,2,3}(\xi) \equiv f_{1,2,3}(\xi)$. Functions $f_{1,2,3}(\xi)$ asymptotically approach unity when $\xi \to \infty$, and the corresponding drag force reduces to the drag forces exerted on an isolated particle. However, when $\xi \to 2$, which corresponds to the minimum distance between the particle centers (when the particles touch each other, and $x = 2a$), the functions $f_1(\xi)$ and $f_3(\xi)$ go to the finite limits: $f_1(\xi) = 0.647$ and $f_{1,2,3}(\xi) = 0.694$, whereas the function $f_2(\xi)$ grows infinitely, $f_2(\xi) \to \infty$ as $\xi \to 2_+$. The physically unacceptable behaviour of the drag forces, in this case, is the consequence of the approximate character of the formula for $f_2(\xi)$. Nevertheless, as noted in Ref. Happel & Brenner, (1983), "*Hocking states that good agreement on collision efficiencies is obtained with his results and experimental data, so it is apparent that under some conditions the approximate treatment is satisfactory*".

Note that in the Coulomb approximation, when the distance between the particles is much longer than their radii or when the charges of spherical particles are localised at their centres, the first term in Equation (2.6) takes the simple form E_{es} / ξ^2. We will study the particle interaction in both cases, with the exact formula for the electrostatic force, $\mathbf{F}_s$ as per Equation (2.1), and with the Coulomb approximation for the electrostatic force $\mathbf{F}_c$ as per Equation (2.2).

Equation (2.8) is independent of (2.9) and can be solved separately. Once its solution is found and $\xi(\theta)$ is determined, Equation (2.9) can then only be solved since Equation (2.9) contains $\xi(\theta)$ via functions $f_3(\xi)$ and $F_3(\xi)$.

For computations we used the following values of parameters: water density $\rho = 10^3\ kg / m^3$, water kinematic viscosity $\nu = 6.05 \cdot 10^{-7}\ m^2 / s$, particle radius $a = 5 \cdot 10^{-5}\ m = 50 \mu\text{m}$, charge values are equal to $q = 1.6 \cdot 10^{-13} C$, water permittivity $\varepsilon = 6.954 \cdot 10^{-10}\ F / m$, particle-to-water density ratio $r = 2.7$ (this corresponds to an aluminium mote). Based on these parameters, the dimensionless parameters are $E_{es} = 3.784 \cdot 10^{-2}$ and $G = 8.272 \cdot 10^{-2}$.

2.4 Particle dynamics in an inviscid fluid

Assuming that two particles with equal charges of absolute value are initially at rest, let us study first the reference case, when the fluid is perfect and viscosity is absent (formally we put $f_{1,2,3}(\xi) = F_{1,2,3}(\xi) \equiv 0$). Then, Equation (2.8) in the Coulomb approximation can be solved analytically; solutions for the like and unlike charged particles can be presented in the implicit forms,

$$\theta = \sqrt{\frac{\xi_0(2r+1)}{-2E_{es}}}\left[\frac{\xi_0}{2}\ln\left|\frac{\sqrt{\xi-\xi_0}+\sqrt{\xi}}{\sqrt{\xi-\xi_0}-\sqrt{\xi}}\right|+\sqrt{\xi(\xi-\xi_0)}\right], \qquad E_{es}<0, \tag{2.13}$$

$$\theta = \sqrt{\frac{\xi_0(2r+1)}{2E_{es}}}\left[\xi_0\left(\arctan\sqrt{\frac{\xi}{\xi_0-\xi}}-\frac{\pi}{2}\right)-\sqrt{\xi(\xi_0-\xi)}\right], \qquad E_{es}>0. \tag{2.14}$$

The former solution corresponds to the repulsive case when $\xi > \xi_0$, whereas the latter corresponds to the attractive case when $\xi < \xi_0$.

The solution of Equation (2.9) without viscosity is trivial – it is simply the motion from the rest with the constant acceleration,

$$\zeta(\theta) = -\frac{G(r-1)\theta^2}{2(2r+1)}$$

Eliminating θ from the expressions for $\xi(\theta)$ and $\zeta(\theta)$, we obtain the particle trajectories in both cases of particle repulsion or attraction:

$$\zeta(\xi) = \frac{G(r-1)\xi_0}{4E_{es}}\left[\frac{\xi_0}{2}\ln\left|\frac{\sqrt{\xi-\xi_0}+\sqrt{\xi}}{\sqrt{\xi-\xi_0}-\sqrt{\xi}}\right|+\sqrt{\xi(\xi-\xi_0)}\right]^2, \qquad E_{es}<0, \tag{2.15}$$

$$\zeta(\xi) = -\frac{G(r-1)\xi_0}{4E_{es}}\left[\xi_0\left(\arctan\sqrt{\frac{\xi}{\xi_0-\xi}}-\frac{\pi}{2}\right)-\sqrt{\xi(\xi_0-\xi)2^2}\right]^2, \qquad E_{es}>0. \tag{2.16}$$

The solution of Equation (2.8) beyond the Coulomb approximation can be readily obtained numerically. The equation was integrated by the fourth-order Runge–Kutta method with the fixed integration step using Mathcad-14 software. The infinite sums in Equation (2.8) were replaced by finite series containing N = 200 terms. The results for attractive and repulsive particles are shown in Figure 2.4 by the solid lines 1 and 1′ here the trajectories for the repulsive particles are

labelled by dashed numbers and go to the right, whereas trajectories for the attractive particles go to the left. In that figure we also show the analytical results obtained in the Coulomb approximation as per Equations (2.15) and (2.16); they are shown by dashed lines 2 and 2′. Lines 3, 3′ and 4, 4′ pertain to the case of viscous fluid when both viscosity coefficients for the SD and BBD forces are equally modified by the functions $f_2(\xi)$ as per Equation (2.11) for the horizontal motion and $f_3(\xi)$ as per Equation (2.12) for the vertical motion. A detailed discussion of the viscosity effect will be presented in the next subsection. Lines 3 and 3′ pertain to the case of exact electrostatic force and lines 4 and 4′ pertain to the Coulomb approximation. In all cases, shown in the figure, the particles started to move from the rest when the distance between them was 4 in dimensionless units. Attractive particle collision occurs when the distance between them becomes $\xi = 2$.

As one can see from this figure, the particles collide in a finite time, when they are attracted by each other due to the electrostatic force. The collision occurs earlier when the exact electrostatic force is taken into consideration compared to the case of the Coulomb approximation. Accordingly, the vertical distance travelled by the particles before they collide is less for the former case compared to the latter case. This can be seen by comparing trajectories 1 and 2, as well as 3 and 4 in Figure 2.5.

The situation is opposite when the particles repulse each other in the perfect fluid: in the case of exact electrostatic force, the horizontal motion is slower than in the case of the Coulomb approximation. Therefore, trajectory 1′ in the former case lies below the trajectory 2′ in the latter case. The repulsive particles move away from each other to infinity. The observed motion is the direct result of the difference between the exact electrostatic forces in comparison with the Coulomb force. The exact force is larger than the Coulomb force for the attractive particles but smaller than the Coulomb force for the repulsive particles (Figure 2.1).

When the distance between the particles becomes large, the exact electrostatic force quickly reduces to the Coulomb force (Figure 2.1). However, if the particles start moving at a relatively small distance between them, the time lag of trajectory 2′ relative to trajectory 1′ still occurs.

In a viscous fluid, the repulsive particles move faster in the horizontal direction when the Coulomb approximation is used. Therefore, trajectory 4′ lies below the trajectory 3′ which corresponds to the exact electrostatic force. This is, apparently, a consequence of a complicated character of the modified BBD force with the variable viscosity coefficient v_{eff}. We will refer to this issue in the next subsection.

Figure 2.5 illustrates the variation of relative particle velocity in the horizontal direction versus the distance between them. When the particles attract each other their relative speed at the moment of collision (at $\xi = 2$) is higher when the exact electrostatic force is considered than in the case of the Coulomb approximation as shown by lines 1 and 2 in Figure 2.5.

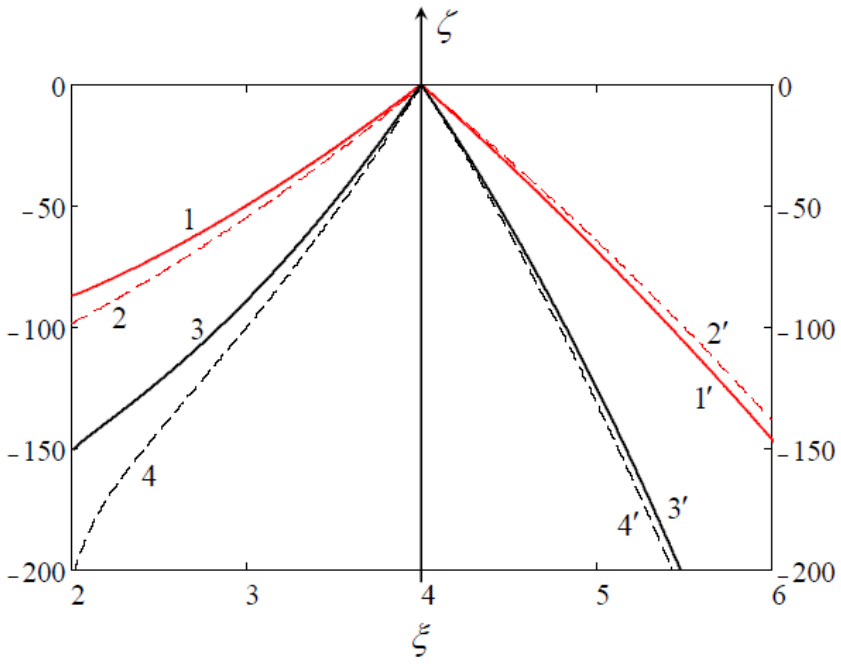

Figure 2.4: Particle trajectories: vertical position of particles, ζ, against the distance between them, ξ, in the dimensionless variables.

When the particles repel from each other, their relative speed varies with the distance almost equally both in the case of exact electrostatic force and in the Coulomb approximation: therefore lines 1′ and 2′ are practically indistinguishable, from each other.

In a viscous fluid, the horizontal speed of the particles is always greater when the exact electrostatic force is used in comparison with the Coulomb force as

shown by lines 3 and 4, as well as lines 3′ and 4′ in Figure 2.5. Notice that the vertical scale for the viscous case represented by lines 3, 4, 3′, and 4′ (shown on the right) is 20 times greater than in the inviscid case (shown on the left) represented by lines 1, 2, 1′, and 2′.

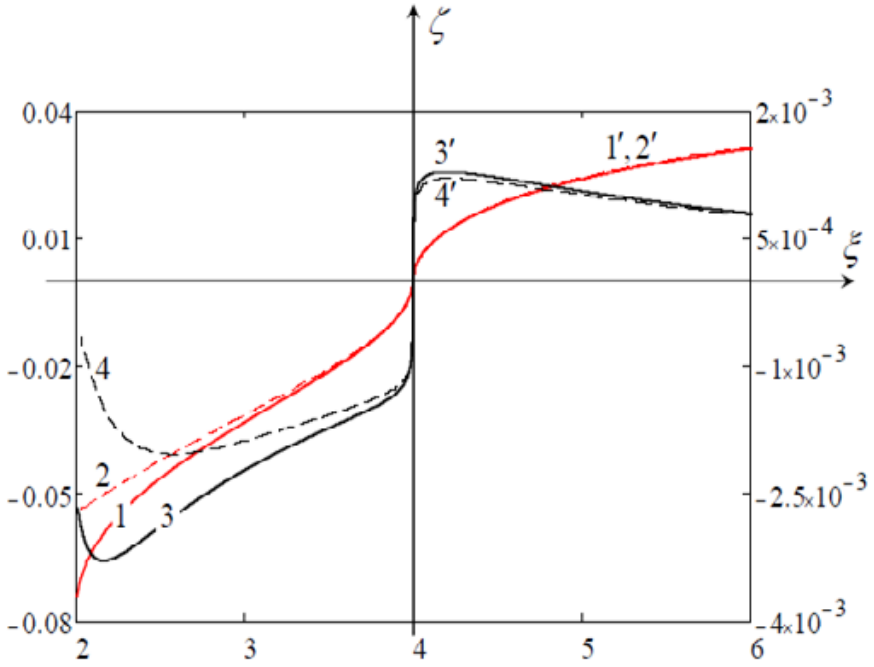

Figure 2.5: Relative horizontal velocity $u(\xi)$ of particles against the distance between them in the dimensionless variables. Curve numbering corresponds to Figure 2.4. The vertical scale for the viscous case represented by lines 3, 4, 3′ , and 4′ is shown on the right.

2.5 Particle dynamics in a viscous fluid

The description of particle dynamics becomes much more complicated when viscosity is taken into account. The simplest case is the motion of uncharged particles with E_{es}=0. Consider first the case when the initial distance between the particles is so large that functions $f_{1,2,3}(\xi)$ and $F_{1,2,3}(\xi)$ can be replaced by unities. In such a case, the set of equations (2.8)–(2.9) can be solved analytically (Stepanyants & Yeoh, 2009), however, the solution is very cumbersome. Here we only present the universal asymptotic form of solution for large time θ assuming that particles commence motion with the zero vertical velocities $\upsilon(0) \equiv d\zeta / d\theta|_{\theta=0} = 0$, but with the non-zero relative horizontal velocity $u(0) \equiv d\xi / d\theta|_{\theta=0} = u_0$,

$$\xi_{as}(\theta) = (1+2r)u_0\left(1-\frac{3}{\sqrt{\pi\theta}}\right),\ u_{as}(\theta) = \frac{3}{2}\frac{2r+1}{\sqrt{\pi}}\frac{u_0}{\theta^{3/2}}, \tag{2.17}$$

$$\zeta_{as}(\theta) = -G(r-1)\left[2(4-r) - 6\sqrt{\frac{\theta}{\pi}} + \theta\right],\ v_{as}(\theta) = -G(r-1)\left(1-\frac{3}{\sqrt{\pi\theta}}\right). \tag{2.18}$$

If the distance between the particles is not large enough, then functions $f_{1,2,3}(\xi)$ and $F_{1,2,3}(\xi)$ cannot be replaced by unities. Neither the Equation (2.8) or Equation (2.9) is integrable in this case, therefore they were integrated numerically by means of a Fortran code using the fourth-order Runge–Kutta scheme and the standard RKGS subroutine with Gill's modification. The infinite sums in Equation (2.8) were replaced by finite series with N=400 terms. The numerical code has been tested against the exact analytical solutions (Stepanyants & Yeoh, 2009) and demonstrated quite reliable results. Examples of the numerical solutions of Equations (2.8)–(2.9) with the different models of viscosity are presented in Figure 2.6.

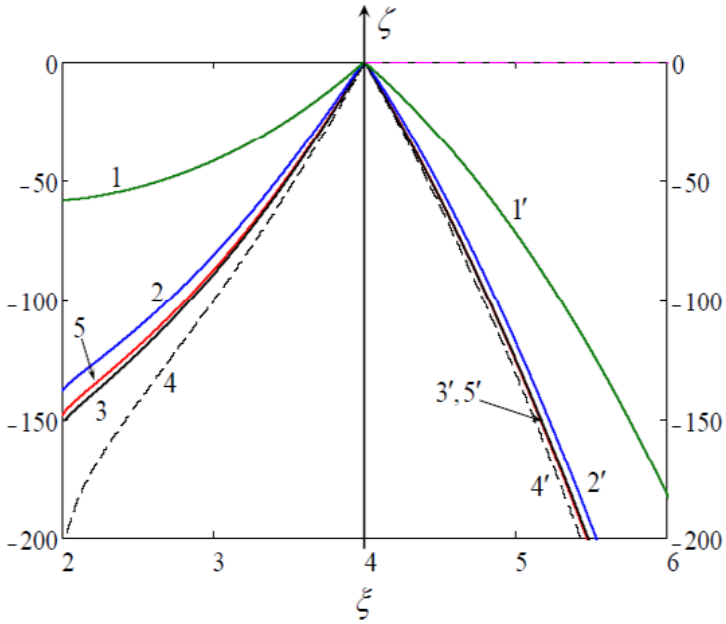

Figure 2.6: Particle trajectories in a viscous fluid with the different models of viscosity.

Lines 3, 3′ and 4, 4′ are the same as in Figure 2.4, i.e. line 3 represents the trajectory of attractive particles when exact electrostatic force is considered and viscosity coefficients are modified in accordance with Equations (2.11) for the horizontal motion and (2.12) for the vertical motion. Line 4 represents the

trajectory when the Coulomb approximation is used for electrostatic force. Lines 3′ and 4′ represent the trajectories for the repulsive particles with the exact electrostatic force and in the Coulomb approximation correspondingly. As one can see, in the repulsive case, trajectories 3′ and 4′ are fairly close to each other whereas in the attractive case the difference between them is quite noticeable at small distances between the particles. In what follows we consider only the exact electrostatic force.

Lines 1 and 1′ represent the particle trajectories in the attractive and repulsive cases respectively when only the SD force is taken into consideration with the constant viscosity, i.e. when the influence of another particle is ignored, as well as influence of the BBD force.

Lines 5 and 5′ represent the particle trajectories in the attractive and repulsive cases respectively when only the SD force is taken into consideration with the modified viscosity, as per Equations (2.11) and (2.12), and the influence of the BBD force is ignored.

Lines 2 and 2′ represent the particle trajectories in the attractive and repulsive cases respectively when the SD force is taken into consideration with the modified viscosity, as per Equations (2.11) and (2.12), and the viscosity coefficient for the BBD force is assumed constant $F_{2,3} = 1$.

As one can see from the figure, the model with only the SD force with a constant viscosity provides results which significantly differ from the results of the other models with variable viscosity and BBD force. In the meantime, lines 5 and 5′ are very close to lines 3 and 3′ respectively.

This indicates that the BBD force does not play a significant role in comparison with the SD force in such motions and, hence, can be neglected. Figure 2.7 illustrates the variation of relative particle velocity in the horizontal direction against the distance between them. Line labels in this figure correspond to the labels of the trajectories used in Figure 2.6. Only the vertical scale of line 5 (but not line 5′!) is 10 times compressed in comparison to all other lines.

Observe that qualitatively the difference between the exact and Coulomb cases is similar to that shown in Figure 2.4. Namely, for the attractive particles, the horizontal motion is faster when the exact electrostatic force is considered, while

for the repulsive particles the horizontal motion is slightly faster when the Coulomb electrostatic force is used.

It is interesting to note that at the initial stage of motion the relative horizontal speed increases very rapidly, after which the speed continues to increase, but at a moderate rate, and then after reaching a maximum value decreases due to the strong influence of the drag force correction $f_2(\xi)$ caused by the close presence of the second particle. If this correction is ignored, then the relative horizontal speed monotonically increases until particle collision. This is seen by comparison of line 1 with other lines 2–5 in Figure 2.7.

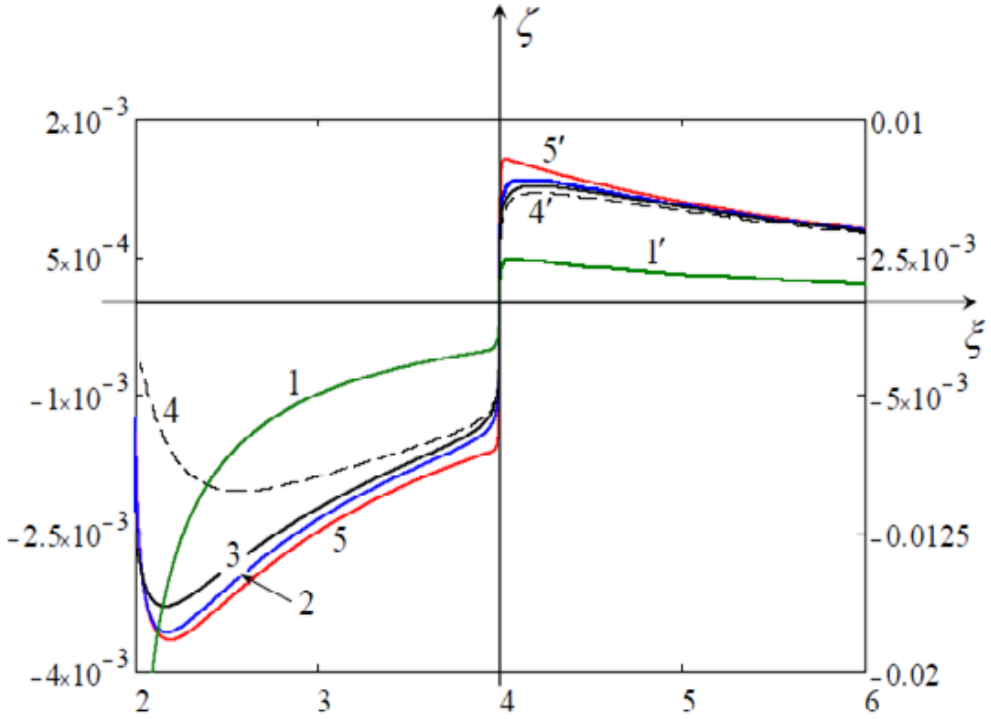

Figure 2.7: Relative horizontal velocity of particles $u(\xi)$ against the distance between them in the dimensionless variables. Curve numbering corresponds to Figure 2.6. The vertical scale for lines 1 and $1'$ are shown on the right. Labels for lines $2'$ and $3'$ are not shown; these two lines are very close to each other and are disposed between the lines $4'$ and $5'$.

As has been noted, in the attraction case the relative horizontal speed is high for the case of exact electrostatic force in comparison to the Coulomb approximation. It is also interesting to note that both the drag-correction factor $f_2(\xi)$ and the electrostatic force infinitely increase when the attractive particles approach each other i.e., when $\xi \to 2$. However, the influence of a variable viscous term prevails

over the electrostatic force resulting in the speed deceleration at the moment of collision.

2.6 Two particles moving one after another

Consider now the case when two particles move one after another as shown in Figure 2.2b). Equations of motion in the scalar dimensionless form follow again from Equations (2.3):

$$(2r+1)\frac{d^2\xi}{d\theta^2} = -\frac{E_{es}}{2}S_n - f_2(\xi)\frac{d\xi}{d\theta} - \frac{3}{\sqrt{\pi}}\int_{-\infty}^{\theta}\frac{d^2\xi}{d\eta^2}\frac{d\eta}{\sqrt{\theta-\eta}}, \tag{2.19}$$

$$(2r+1)\frac{d^2\zeta}{d\theta^2} = -G(r-1) - f_1(\xi)\frac{d\zeta}{d\theta} - \frac{3}{\sqrt{\pi}}\int_{-\infty}^{\theta}\frac{d^2\zeta}{d\eta^2}\frac{d\eta}{\sqrt{\theta-\eta}}, \tag{2.20}$$

where $\zeta = (z_1 + z_2)/2R$ is the dimensionless coordinate of the mass centre, and the other dimensionless quantities are as defined after Equation (2.9). The function $f_1(\xi)$ is as defined in Equation (2.10).

Equation (2.19) describes time variation of the relative distance between the particles; it is exactly the same as in Equation (2.8), whereas Equation (2.20) slightly differs from Equation (2.9) due to the replacement of function $f_3(\xi)$ by the function $f_1(\xi)$. The difference between these two functions is not large, as one can see from Figure 2.3, therefore the solution of Equations (2.19) and (2.20) does not differ too much from the solution of Equations (2.8) and (2.9).

In Figure 2.8 we present a comparison of two trajectories when the exact electrostatic force was used with the modified viscosity coefficient of SD force only, whereas the BBD force was taken with the constant coefficient. Lines 5 and 5′ pertain to the case when particles move side-by-side, and lines 6 and 6′ pertain to the case when particles move vertically one after another. In the latter case, the drag force for the motion of mass centre is less than in the former case ($f_1(\xi) < f_3(\xi)$), therefore the traversed path by mass centre before the particle collision in the latter case $(z \approx -166.5)$ is slightly larger than in the former case $(z \approx -148.5)$.

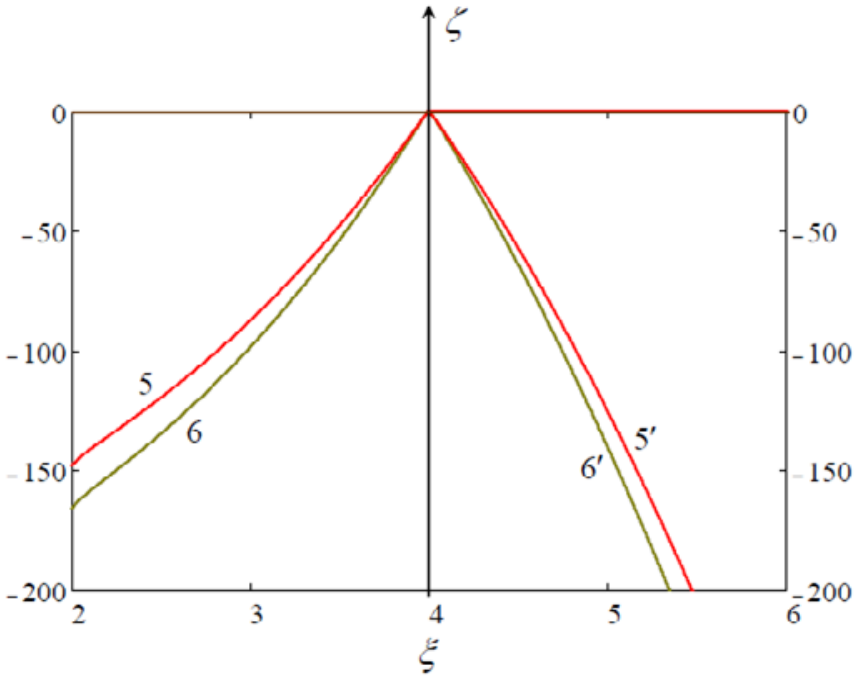

Figure 2.8: The trajectories of two particles moving side-by-side (lines 5 and 5′) and vertically one after another (lines 6 and 6′) in a viscous fluid.

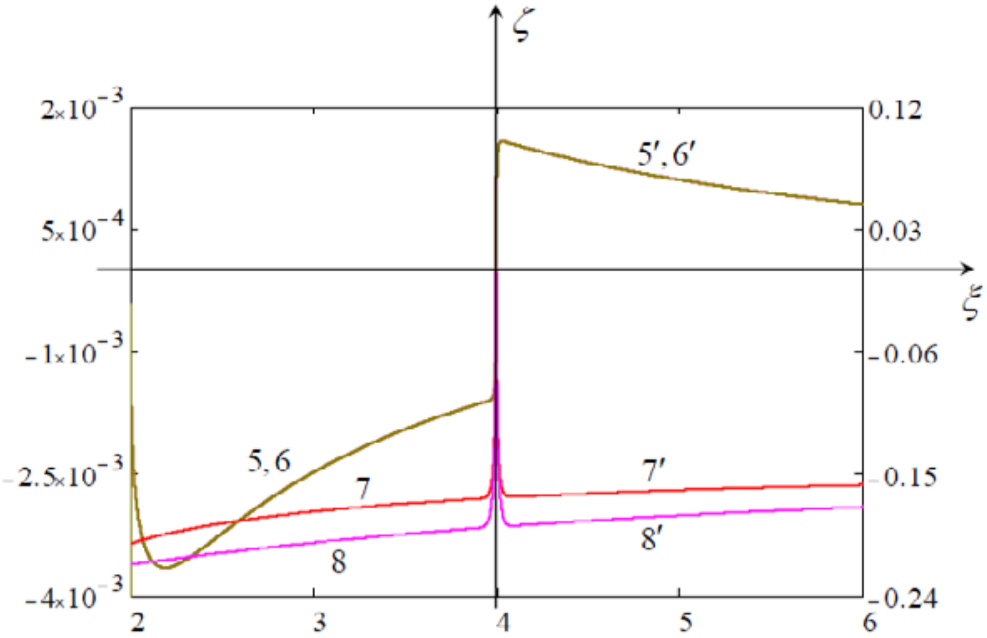

Figure 2.9: Relative velocity and the velocity of the mass centre of two particles against the distance between them in the dimensionless variables. Lines 5, 6 and 5′, 6′ pertain to the relative velocity of attractive and repulsive particles. Lines 7, and 7′ pertain to the side-by-side vertical motion of two particles, and lines 8, and 8′ pertain to the vertical motion of two particles one after another. The vertical scale for lines 7, 8, 7′, and 8′ is shown on the right.

Because Equations (2.8) and (2.19) are the same, the relative particle velocities are equal in the corresponding cases of side-by-side and vertical motions (see lines 5, 5′ and 6, 6′ in Figure 2.9). But the vertical motion of mass centres in these two cases is slightly different because of the difference in Equations (2.9) and (2.20) as shown by lines 7, 7′ and 8, 8′ in Figure 2.9.

2.7 Conclusion:

We have considered the dynamics of two unlike and like charged particles in viscous fluid in the creeping flow approximation. Relative particle dynamics have been studied under different models of electrostatic force acting between the particles: the force between two conducting spheres as derived by Saranin (1999) and Coulomb's force between point-like particles. Two types of viscous drag forces were taken into consideration: the quasi-stationary Stokes drag force and the transient Boussinesq–Basset drag force. Different models of viscous drag forces were analysed, when the viscosity coefficient is constant, in the case of a single particle, and when it is modified due to the presence of a second particle. A comparison of particle trajectories under the influence of all these forces was made and compared with the case of an inviscid fluid.

Using the typical value of parameters (see the paragraph before the subsection 2.3.), we obtain that two aluminium micro-particles of a radii 50 μm approaching each other from the distance 200 μm traverse 7.5 mm in the vertical direction before their collision. The maximal relative velocity between the particles is ~ 0.44 mm/s, and their vertical velocity attains ~ 2.28 cm/s.

Results obtained can be useful for the development of control methods of micro- and nano-particle dynamics in viscous fluids in application to technological processes and medicine (Sarvazyan & Ostrovsky, 2009). The theoretical analysis presented in this Chapter provides us with the estimates of typical particle approach speeds, terminal velocities of falling down particles in viscous fluids, and traversed paths. This can be used in the development of facilities for the control of particle motion by external forces, acoustic or electro-magnetic. Such estimates will allow researcher and engineers to estimate further the characteristic values of field strengths for the effective control of particle motion. This can be especially

important for preventing particles ensembles from sticking together and aggregation. In some cases, contrary, estimates of strength of external fields can be useful to develop a device, which promotes effective gathering of all particles together.

The content of this Chapter is based on the published paper: Hassan, H.K. & Stepanyants, Y.A. (2015). Dynamics of two charged particles in a creeping flow. *Journal of Physical Mathematics*, v. 6, n. 2, 7 p.

In this Chapter, only two charged particles were considered as the simplest basic model to demonstrate the main physical effects and gain insight in the complex problem. However, the results obtained can be further generalized for the ensemble of many particles (see, for example, (Sazhin et al., 2008)), but this will lead to the serious complication of equations and interpretation of results.

Chapter 3: Particle dynamics in a viscous fluid under the action of acoustic radiation force

3.1 Introduction

Complex dynamics of small particles under the action of acoustic radiation force is considered in this chapter. This work extends the previous studies of Ostrovsky & Sarvazyan (2009) and Ostrovsky (2015) in two aspects. Firstly, here the particle material can have an arbitrary compressibility and sound speed, whereas in the previous papers the authors considered only the limiting case of hard particles with the infinite sound speed. Secondly, in addition to the viscosity effect described by the Stokes drag force, the Boussinesq–Basset drag (BBD) force and the inertial force together with the added mass effect are accounted for. Although, as was assumed in the earlier publications, the latter effects are usually small, however, their influence can be noticeable in specific cases considered in this chapter. The control of particle motion by switching of acoustic modes in a resonator is also studied for particles of different properties. Quantitative estimates are given for particles made of different materials.

3.2 The governing equation for particle motion in a standing acoustic field

Consider the equation of motion of a small (as compared to the sound wavelength) spherical particle of density ρ_p and radius a in a fluid taking into account the Stokes drag force, an added mass effect, and the transient Boussinesq–Basset drag force (Stepanyants & Yeoh, 2009):

$$\left(\rho_p + \frac{\rho_f}{2}\right) V_p \frac{d^2\mathbf{r}}{dt^2} = -6\pi\rho_f \nu_a \left(\frac{d\mathbf{r}}{dt} + \frac{a}{\sqrt{\pi\nu}} \int_{-\infty}^{t} \frac{d^2\mathbf{r}}{d\theta^2} \frac{d\theta}{\sqrt{t-\theta}}\right) + \mathbf{F}_a, \tag{3.1}$$

where $\mathbf{r}$ is the particle coordinate, ρ_f is the fluid density, ν is the kinematic viscosity of a fluid, and V_p is the particle volume. The added mass effect is taken into account for a spherical particle through the factor $\rho_f/2$ included in the inertial term on the

left-hand side of the equation. The first term in the brackets in the right-hand side together with the coefficient $6\pi\rho_f \nu_a$ represents the Stokes drag force, whereas the second integral term in the brackets together with the coefficient $6\pi\rho_f \nu_a$ represents the BBD force (details can be found, e.g., in Refs. (Lovalenti & Bardy, 1993; Stepanyants & Yeoh, 2009; Landau & Lifshitz, 1988)). The expression for the period averaged acoustic force $\mathbf{F}_a$ acting on a small spherical particle has the form (Gorkov, 1962)

$$\mathbf{F}_a = -\nabla U, \quad U = 2\pi\rho a^3 \left(\frac{\left\langle p_a^2 \right\rangle}{3\rho_f^2 c_f^2} f_1 - \frac{\left\langle u_a^2 \right\rangle}{2} f_2 \right). \tag{3.2}$$

Here the angular brackets, $\langle ... \rangle$, denote period averaging of the wave pressure P_a and the acoustic velocity u_a, and

$$f_1 = 1 - \frac{c_f^2 \rho_f}{c_p^2 \rho_p}, \qquad f_2 = 2\frac{\rho_p - \rho_f}{2\rho_p + \rho_f}, \tag{3.3}$$

where c_f and c_p are the sound speed values in the ambient liquid and the particle material, respectively.

In many practical cases for small particles in Equation (3.1) the viscous Stokes drag force dominates over the BBD force and effect of inertia. In such cases (which we call the quasi-static approximation) the balance between the radiation force and Stokes drag force yields:

$$\mathbf{u}_a = \frac{\mathbf{F}_a}{6\pi\rho_f \nu a}. \tag{3.4}$$

Below we examine the influence of factors that were ignored in the previous publications (Sarvazyan & Ostrovsky, 2009; Ostrovsky, 2015) and consider a standing acoustic wave in a resonator. We will study first a plane resonator with a single acoustic mode and two modes periodically switching on and off to replace each other. Then a more complex cylindrical resonator will be studied.

3.3 Solid particle dynamics in a plane geometry

3.3.1 Single mode regime

Consider first standing waves in a plane resonator of a length L. Let a wave with the amplitude P_0 be defined as

$$p_a = P_0 \cos kx \sin\left(2\pi f t\right), \qquad u_a = \frac{P_0}{\rho_f c_f} \sin kx \cos\left(2\pi f t\right), \tag{3.5}$$

where $k = 2\pi/\lambda$ is the wavenumber, λ is the wavelength, and f is the frequency of the acoustic wave.

Substituting this into Equation (3.1) we obtain the radiation force in the form (see, e.g., (Ostrovsky, 2015)):

$$F(x) = \frac{V_p k P_0^2}{2\rho_f c_f^2} \Phi\left(r, s\right) \sin 2kx, \tag{3.6}$$

where the function $\Phi\left(r, s\right)$ is defined by the formula

$$\Phi\left(r, s\right) = \frac{5r - 2}{2r + 1} - \frac{1}{s^2 r}. \tag{3.7}$$

Here the values of r and s are given by, $r = \rho_p / \rho_f$, and $s = c_p / c_f$.

According to Equations (3.4) and (3.6), in the plane quasi-static case the particle velocity has the form

$$u(x) = -\frac{\pi a^2 f P_0^2}{9\rho_f^2 c_f^3 \nu} \Phi\left(r, s\right) \sin \frac{4\pi f x}{c_f}. \tag{3.8}$$

The function Φ defines a dependence of the particle dynamics on the physical properties of a particle with respect to the parameters of the ambient fluid. Figure 3.1 shows the 3D plot of the function $\Phi\left(r, s\right)$. As one can see, this is a smooth surface which asymptotically attains the maximum value $\Phi_{\max} = 5/2$, when r infinitely increases for any finite non-zero value of s. This limiting case $r \to \infty$ was studied by

Sarvazyan & Ostrovsky (2009). Here we consider a range of parameters r and s within the framework of general equation (3.1).

Notice that function $\Phi(r,s)$ can be of either sign. For relatively soft particles with $s < s_c$ this function is negative, where

$$s_c^2 = \frac{2r+1}{r(5r-2)}. \tag{3.9}$$

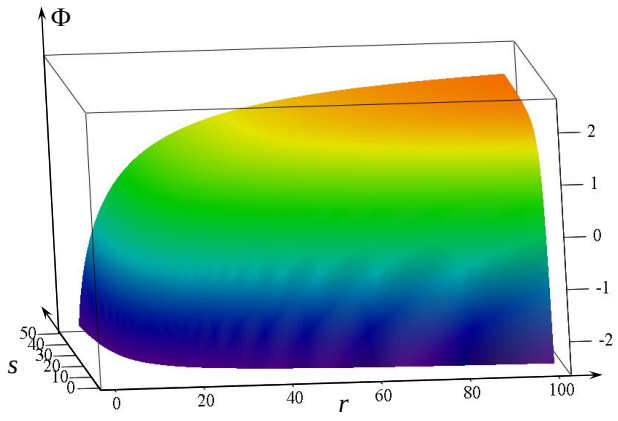

Figure 3.1: Dependence of function Φ on the parameters r and s as per Equation (3.7).

In particular, $\Phi(r,s)$ is negative regardless of the value of s if $r < 2/5$. Below we will consider one case of light particle motion with a negative $\Phi(r,s)$ and compare the result with the cases of particle motion with the positive values of $\Phi(r,s)$.

In what follows we shall use the dimensionless form of Equation (3.1) (cf. (Stepanyants & Yeoh, 2009)):

$$(2r+1)\frac{d^2\xi}{d\tau^2} = -\frac{d\xi}{d\tau} - \frac{3}{\sqrt{\pi}}\int_{-\infty}^{\tau}\frac{d^2\xi}{d\vartheta^2}\frac{d\vartheta}{\sqrt{\tau-\vartheta}} - \sin(nK\xi), \tag{3.10}$$

where $\xi = 2\pi_x/KL$, $\tau = t/\gamma$, $\gamma = a^2/9\nu$, n is the mode number, and $K = \dfrac{2\pi^2 a^4 P_0^2 f}{81\rho_f^2\nu^2 c_f^3 L}\Phi(r,s)$. The length of acoustic resonator L can be expressed in terms of

the wavelength λ of a sound wave or in terms of a frequency *f*: $L = n\lambda/2 = nc_f T/2 = nc_f/2f$, where the mode number *n* determines the number of half-lengths of the acoustic wave in the resonator.

For comparison, in specific calculations, we use the parameters similar to those used in Sarvazyan & Ostrovsky (2009); namely, the ambient fluid is a water, for which we take the following parameters at *T* = 20°C: $\rho_f = 10^3\ kg/m^3$, $c_f = 1500\ m/s$, and $\nu = 10^{-6}\ m^2/s$. For the particle radius, we choose $a = 10\ \mu m$, for the length of a resonator we set *L* = 2 mm, and for the amplitude of acoustic pressure, we use $P_0 = 200\ KPa$. With these parameters, we obtain $\gamma = 1.1 \cdot 10^{-5} s$ for Equation (3.10).

As mentioned, different particle materials were used in this study for quantitative estimates. In Table 1 the values for each parameter for different particle types are presented.

Table 3.1: The values of parameters for different particle types.

Particle type	Alumi-nium	gold	ice	plexiglas	silica	Biological cells	light particle*)
$\rho_p,\ Kg/m^3$	$2.7 \cdot 10^3$	$19.3 \cdot 10^3$	$0.97 \cdot 10^3$	$1.18 \cdot 10^3$	$2.2 \cdot 10^3$	$1.1 \cdot 10^3$	$0.2 \cdot 10^3$
$r = \rho_p/\rho_f$	2.7	19.3	0.97	1.18	2.2	1.1	0.2
$c_p,\ m/s$	6400	3240	3980	2600	6000	1.575	1500
$s = c_p/c_f$	4.267	2.160	2.653	1.733	4.0	1.05	1.0
$\Phi(r,s)$	1.777	2.375	0.823	0.879	1.638	0.269	–5.714

*) As an example we consider a small density gaseous particle (a bubble) covered by a solid solvable shell. Such particles can be used to transport gaseous contents, for example, in medicine and food technology.

In Sarvazyan & Ostrovsky, (2009) the basic equation of motion (3.1) was studied in the dimensional form in the quasi-static approximation, when both the inertial term on the left-hand side and BBD force on the right-hand side were neglected. First, we will consider a similar case when a particle moves in a viscous fluid under the action of acoustic radiation force, but also takes into account arbitrary particle properties such as density and sound speed in the particle material. In this case equation (3.10) is reduced to

$$\frac{d\xi}{d\tau} = -\sin(Kn\xi). \tag{3.11}$$

Solution to this equation can be readily obtained (cf. (Sarvazyan & Ostrovsky, 2009); a typo in that paper is corrected here):

$$\xi = \frac{2}{Kn}\arctan\left[\tan\left(\frac{Kn}{2}\xi_0\right)e^{-Kn\tau}\right], \tag{3.12}$$

where ξ_0 is the initial position of the particle at $\tau = 0$.

The full equation (3.10) was solved numerically for three different particle types, infinitely hard and dense (as the reference case), aluminium and ice. These solutions together with the approximate analytical solution (3.9) are shown in Figure 3.2. For the first reference case, all parameters were chosen the same as in Sarvazyan & Ostrovsky, (2009) with the same initial conditions of $\xi_0 = 2.18\cdot 10^3$, $V_0 \equiv \left(d\xi / d\tau\right)\Big|_{\tau=0} = -0.0997$, and parameter n = 8. We have tested the influence of the integral BBD term, as well as the inertial term and found that it was small as shown in Figure 3.2. Line 1 in Figure 3.2 illustrates the approximate solution (3.12) for the reference case with Φ=5/2, and the dots show the numerical data when all factors in Equation (3.10) including the BBD force were taken into consideration. The inset represents the magnified portion of Figure 3.2 and demonstrates the difference between the approximate (line 1) and numerical solutions (dots) for the reference case when the particle approaches the equilibrium state.

Similar calculations were carried out for other particles with different properties. In all cases, the influence of the inertial effect and BBD force was relatively small, except

the initial period of motion (see below). Figure 3.2 shows the corresponding plots for particles of a moderate density (aluminium, $r = 2.7$, $s = 4.267$, $\Phi = 1.777$) and of a relatively small density (ice, $r = 0.97$, $s = 2.653$, $\Phi = 0.823$). For a relatively dense gold particle ($r = 19.3$, $s = 2.16$, $\Phi = 2.375$) the result is close to line 1 in Figure 3.2; it is not shown separately to avoid figure complication.

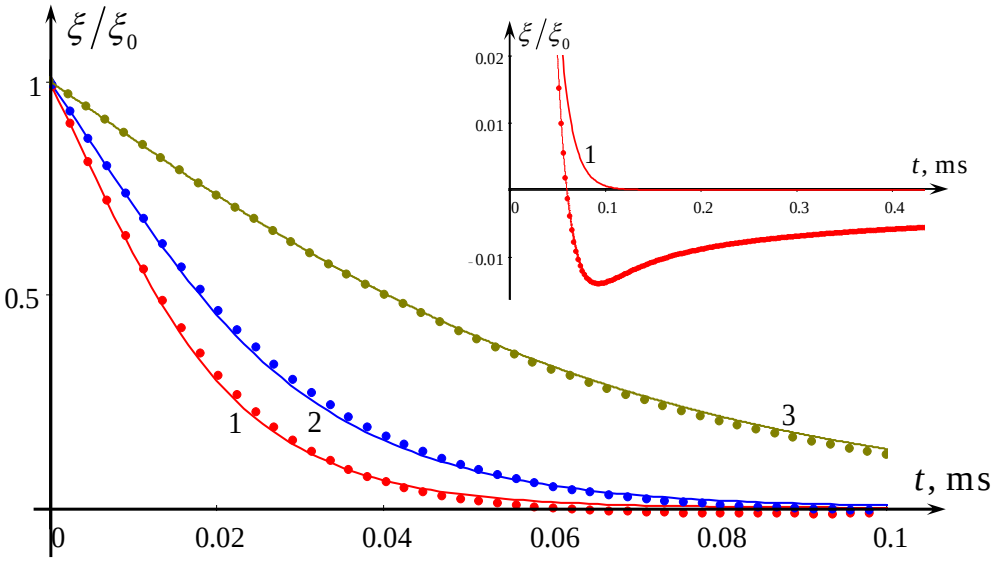

Figure 3.2: Dependence of normalised particle position on time as per Equation (3.9) (solid lines) for different particle types. Line 1 pertains to the reference case of $\Phi = 5/2$ (very dense incompressible particle), line 2 – an aluminium particle ($\Phi = 1.777$), line 3 – an ice particle ($\Phi = 0.823$). Dots show the numerical results when all factors including the BBD and inertia forces are taken into account.

Figure 3.3 shows the dependence of particle speed on time for the same values of the parameter Φ as in Figure 3.2, and Figure 3.4 shows the dependence of particle speed on the distance from the equilibrium point. In the latter case the approximate theoretical dependence (3.11) is universal for all sorts of particles (see line 1 in Figure 3.4). The numerical data obtained with the inertial and BBD forces are almost similar to each other, but they slightly deviate from the approximate theoretical lines. A small portion of Figure 3.4(a), is magnified and presented in Figure 3.4(b). From the latter

figure, one can see a noticeable difference (up to ~3%) between the approximate analytical solution (line 1) and numerical data (triangles and dots) at the early stage of particle motion.

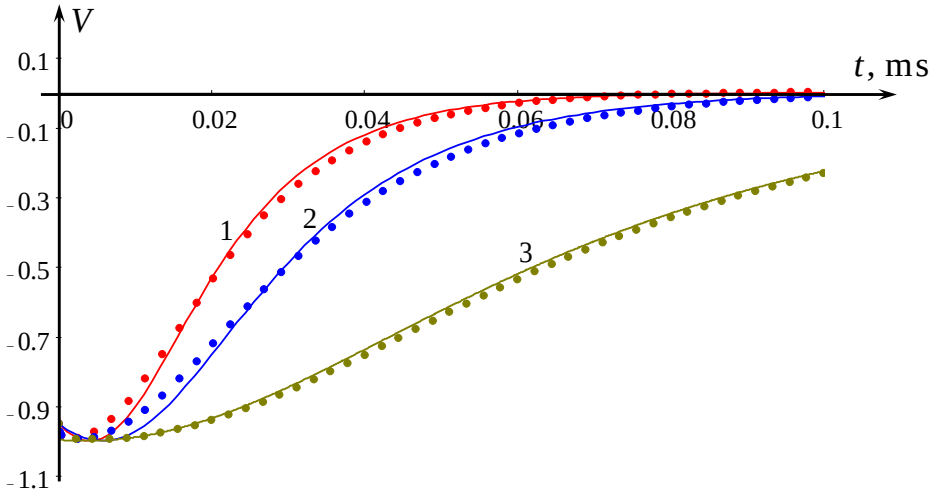

Figure 3.3: Dependence of particle speed on time as per Equation (3.11) (solid lines) for different particles. Line 1 pertains to the reference case of $\Phi = 5/2$ (very dense incompressible particle), line 2 – $\Phi = 1.777$ (aluminium particle), line 3 – $\Phi = 0.823$ (ice particle). Dots show the numerical results when all factors including the BBD force are taken into account.

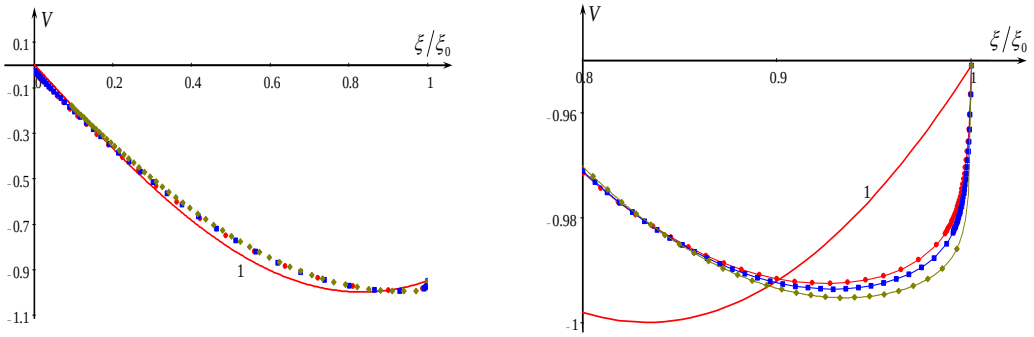

Figure 3.4: Particle speed against the normalised distance (solid line 1). Symbols represent the numerical data for different kinds of particles when all factors including the BBD force are taken into account: dots – represent the reference case with $\Phi = 5/2$; squares pertain to the aluminium particle ($\Phi = 1.777$), and rhombuses pertain to the ice particle ($\Phi = 0.823$). Panel (b) represents the magnified fragment of Figure 3.4(a) near $\zeta/\zeta_0 = 1$.

Another effect of the BBD force manifests itself at the terminal stage of particle motion when it approaches the equilibrium state. This is clearly seen from the inset in Figure 3.2 by the comparison of the approximate solution as per Equation (3.12) (line 1) with the numerical data shown by dots. Without the BBD force, a particle approaches the equilibrium state monotonically and exponentially quickly in time, whereas under the influence of BBD force it approaches the equilibrium non-monotonically and much more slowly, as $t^{-1/2}$ (Stepanyants & Yeoh, 2009). The particle displacement with the BBD force becomes negative at some instance of time (see dots in the inset), and then gradually approaches zero. This means that the particle passes through the equilibrium position and then slowly returns to it again.

In the critical case when the parameter $\Phi(r,s)=0$ (see Equation (3.7)), the governing parameter K (in Equation (3.10)) vanishes. In this case a particle is not affected by the acoustic field and remains at rest at any initial position. When, $s < s_c$, the parameters $\Phi(r,s)$ and K become negative. In this case all equilibrium states change – the stable states become unstable and vice versa. Therefore, a particle with $\Phi(r,s)<0$ moves in the opposite direction with respect to the particle with $\Phi(r,s)>0$. This is illustrated in Figure 3.5 with the approximate solutions (3.12) for the reference case of $\Phi(r,s)=5/2$ and for the case of a light particle with $\Phi(r,s)=-5.714$ $(r=0.2,\ s=1)$. Notice that, in the case of $\Phi(r,s)<0,$ the particles positions are negative at all times, but Figure 3.5 shows positions normalised by the negative initial condition, therefore the scaled particle positions shown by line 2 remains positive.

Thus, one can conclude that a simplified description of particle motion by means of formulae (3.11) and (3.12) is qualitatively correct and even provides quantitatively satisfactory results. For more accurate description one should take into account the inertial and BBD forces, but this leads to the necessity to solve the basic equations of motion numerically.

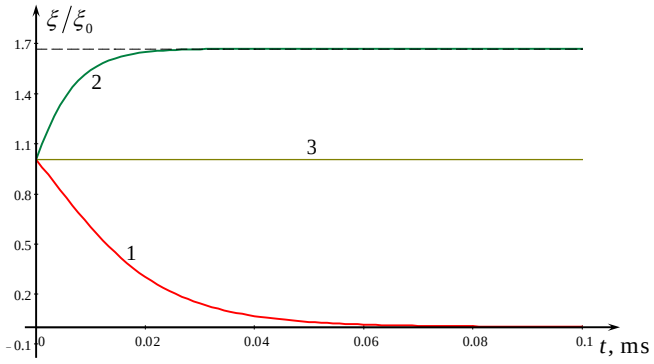

Figure 3.5: Dependence of normalised particle position on time as per Equation (3.12) for different particle types. Line 1 pertains to the reference case of $\Phi = 5/2$, line 2 – to the particle with $\Phi = -5.714$, and line 3 – to the particle with $\Phi = 0$. The dashed line shows the stable equilibrium state for a particle with negative Φ.

3.3.2 Periodic switching between two acoustic modes in the resonator

Consider now a more complex process briefly studied in Sarvazyan & Ostrovsky, (2009) for hard particles. Let the third and fourth modes of the resonator, having the same parameters as above, be alternately switched between each other. As was shown in Sarvazyan & Ostrovsky, (2009), this effect can be used for enhancing the stirring and mixing processes in microfluidics. It can also be used to deliver a medicine to a certain organ and dissolve it effectively in the process of particle oscillations around the required position (see, e.g., (Schmid et al. 2016)). In such fields the radiation force has the form

$$F_a = \Psi_3 e^{-2b_3 t} \sin\left(\frac{6\pi x}{L}\right) + \Psi_4 \left(1 - e^{-b_4 t}\right)^2 \sin\left(\frac{8\pi x}{L}\right), \tag{3.13}$$

where $b_{3,4}$ are the damping rates of the mode numbers $n_3 = 3$ and $n_4 = 4$ which are caused by the dissipation of acoustic field in the fluid and energy losses through the resonator walls. For the sake of simplicity, we set $b_3 = b_4 = b = 0.035\ s^{-1}$ and $\Psi_3 = \Psi_4 = \Psi$, where

$$\Psi = \frac{2\pi^2 a^3 P_0^2 f}{3\rho_f c_f^3} \Phi(r, s), \tag{3.14}$$

For the initial condition, we assume that at $t = 0$ a particle starts moving under the action of a third-mode acoustic field from the rest being at the initial position $x = x_0$. Substituting expressions (3.13) and (3.14) for $\Psi_{3,4} = \Psi$ into Equation (3.1) and assuming that there is a periodic switching between the modes 3 and 4 with the period $2\tau_s$, we obtain the dimensionless form of Equation (3.1):

$$(2r+1)\frac{d^2\xi}{d\tau^2} = -\frac{d\xi}{d\tau} - \frac{3}{\sqrt{\pi}}\int_{-\infty}^{\tau}\frac{d^2\xi}{d\vartheta^2}\frac{d\vartheta}{\sqrt{\tau-\vartheta}} -$$

$$\sin(n_3 K\xi)\left\{\left[H(\tau)-H(\tau-\tau_s)\right]e^{-2b\gamma\tau} + \left[H(\tau-\tau_s)-H(\tau-2\tau_s)\right]e^{-2b\gamma\tau_s}\left[1-e^{-b\gamma(\tau-\tau_s)}\right]^2 +\right.$$

$$\left.\left[H(\tau-2\tau_s)-H(\tau-3\tau_s)\right]e^{-2b\gamma\tau_s}\left(1-e^{-b\gamma\tau_s}\right)^2 e^{-2b\gamma(\tau-2\tau_s)} + \cdots\right\} + \qquad (3.15)$$

$$\sin\left(n_4\frac{f_4}{f_3}K\xi\right)\left\{\left[H(\tau)-H(\tau-\tau_s)\right]\left(1-e^{-b\gamma\tau}\right)^2 + \left[H(\tau-\tau_s)-H(\tau-2\tau_s)\right]\left(1-e^{-b\gamma\tau_s}\right)^2 e^{-2b\gamma(\tau-\tau_s)} +\right.$$

$$\left.\left[H(\tau-2\tau_s)-H(\tau-3\tau_s)\right]e^{-2b\gamma\tau_s}\left(1-e^{-b\gamma\tau_s}\right)^2\left[1-e^{-b\gamma(\tau-2\tau_s)}\right]^2 + \cdots\right\}.$$

Here the scaling of variables are the same as in Equation (3.10), and the dimensionless parameter *K* contains a frequency of the third mode.

In the process of mode switching one mode decays with the characteristic time scale $1/b$ and another mode onsets at the same time. When $b \neq 0$, Equation (3.15) is non-integrable even in the quasi-static regime. Only the approximate analytical solutions can be obtained in this case separately for the decaying mode 3 and the increasing mode 4; this has been done in Sarvazyan & Ostrovsky, (2009). In the dimensionless variables used here the solutions for these two modes read:

$$\xi_d = \frac{2}{Kn_3}\arctan\left[\tan\left(\frac{Kn_3}{2}\xi_0\right)\exp\left(\frac{Kn_3}{2b\gamma}e^{-2b\gamma\tau}\right)\right], \qquad (3.16)$$

and

$$\xi_i = \frac{2f_3}{Kf_4n_4}\arctan\left\{\tan\left(\frac{Kf_4n_4}{2f_3}\xi_0\right)\exp\left[\frac{Kf_4n_4}{2b\gamma f_3}\left(2b\gamma\tau + 4e^{-b\gamma\tau} - 3 - e^{-2b\gamma\tau}\right)\right]\right\}. \qquad (3.17)$$

According to Equation (3.16), a particle being initially at the position $\xi = \xi_0$ moves under the action of acoustic field to the equilibrium state at $\xi = 0$. If the switching between the modes occurs at $t = t_s$, then the particle starts moving to another equilibrium state $\xi_{eq} = \pi f_3 / (K f_4 n_4)$. This is illustrated at Figure 3.6, where the switching time was chosen at $t_s = 180\ ms$ as in Sarvazyan & Ostrovsky, (2009). In Figure 3.6(a) one can see a behaviour of a relatively heavy gold particle with $\Phi = 2.375$, and in Figure 3.6(b) – a relatively light ice particle with $\Phi = 0.823$. Odd lines 1, 3, etc, pertain to particle motion under the action of the third acoustic mode, and even lines 2, 4, etc – to particle motion under the action of the fourth acoustic mode. Dashed horizontal lines in Figure 3.6 show the equilibrium particle position ξ_{eq} which particle would attain if only the fourth mode acts upon it.

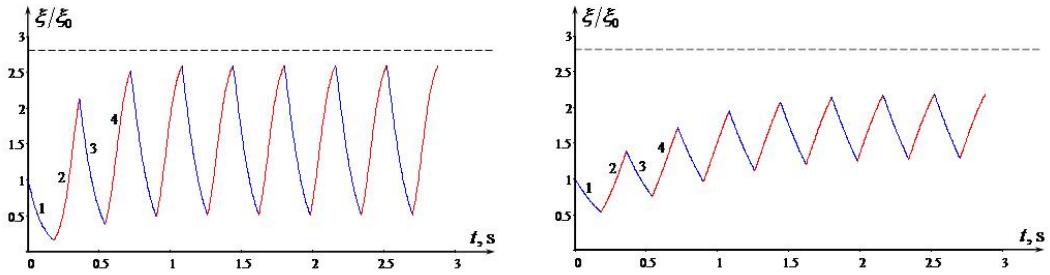

(a) (b)

Figure 3.6: Dependences of particle position on time when the acoustic field periodically switches from mode 3 to mode 4 and back. Odd decreasing lines (1, 3, …) pertain to mode 3, and even increasing lines (2, 4, …) pertain to mode 4. Panel (a) – for a gold particle, panel (b) – for an ice particle. Dashed horizontal lines show another equilibrium position for particles in the presence of mode 4 only.

Figures 3.7(a) and 3.7(b) show the corresponding particle speeds under the action of modes 3 and 4. A transition from one mode to the next actually occurs smoothly, but within a very short time interval. The transient time is controlled by the parameter *b*, which is of the order of $\tau_t = 1/\gamma b$. In the dimensional variables the transient time is $t_t = 28.6\ \mu s$, whereas the switching time is much greater, $t_s = 180$ ms $\approx 6.3 \cdot 10^3 t_t$. That is why the transition between the modes looks so sharp.

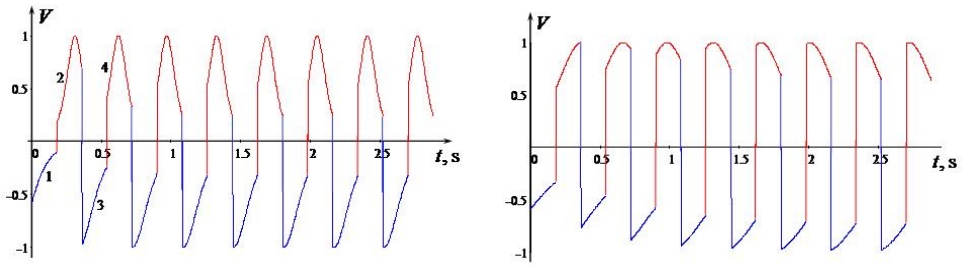

(a) (b)

Figure 3.7: Dependence of particle speed on time when the switching between the modes occurs (see Figure 3.6). Panel (a) – gold particle, panel (b) – ice particle.

The behaviour of heavy and light particles in the acoustic field is somewhat different. During the same time interval τ_s the heavy particle (e.g., gold) displaces for a larger distance than the light particle (e.g., ice), therefore the amplitudes of particle oscillations in Figures 3.6 (a) and (b) are different. Both particles in the process of oscillations experience a slow drift until their centres reach an equilibrium position. Then the particles oscillate around the central positions when the acoustic modes periodically switch. A slow drift of the central particle position $\xi_c = \left(\xi_{max} + \xi_{min}\right)/\left(2\xi_0\right)$ versus time is shown in Figure 3.8 for the gold particle (line 1) and the ice (line 2) particle.

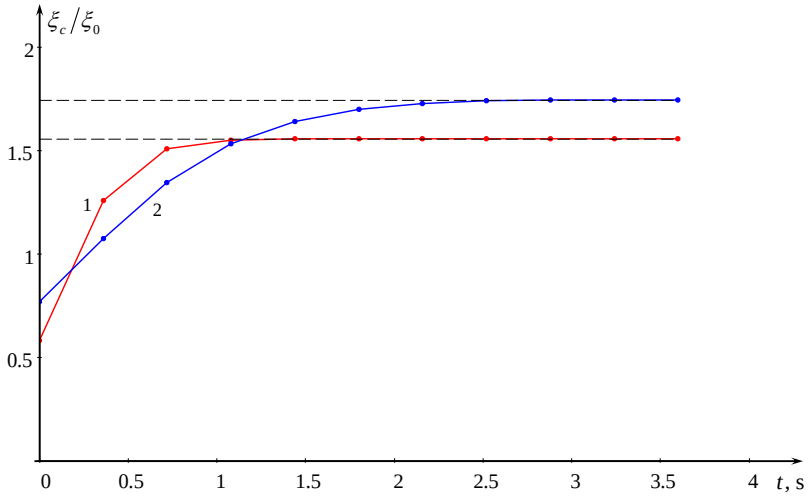

Figure 3.8: Dependencies of period averaged particle positions in the process of oscillations for the gold particle (line 1) and ice particle (line 2) on time. The central positions were normalised by the individual initial particle positions for each of these two particles.

A similar behaviour was observed for the particles of different properties listed in Table 1, when the parameter Φ (see Equation (3.7)) is positive. However, as mentioned, for some particles this parameter can be negative. As an example, we consider a particle with $r = 0.2$ and $s = 1$ (see the last column in Table 3.1). For such a particle, the initial coordinate is negative and its further displacement is also negative as per Equations (3.16) and (3.17), but the ratio of the current particle coordinate to the initial coordinate is positive. It is shown in Figure 3.9 as a function of time. The specific feature of this particle behaviour is that the equilibrium state at $\xi = 0$ is now unstable and the particle moves under the action of the third acoustic mode to the nonzero equilibrium state $\xi_{1\infty} = \pi / \left[K(f_3) n_3 \right]$ given by the upper dashed line in Figure 3.9. Under the action of the fourth acoustic mode, the particle moves to another equilibrium state $\xi_{2\infty} = \pi \ f_3 / \left[K(f_3) \, f_4 n_4 \right]$ shown by the lower dashed line in Figure 3.9. In the process of oscillation the particle also experiences a drift, but in a relatively short time; after two periods of oscillations, the particle centre arrives in a stable position.

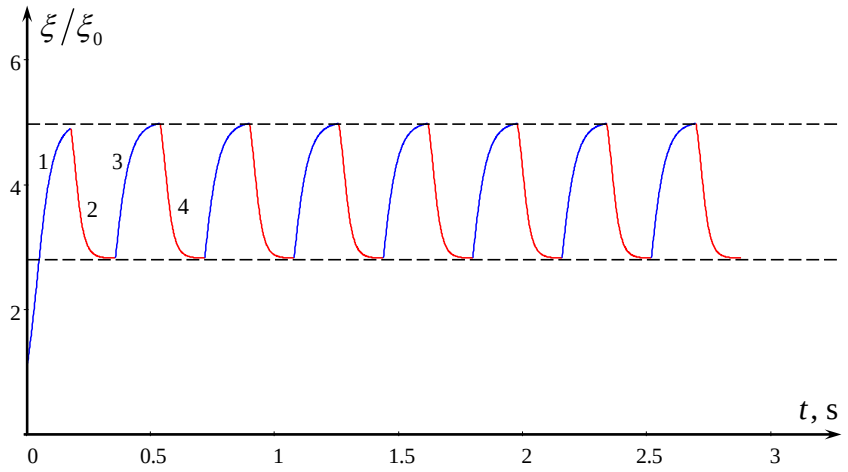

Figure 3.9: Dependence of particle position on time for a light microparticle with $r = 0.2$ and $s = 1$. Decreasing lines (1, 3, etc.) correspond to the particle motion under the action of the third acoustic mode and increasing lines (2, 4, etc.) correspond to the particle motion under the action of the fourth acoustic mode. Dashed horizontal lines show two equilibrium positions for the particle in the presence of mode 3 only (upper line) and mode 4 only (lower line).

In conclusion of this section, consider also a case of a nanoparticle with a silica content recently described in Schmid et al., (2016). The typical parameters of such particle are: radius $a = 0.4\ \mu\text{m}$, density $\rho_p = 2.2 \cdot 10^3\ Kg/m^3$, sound speed $c_p = 6000\ m/s$. We conditionally assume that the particle consists entirely of silica, albeit its content as per Schmid et al. (2016) is more complex. The corresponding dimensionless parameter is $\Phi = 1.638$. For the same parameters of the acoustic field, the effect of radiation force is much weaker and it takes much longer time to displace the particle to the equilibrium state in comparison with the microparticles considered previously in this chapter. If the acoustic modes are periodically switched from the mode 3 to mode 4 after each 180 s, then, as above, the particle drifts and oscillates around the mean position as shown in Figure 3.10. This is qualitatively similar to Figure 3.6, but the comparable magnitudes of oscillations are achieved at much larger periods of switching.

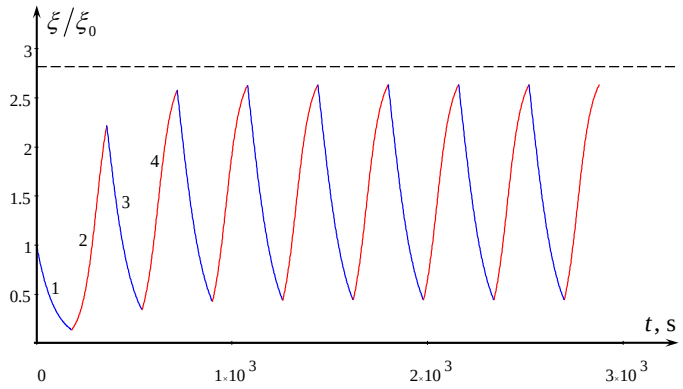

Figure 3.10: Dependence of particle position on time for a realistic nanoparticle with a silica core. Decreasing lines (1, 3, etc.) correspond to the particle motion under the action of the third acoustic mode and increasing lines (2, 4, etc.) – to the particle motion under the action of the fourth acoustic mode. The dashed horizontal line shows another equilibrium position for the particle in the presence of mode 4 only.

3.4 Particle dynamics in the cylindrical resonator

In this section, we consider a motion of an individual particle in the axisymmetric standing acoustic field. Such configuration is also used in bio-medical applications, as

well as in technology. As has been shown in Ostrovsky, (2015), the acoustic radiation force acting on a particle in this case is

$$F_a = \frac{8}{3}\frac{\pi^2 a^3 P_0^2 f}{\rho_f c_f^2}\Phi(r,s)\mathrm{J}_1(kR)\left[\mathrm{J}_0(kR) - \frac{3}{\Phi(r,s)}\frac{r-1}{2r+1}\mathrm{J}_2(kR)\right], \tag{3.18}$$

where the function $\Phi(r,s)$ is defined in Equation (3.7), and $\mathrm{J}_0(x)$, $\mathrm{J}_1(x)$, and $\mathrm{J}_2(x)$ are the Bessel functions of the first kind.

Substituting this force into Equation (3.1), we obtain in the dimensionless variables (cf. Equation (3.10)) the equation:

$$(2r+1)\frac{d^2\xi}{d\tau^2} = -\frac{d\xi}{d\tau} - \frac{3}{\sqrt{\pi}}S\int_{-\infty}^{\tau}\frac{d^2\xi}{d\vartheta^2}\frac{d\vartheta}{\sqrt{\tau-\vartheta}} - 4\mathrm{J}_1(nK\xi)\left[\mathrm{J}_0(nK\xi) - \frac{3}{\Phi(r,s)}\frac{r-1}{2r+1}\mathrm{J}_2(nK\xi)\right], \tag{3.19}$$

where $\xi = 2\pi R/KL$, L is now the radius of a cylindrical acoustic resonator, n is the mode number, and other parameters are the same as defined after Equation (3.10).

Neglecting the inertial and BBD forces, we first consider the simplified version of Equation (3.19):

$$\frac{d\xi}{d\tau} = -4\mathrm{J}_1(nK\xi)\left[\mathrm{J}_0(nK\xi) - \frac{3}{\Phi(r,s)}\frac{r-1}{2r+1}\mathrm{J}_2(nK\xi)\right]. \tag{3.20}$$

Solution to this equation can be presented in terms of hypergeometric functions, but it can also be easily integrated numerically. In contrast to the solution in Equation (3.12), the solution of Equation (3.20) is not periodic in space, therefore the particle trajectory and its final state are dependent on the initial position ξ_0 in a more complex way than for a plane standing wave. The equilibrium states can be found from Equation (3.20) by equating the function in the right-hand side of this equation to zero. Solving this transcendental equation, one obtains numerous critical points ξ_0. Some of these points correspond to stable equilibrium states, and others to unstable states. Figure 3.11 illustrates the typical trajectories of a very heavy ($r >> 1$) and hard ($s >> 1$) particle with $\Phi = 5/2$ and $n = 3$.

Within the limits of this figure the stable equilibrium states correspond to $\xi = 0$ and $2.36 \cdot 10^4$ (dashed line 2), and the unstable equilibrium states correspond to $\xi = 1.24 \cdot 10^4$ (dashed line 1) and $3.31 \cdot 10^4$ (dashed line 3). If the initial particle displacement is less than $\xi_1 = 1.24 \cdot 10^4$, then the particle moves to the centre $\xi = 0$ (see the three lines below dashed line 1). If the initial particle displacement is between $\xi_1 = 1.24 \cdot 10^4$ and $\xi_3 = 3.31 \cdot 10^4$, then the particle moves to the next stable equilibrium state of $\xi_2 = 2.36 \cdot 10^4$ (see the three lines between dashed lines 1 and 3), and so on. One can easily show that the stable equilibrium states occur at the nodes of acoustic force F_a, in Equation (3.18), which have a positive gradient with respect to *R*, whereas unstable equilibrium states occur at the nodes of acoustic force F_a with a negative gradient with respect to *R*. Thus, one can conclude that if there is an ensemble of particles randomly distributed in the cylindrical acoustic resonator, then under the action of a standing acoustic field they will be separated and bunched at the certain nodes of the acoustic field.

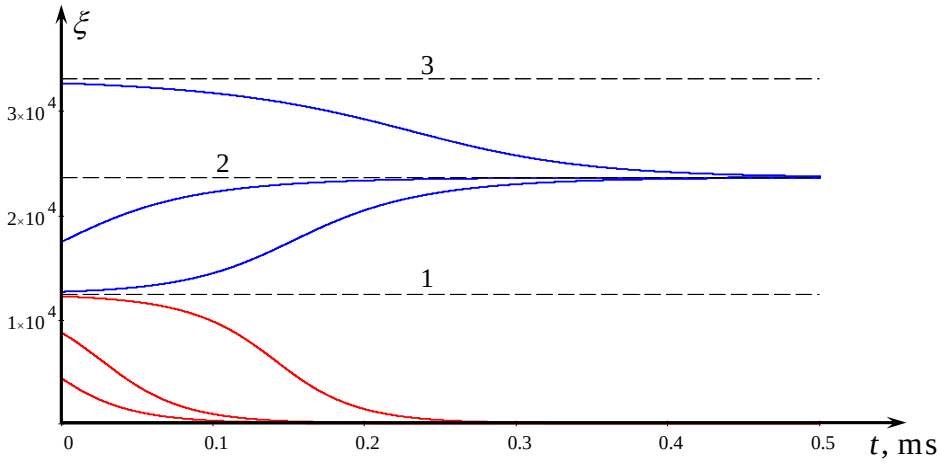

Figure 3.11: Dependence of particle position on time at different initial conditions in a cylindrical resonator.

Qualitatively similar results were obtained for other particle types (gold, aluminium, silica, ice) with finite values of *r* and *s*.

3.5 Conclusion

In this chapter, the complex dynamics of small rigid particles under the action of acoustic radiation force was considered. We have studied different realistic particles of arbitrary compressibility and density. Our analysis was based on a more advanced model in comparison with those that were used in the earlier works of Sarvazyan & Ostrovsky, (2009); and Ostrovsky, (2015). In addition to the Stokes drag force, the model used in this chapter includes the particle inertia, added mass, and the Boussinesq–Basset drag force, the effects which were ignored in these papers. It is confirmed through the numerical solutions that all these additional effects are usually small and can be neglected, except for the particular cases when their influence become noticeable. This happens, in particular, at the very early stages of particle motion, see Figure 3.4(b), as well as at the final stage, when a particle approaches the equilibrium state as shown in Figure 3.2. Under the influence of a BBD force, the character of motion becomes non-monotonic and non-exponential in time: the equilibrium is approached as $t^{-1/2}$ (Stepanyants & Yeoh, 2009).

The particle motion was considered both for the plane and cylindrical geometries. Stable positions where particles eventually move to, under the action of a single-mode acoustic field, have been found.

We also considered particle motion due to periodic switching between two acoustic modes when a particle can experience a slow drift and simultaneous oscillations when approaching an equilibrium position.

As was mentioned in the previous publications, the motion of particles under the action of the acoustic radiation force has a variety of potential applications. It can be used, in particular, for stirring and mixing of particles (Sarvazyan & Ostrovsky, 2009), as well as for their separation and collection at certain places, from where they can be subsequently removed to provide a cleaning of a fluid. Another possibility is enhancing drug particle dissolution in the process of oscillations, based on the existing technology which allows for the creation of nanoparticles containing a solvable drug (Schmid et al., 2016). Acoustic radiation force in resonators has been used for food and water quality control and monitoring (Priev & Sarvazyan, 2009; Priev &

Barenholz, 2010; Ostrovsky et al. 2011). It is hoped that, besides the new theoretical results, the models considered here can contribute to the aforementioned practical applications.

The content of this Chapter is based on the published paper: Hassan, H.K., Ostrovsky, L.A., & Stepanyants, Y.A. (2017). Particle dynamics in a viscous fluid under the action of acoustic radiation force. *Interdisciplinary Journal of Discontinuity, Nonlinearity, and Complexity*, v. 6, n. 3, 317–327.

In this Chapter, it was considered a typical sinusoidal acoustic signal, but in principle, the similar approach can be developed for more complex types of oscillations, in particular, for the solitary impacts on particles, multi-mode particle control, or breather-type external forcing.

Chapter 4: Resonance properties of forced oscillations of particles and gaseous bubbles in a viscous fluid at small Reynolds numbers

4.1 Introduction

Oscillation is the frequent variation with time of an objects position or state. The oscillations occur everywhere in nature, technology, economy, biology, etc. There are natural oscillations and artificially generated oscillations by an external force such as, by acoustic radiation force, magnetic force or electric force. Such oscillations are called forced oscillations. Without an external force, oscillations in real systems usually decay with time due to dissipation. However under the action of an external force, oscillations can occur for an indefinite time. At a certain frequency of the external force, oscillations can be of very high amplitude; in this case they say that resonance occurs in the system. Resonance can play both positive and negative roles in nature and in industry. Therefore, it is important to know the resonance property of a particular system to control the vibrations and oscillations which potentially can happen in the system.

In simple models of linear oscillators with damping, the dissipation is proportional to the derivative of an unknown quantity. For example, for the oscillating particle in a fluid, the drag force (Stokes drag force) is proportional to the derivative of particle displacement (particle speed). Resonance properties of such oscillators are very-well known (Siebert, 1986; Klepper & Kolenkow, 2014). However, the Stokes drag force alone is applicable only to a stationary moving particle. For a transient (in particular, oscillating) motion one additional drag force should be taken into account – the memory integral drag force. This force in application to solid particles is known as the Boussinesq–Basset drag force. A similar modification is known for gaseous bubbles oscillating in a viscous fluid. Resonance properties of particles and bubbles under the influence of memory integral drag forces have not been studied thus far.

We consider small oscillations of micro-particles and gaseous bubbles, in a viscous fluid, due to the action of a sinusoidal external force. Exact solutions to the governing

integro-differential equations containing both Stokes and memory-integral drag forces will be obtained. The main aim of this study is to clarify the influence of the memory-integral drag force on the resonance characteristics of oscillating particles or gaseous bubbles in a viscous fluid at small Reynolds numbers. The resonant curves (amplitude versus frequency of external force), as well as phase-frequency dependences, are obtained for both these and compared with the corresponding dependences of the traditional oscillator with the Stokes drag force only applied.

4.2 Oscillating solid particle in a viscous fluid

Let us consider first small oscillations of a solid spherical particle of density ρ_p and radius a in a viscous fluid. Particle motion can be caused by the influence of an external harmonic force having the amplitude $\tilde{A}$ and frequency $\tilde{\omega}$. A corresponding equation of motion, for the one-dimensional case, in the creeping flow regime (i.e. the flow with very small Reynolds number, Re << 1) is (Lovalenti & Brady, 1993; Stepanyants & Yeoh, 2009; Stepanyants & Yeoh, 201):

$$\left(r+\frac{1}{2}\right)\frac{d^2z}{dt^2}+\frac{9}{2}\frac{\mu}{a^2\rho_f}\frac{dz}{dt}+\frac{9}{2a}\sqrt{\frac{\mu}{\pi\rho_f}}\int_{-\infty}^{t}\frac{d^2z(t)}{d\tau^2}\frac{d\tau}{\sqrt{t-\tau}}+\tilde{\omega}_0^2 z=\tilde{A}\sin\tilde{\omega}t\,, \qquad (4.1)$$

where z is the particle coordinate; $r \equiv \rho_p/\rho_f$ is the ratio of particle to fluid density; μ is the dynamic viscosity of a fluid, and $\tilde{\omega}_0$ is the frequency of free oscillations of a particle in the absence of dissipation (ν = 0). In this equation, the second term in the left-hand side describes the quasi-stationary Stokes drag (SD) force, while the integral term describes the well-known Boussinesq–Basset drag (BBD) force (Lovalenti & Brady, 1993; Landau & Lifshitz, 1993). The added mass effect for a spherical particle is accounted for through the coefficient 1/2 within the bracket on the left-hand side of equation (Landau & Lifshitz, 1993).

We assume that a particle begins from rest and commences an instantaneous motion at t = 0 with the initial velocity V_0, i.e. its velocity experiences a sudden jump from zero to V_0 and then varies in accordance with the equation of motion (Lovalenti & Brady, 1993). Thus, the particle velocity, including the initial jump, can be expressed

through the unit Heaviside function $H(t)$: $(dz/dt)_{tot} = H(t)(dz/dt)_{pos}$, where $(dz/dt)_{tot}$ is the velocity at any instant of time, whereas $(dz/dt)_{pos}$ relates to the velocity at positive times only. Correspondingly, the acceleration is $(d^2z/dt^2)_{tot} = \delta(t)(dz/dt)_{pos} + H(t)(d^2z/dt^2)_{pos}$, where $\delta(t) \equiv dH(t)/dt$ is the Dirac delta-function. Taking into consideration the effect of the Dirac delta-function under the integral, Equation (4.1) for $t > 0$ can be presented in the form (the index "pos" has been omitted):

$$\left(r + \frac{1}{2}\right)\frac{d^2z}{dt^2} + \frac{9\mu}{2a^2\rho_f}\left[\frac{dz}{dt} + \frac{aV_0}{\sqrt{\pi\nu t}} + a\sqrt{\frac{\rho_f}{\pi\mu}}\int_{0+}^{t}\frac{d^2z(t)}{d\tau^2}\frac{d\tau}{\sqrt{t-\tau}}\right] + \tilde{\omega}_0^2 z = \tilde{A}\sin\tilde{\omega}t. \quad (4.2)$$

The equation of motion can be expressed in the dimensionless form by introducing the following normalised variables: $\zeta = z/a$, $\theta = 9\mu t/a^2\rho_f$, and $\upsilon_0 = V_0 a\rho_f/9\mu$. Equation (4.2) after that reduces to (Stepanyants & Yeoh, 2009; Stepanyants & Yeoh, 2010):

$$\frac{d^2\zeta}{d\theta^2} + \alpha\frac{d\zeta}{d\theta} + \frac{\beta}{\sqrt{\pi}}\left[\frac{\upsilon_0}{\sqrt{\theta}} + \int_0^{\theta}\frac{d^2\zeta(\vartheta)}{d\vartheta^2}\frac{d\vartheta}{\sqrt{\theta-\vartheta}}\right] + \omega_0^2\zeta = A\sin\omega\theta, \quad (4.3)$$

where $\alpha = 1/(1 + 2r)$, $\beta = 1/(1 + 2r)$, $\omega_0 = \tilde{\omega}_0\sqrt{2a^3\rho_f^2/81\mu^2(2r+1)}$, $\omega = \tilde{\omega}a^2\rho_f/9\mu$ and $A = 2\tilde{A}a^3\rho_f^2/81\mu^2(2r+1)$.

Although the coefficients α and β are equal, we denote them by different letters. This allows us to switch off either the SD force by setting $\alpha = 0$ or BBD force by setting $\beta = 0$ and allows study the influence of the corresponding drag forces separately. We assume further that the viscosity of an ambient fluid is relatively small, so that the frequency of free oscillations $\omega_0 >> \alpha, \beta$ whilst the Reynolds number is still small, $\mathrm{Re} = aV\rho_f/\mu << 1$. This can be achieved, for example, by a smallness of particle radius a.

As this is a linear equation with respect to ζ, its general solution consists of two parts, the general solution of a homogeneous equation and a particular solution of a non-homogeneous equation. The general solution of a homogeneous equation with $A = 0$ can be readily obtained with the help of the Laplace transform subject to the initial conditions $\zeta(0) = \zeta_0$ and $\dot{\zeta}(0) = \upsilon_0$. Here the dot on the top of a letter stands for a derivative with respect to the dimensionless time θ. This has been done in Stepanyants &Yeoh, (2009), and Stepanyants &Yeoh, (2010). We do not reproduce here the lengthy solution from those papers; it has been analysed there in detail and represented for slowly decaying oscillations (provided that the decay coefficients α and β are small compared to ω_0).

The most important issue to us is the solution of the forced equation (4.3) for non-zero $A \neq 0$. To construct such a solution we choose a trial solution of the form $\zeta(\theta) = B\cos\omega\theta + C\sin\omega\theta$ and assume for simplicity that the particle is at the rest at the initial instant of time, so that $\zeta_0 = \upsilon_0 = 0$. With this trial solution chosen above the integral term in Equation (4.3) can be readily evaluated (see also Ref. (Visitskii, Petrov & Shunderyuk, 2009)):

$$\int_0^\theta \frac{d^2\zeta(\vartheta)}{d\vartheta^2}\frac{d\vartheta}{\sqrt{\theta-\vartheta}} = -\frac{\omega^{3/2}}{2}\sqrt{\frac{\pi}{2}}\left[B\left(\sin\omega\theta+\cos\omega\theta\right)+C\left(\sin\omega\theta-\cos\omega\theta\right)\right]. \quad (4.4)$$

Substituting then the trial solution into Equation (4.3) and using Equation (4.4), we obtain after some manipulations

$$B = -\frac{A}{6}\omega\frac{2\alpha+3\beta\sqrt{2\omega}/2}{\left(\omega_0^2-\omega^2-\sqrt{2}\beta\omega^{3/2}/4\right)^2+\left(\alpha+3\beta\sqrt{2\omega}/4\right)^2\omega^2/9}, \quad (4.5)$$

and

$$C = A\frac{\omega_0^2-\omega^2-\beta\sqrt{2}\omega^{3/2}/4}{\left(\omega_0^2-\omega^2-\sqrt{2}\beta\omega^{3/2}/4\right)^2+\left(\alpha+3\beta\sqrt{2\omega}/4\right)^2\omega^2/9}. \quad (4.6)$$

Let us present now the forced solution in the equivalent form

$$\zeta(\theta) = B\cos\omega\theta + C\sin\omega\theta = Amp(\omega_0,\omega)\sin(\omega\theta+\varphi), \quad (4.7)$$

where the amplitude of forced oscillations is

$$Amp\left(\omega_0,\omega\right)=\sqrt{B^2+C^2}=\frac{A}{\sqrt{\left(\omega_0^2-\omega^2-\sqrt{2}\beta\omega^{5/2}\right)^2+\frac{1}{9}\omega^2\left(\alpha+3\sqrt{2}\beta\omega^{3/2}\right)^2}},\quad(4.8)$$

and the phase φ is determined from the equation

$$\tan\varphi=\frac{B}{C}=\frac{\omega}{12}\frac{2\alpha+3\beta\sqrt{2\omega}}{\omega_0^2-\omega^2-\left(\sqrt{2}/4\right)\beta\omega^{3/2}}.\quad(4.9)$$

These expressions can be presented in the traditional dimensionless forms if we normalise the frequency $\nu=\omega/\omega_0$ and introduce the quality factors, $Q_\alpha=\omega_0/\alpha$ and $Q_\beta=8\omega_0/\beta^2$. The quality factor Q_α is well known in the theory of oscillations (see, Klepper & Kolenkow, (2014)), whereas the other quality factor Q_β is new. Taking into account our definitions of coefficients α and β, we can express the quality factors in terms of the frequency ω_0 and the relative particle density r: $Q_\alpha=\omega_0\left(1+2r\right)$ and $Q_\beta=8\omega_0\left(1+2r\right)^2$. Normalising the amplitude of particle oscillation as $A_n=\omega_0^2 Amp/A$, we then the amplitude-frequency dependence (4.8) in dimensionless form is given by

$$A_n\left(\nu,Q_\alpha,Q_\beta\right)=\frac{1}{\sqrt{\left(1-\nu^2-\nu\sqrt{\nu/Q_\beta}\right)^2+\nu^2\left(1/Q_\alpha+\sqrt{\nu/Q_\beta}\right)^2}},\quad(4.10)$$

The phase-frequency dependence (4.9) in the dimensionless form can also be written as

$$\varphi\left(\nu,Q_\alpha,Q_\beta\right)=\tan^{-1}\left(\frac{\nu}{Q_\alpha}\frac{1+Q_\alpha\sqrt{\nu/Q_\beta}}{\nu^2-1+\nu\sqrt{\nu/Q_\beta}}\right).\quad(4.11)$$

If the BBD force is neglected ($Q_\beta\to\infty$), then the dependences (4.10) and (4.11) naturally reduce to the classic ones (Siebert, 1986; Klepper & Kolenkow, 2014):

$$A_n(\nu, Q_\alpha) = \left[\left(1-\nu^2\right)^2 + \nu^2 / Q_\alpha^2\right]^{-1}, \qquad \varphi(\nu, Q_\alpha) = \tan^{-1}\left(\nu / Q_\alpha \left(\nu^2 - 1\right)\right). \tag{4.12}$$

Plots of $A_n(\nu, Q_\alpha, Q_\beta)$ and $\varphi(\nu, Q_\alpha, Q_\beta)$ as functions of the normalised frequency ν are shown in Figures 4.1a) and 4.1b), respectively. Line 1 pertain to the case when only the Stokes drag force is taken into account and the BBD force is ignored. The parameter Q_α = 700 was chosen; it corresponds to ω_0 = 100 and r = 3 in Equation (4.3). Line 2 pertain to the case when both Stokes and BBD forces are both taken into account with the same parameters for ω_0 and r which gives Q_β = 39200.

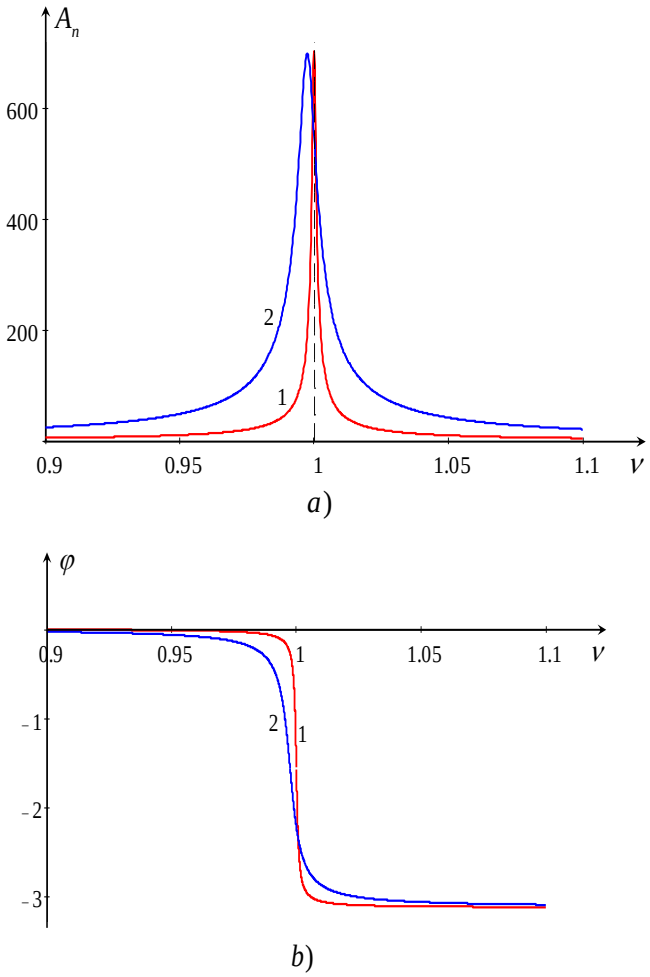

Figure 4.1: The amplitude-frequency dependence (a) and phase-frequency dependence (b) for oscillating solid particle in a viscous fluid under the influence of only the Stokes drag force (lines 1) and both Stokes and BBD drag forces (lines 2). Function A_n for line 2 in frame (a) was multiplied by the factor 4.5.

Thus, from this analysis, one can see that, under the influence of BBD force, the maximum of the resonance curve becomes about 4.5 times smaller and correspondingly 4.5 times wider. It is also shifted to the left from $v = 1$ as shown in Figure 4.1a).

4.3 Oscillating bubble in a viscous fluid

Consider now another limiting case – small oscillations of a gaseous spherical bubble of a density ρ_b and a radius a in a viscous fluid. The bubble sphericity can be maintained by a surface tension which is very important for small-radius bubbles. The basic equation of motion in the dimensionless variables is similar to Equation (4.3), but contains different coefficients of viscous terms and the different kernel of memory-integral drag (MID) force (the same dimensionless variables as used in the last section can be used in this case too). Now instead of a Stokes drag force, the corresponding term is proportional to the first derivative $d\zeta/d\theta$ and is known as the Hadamard–Rybczynski drag (HRD) force (Landau & Lifshitz, 1993; Stepanyants & Yeoh, 2009), and the basic equation reads (its derivation is similar to that presented above for a solid particle):

$$\frac{d^2\zeta}{d\theta^2} + \frac{2}{9}\left[\alpha\frac{d\zeta}{d\theta} + 6\beta\left(\frac{\upsilon_0}{\sqrt{\theta}} + \int_0^\theta \frac{d^2\zeta(\vartheta)}{d\vartheta^2} e^{\theta-\vartheta}\,\mathrm{erfc}\left(\sqrt{\theta-\vartheta}\right)d\vartheta\right)\right] + \omega_0^2\zeta = A\sin\omega\theta. \quad (4.13)$$

Here $\mathrm{erfc}(x) = 1 - \mathrm{erf}(x)$ is the complementary error function Weisstein, (2003), and $\alpha = \beta = 1$, because the ratio of bubble density to the fluid density is negligible, $r = \rho_b/\rho_f \approx 0$. However, we will keep the parameters α and β as arbitrary to investigate the influence of the HRD and MID forces separately.

Assuming again the zero initial conditions and focusing on the steady oscillations of a bubble after a transient decay process, we choose a trial solution in the form $\zeta(\theta) = B\cos\omega\theta + C\sin\omega\theta$. Evaluate first the integral term in Equation (4.13) with the trial solution

$$I(\theta) = \int_0^\theta \frac{d^2\zeta(\vartheta)}{d\vartheta^2} e^{\theta-\vartheta} \operatorname{erfc}\left(\sqrt{\theta-\vartheta}\right) d\vartheta$$
$$= -\omega^2 \int_0^\theta \left(B\cos\omega\vartheta + C\sin\omega\vartheta\right) e^{\theta-\vartheta} \operatorname{erfc}\left(\sqrt{\theta-\vartheta}\right) d\vartheta. \tag{4.14}$$

To evaluate this integral, consider its Laplace transform

$$\hat{I}(s) = -\omega^2 \frac{Bs + C\omega}{s^2+\omega^2} \frac{1}{\sqrt{s}\left(\sqrt{s}+1\right)} = -\omega^2 \frac{Bs + C\omega}{s^2+\omega^2} \left[\frac{1}{s-1} - \frac{\sqrt{s}}{s(s-1)}\right]. \tag{4.15}$$

This expression can be further presented in terms of a sum of simplest ratios:

$$\hat{I}(s) = -\frac{\omega^2}{\omega^2+1}\left[\left(B\omega - C\right)\frac{\omega}{s^2+\omega^2} - \left(B + C\omega\right)\frac{s}{s^2+\omega^2} + \left(B + C\omega\right)\frac{1}{s-1} + \frac{C}{\omega}\frac{\omega^2+1}{\sqrt{s}}\right.$$
$$\left. - \left(B + C\omega\right)\frac{\sqrt{s}}{s-1} + \left(B + C\omega\right)\frac{\sqrt{s}}{s^2+\omega^2} + \frac{B\omega - C}{\omega}\frac{s\sqrt{s}}{s^2+\omega^2}\right]. \tag{4.16}$$

The inverse Laplace transform then gives:

$$I(\theta) = -\frac{\omega^2}{\omega^2+1}\left\{\left(B + C\omega\right)e^{\theta}\left[1 - \operatorname{erf}\left(\sqrt{\theta}\right)\right] + \left(B\omega - C\right)\sin\omega\theta - \left(B + C\omega\right)\cos\omega\theta\right.$$
$$- \frac{\sqrt{i}}{2\omega} e^{i\omega t} \operatorname{erf}\left(\sqrt{i\omega t}\right)\left[B\omega - C + i\sqrt{\omega}\left(B + C\omega\right)\right]$$
$$\left. - \frac{\sqrt{-i}}{2\omega} e^{-i\omega t} \operatorname{erf}\left(\sqrt{-i\omega t}\right)\left[B\omega - C - i\sqrt{\omega}\left(B + C\omega\right)\right]\right\}. \tag{4.17}$$

The first term in the curly brackets $e^{\theta}\left[1 - \operatorname{erf}\left(\sqrt{\theta}\right)\right]$ quickly vanishes when $t \to \infty$. All other terms after simplification reduce to:

$$I(\theta) = -\omega\left(B\sin\omega\theta - C\cos\omega\theta\right). \tag{4.18}$$

Substituting the trial solution into Equation (4.13) and using Equation (4.18), we obtain after simple manipulations:

$$B = -\frac{2A}{9}\omega \frac{\alpha + 6\beta}{\left(\omega^2 - \omega_0^2\right)^2 + 4\left(\alpha + 6\beta\right)^2 \omega^2 / 81},$$

and

$$C = -A\frac{\omega^2 - \omega_0^2}{\left(\omega^2 - \omega_0^2\right)^2 + 4\left(\alpha + 6\beta\right)^2 \omega^2 / 81}. \tag{4.19}$$

The forced solution can be written in the equivalent form:

$$\zeta\left(\theta\right) = B\cos\omega\theta + C\sin\omega\theta = Amp\left(\omega_0, \omega\right)\sin\left(\omega\theta + \varphi\right), \tag{4.20}$$

where the amplitude of forced oscillations is:

$$Amp\left(\omega_0, \omega\right) = \sqrt{B^2 + C^2} = \frac{A}{\sqrt{\left(\omega^2 - \omega_0^2\right)^2 + 4\left(\alpha + 6\beta\right)^2 \omega^2 / 81}}, \tag{4.21}$$

and the phase φ is determined from the equation:

$$\tan\varphi = \frac{B}{C} = \frac{2\omega}{9}\frac{\alpha + 6\beta}{\omega^2 - \omega_0^2}. \tag{4.22}$$

These expressions can be again presented in the traditional dimensionless forms, if we normalise the frequency $\nu = \omega/\omega_0$ and introduce the quality factors, $Q_\alpha = 3\omega_0/2\alpha$ and $Q_\beta = 3\omega_0/4\beta$. Normalising the amplitude of particle oscillation $A_n = \omega_0^2 Amp/A$, we finally present the amplitude-frequency dependence (4.21) in the form as:

$$A_n\left(\nu, Q_\alpha, Q_\beta\right) = \frac{1}{\sqrt{\left(1 - \nu^2\right)^2 + \nu^2\left(1/Q_\alpha + 1/Q_\beta\right)^2}}. \tag{4.23}$$

The phase-frequency dependence (4.22) in the dimensionless form is:

$$\varphi\left(\nu, Q_\alpha, Q_\beta\right) = \left(\frac{1}{Q_\alpha} + \frac{1}{Q_\beta}\right)\frac{\nu}{\nu^2 - 1}. \tag{4.24}$$

The maximum of the resonance curve occurs at $\nu_m = \sqrt{1 - \left(Q_\alpha + Q_\beta\right)^2 / 2Q_\alpha^2 Q_\beta^2}$ and equals to:

$$\left(A_n\right)_{\max} = \frac{2Q_\alpha^2 Q_\beta^2}{\left(Q_\alpha + Q_\beta\right)\sqrt{4Q_\alpha^2 Q_\beta^2 - \left(Q_\alpha + Q_\beta\right)^2}}. \tag{4.25}$$

These expressions reduce to the classic ones (Siebert, 1986; Klepper & Kolenkow, 2014), when $Q_\beta \to \infty$: $\nu_{m|_{Q_\beta\to\infty}} = \sqrt{1-1/2Q_\alpha^2}$, $(A_n)_{\max}\big|_{Q_\beta\to\infty} = \dfrac{Q_\alpha}{\sqrt{1-1/4Q_\alpha^2}}$.

The ratio of the maxima is

$$\frac{(A_n)_{\max}\big|_{Q_\beta\to\infty}}{(A_n)_{\max}} = \frac{Q_\alpha + Q_\beta}{Q_\beta^2}\sqrt{\frac{4Q_\alpha^2Q_\beta^2 - (Q_\alpha+Q_\beta)^2}{4Q_\alpha^2-1}}. \qquad (4.26)$$

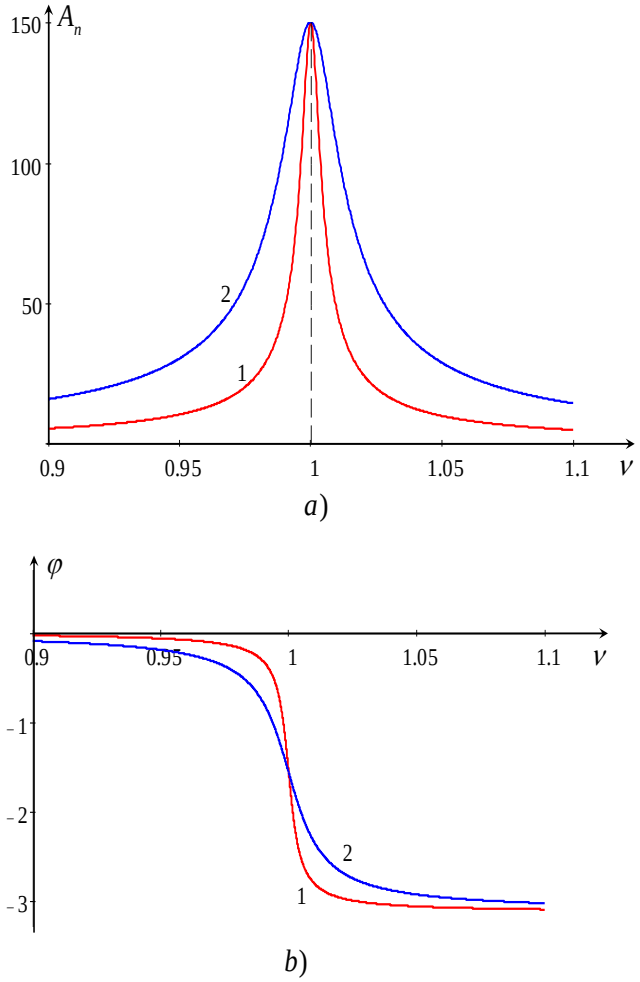

Figure 4.2: The amplitude-frequency dependence (a) and phase-frequency dependence (b) for oscillating bubble in a viscous fluid under the influence of only the HRD force (lines 1) and both HRD and MID forces (lines 2). Function A_n for line Thus, from this analysis one can see that under the influence of MID force the 2 in frame (a) was multiplied by the factor 3. The plots were generated for Q_α=150 and Q_β =75.

For ω_0 = 100, we obtain Q_α = 150 and Q_β = 75; therefore the maxima ratio as per Equation (4.26) is 3. Plots of dependences of $A_n(\nu\ ,\ Q_\alpha,\ Q_\beta)$ and $\varphi(\nu\ ,\ Q_\alpha,\ Q_\beta)$ as functions of the normalised frequency ν are shown in Figures 4.2a) and 4.2b), respectively. Lines 1 pertain to the case when only the HRD force is taken into account, and the MID force is ignored.

It is of interest to compare the resonant curves of a solid particle of negligible density in comparison with the density of ambient fluid and a gaseous bubble. At first glance these two objects become equivalent, but due to different boundary conditions at the solid-liquid and gas-liquid interfaces, the flow around these objects is different. As a result of that, the dissipation coefficients are also different; these reflect, in particular, in the different coefficients of Stokes and Hadamard–Rybczynski drag forces (cf. Equations (4.3) and (4.13)) (see, e.g., Ref. (Landau & Lifshitz, 1993)). In Figure 4.3 we present in the same scale a comparison of resonant characteristics of a solid particle with r = 0 (Figure 4.3a)) and a gaseous bubble (Figure 4.3b)). Lines 1 pertain to the cases when the MID forces are ignored, and lines 2 pertain to the cases when these forces are taken into account. As one can see, the resonant curves of a bubble are taller and a bit narrower. In both cases, the influences of MID forces lead to a 3–5 times reduction of the resonance curves.

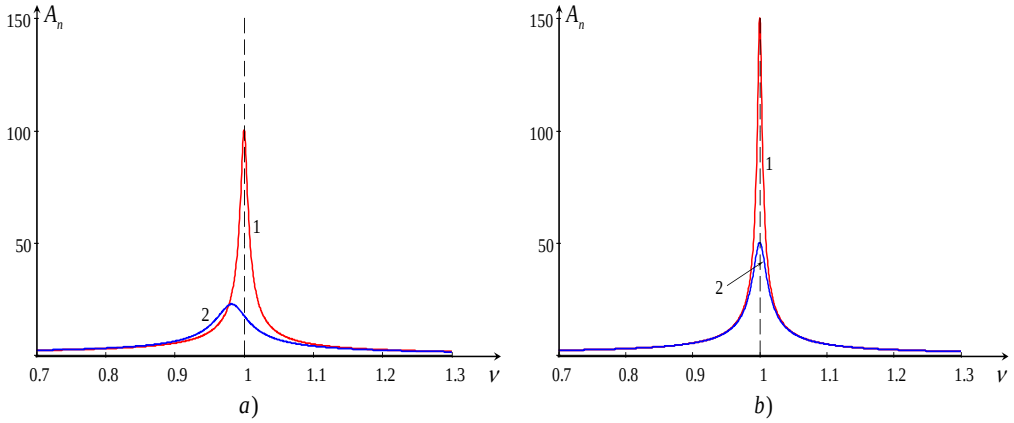

Figure 4.3: The amplitude-frequency dependences of a solid particle of a) negligible small density b) gaseous bubble oscillating in a viscous fluid when the MID force is ignored (lines 1) and when it is taken into consideration (lines 2).

4.4 Conclusion

We can conclude that the influence of a MID force on the resonance characteristics of oscillating solid particles and gaseous bubbles in a viscous fluid under the action of an external sinusoidal force is significant. The MID force leads to the widening of resonance curves and the reduction of resonance peaks which is equivalent, to a certain extent, to the reduction of the quality factor Q_α of the corresponding classical linear oscillator. The results obtained in this study can be helpful in applied problems of micro- and nano-particles and bubble control by acoustic or electromagnetic fields and, possibly, by other external forces (see, e.g., the recent review by Ostrovsty & Stepanyants (2017) and references therein). One of the most promising application of this study pertains to the dissolution of drugs near a particular organ by resonant forcing on the micro-particle by external acoustic field. In this case, it is important to know the resonance frequency, width of a resonance curve, and quality of the resonance system. All these parameters can be correctly estimated only by taking into account all possible drag forces.

The content of this Chapter is based on the published paper: Hassan, H.K., & Stepanyants, Y.A. (2017). Resonance properties of forced oscillations of particles and gaseous bubbles in a viscous fluid at small Reynolds numbers. *Physics of Fluids*, v. 29, n. 10, 101703, 5 p.

We considered here a linear response of the system on relatively small external excitation, however when the amplitude of oscillations becomes large, it is necessary to take into account possible nonlinear effects. In this case, the nonlinear resonance and hysteresis can appear in the system (see e.g. (Svobodny, 1998)). This can be a future area of study.

Chapter 5 Research outcome and further work

5.1. Research outcome

The objective of this research was to investigate the dynamics of particles and bubbles in creeping flows of viscous fluids under the impact of various external forces: electric, acoustic, and memory drag forces. Both analytical and numerical methods were used to obtain interesting results describing the dynamics of two charged particles in a creeping flow and the dynamics of particles under the action of acoustic radiation force. The dynamics of two charged particles in viscous fluid in the creeping flow with two types of viscous drag forces in this Thesis was considered and studied for the first time, moreover, the complex dynamics of small rigid particles under the action of acoustic radiation force was considered for the first time with two types of viscous drag forces the Stokes drag force, and the Boussinesq–Basset drag force. The equation of particle motion in creeping flows with two types of viscous drag forces was solved by means of well-developed solvers realised in FORTRAN (the numerical code is presented in the Appendix).

The resonance properties of forced oscillations of particles and gaseous bubbles in a viscous fluid at small Reynolds numbers was the subject of investigation in this Thesis too. The results obtained show that the memory-integral drag forces play a significant role in the resonance characteristics of oscillating solid particles and gaseous bubbles in a viscous fluid under the action of an external sinusoidal force. To validate the analytical results, the numerical solutions were obtained in the Thesis using the numerical codes (realised in FORTRAN) for the solution of governing equation of forced oscillations.

Chapter 2 presents the case of dynamics of two unlike and like charged particles in viscous fluid in the creeping flow. Charge redistribution within conducting particles was taken into account as per Saranin (1999) and the results obtained were compared against the case of classical Coulomb's force acting between two spherical uniformly charged particles. Two models of particles motion were studied in this chapter: when

the particles move side-by-side and when they move one after another along the same vertical line.

Although in this Chapter it was considered the simplest model of interaction of two charged particles, the results obtained provide a physical insight and can be further generalized to *n*-particles on the basis of the developed approach. However, the equations of motion of many particles become much more complicated, which requires the application of numerical simulation.

Chapter 3 represents a study of the problem of complex dynamics of small rigid particles under the action of acoustic radiation force. Two different cases were considered: particle motion in the plane and in cylindrical geometries. The results obtained in this chapter generalise and specify (make more exact) the results derived in Sarvazyan & Ostrovsky, (2009), and Ostrovsky, (2015) where simplified models were used without memory, inertial, and added mass forces. The results obtained were validated by the numerical solutions and have demonstrated the range of applicability of simplified models. In this Chapter, it was considered a typical sinusoidal acoustic signal, but in principle, a similar approach can be developed for more complex types of oscillations, in particular, for the solitary impacts on particles or breather-type oscillations.

Chapter 4 presents the influence of memory-integral drag (MID) forces on the resonance characteristics of oscillating solid particles and gaseous bubbles in a viscous fluid under the action of an external sinusoidal force. The governing integro-differential equations which take into account the both the Stokes drag force and the memory-integral drag force have been studied analytically, and the results obtained for the resonance curves were compared with the classical resonance properties of a damped oscillator. It has been shown that the MID force leads to the widening of resonance curves and the reduction of resonance peaks. The results obtained in this Chapter pertain to a linear system described by the equation of a harmonic oscillator with dissipations and external force. Based on the developed approach one can consider a nonlinear oscillator with the same types of dissipations. Then the typical nonlinear phenomena, such as the hysteresis, harmonic generation, asymmetry in the

resonance curve, etc., can appear in the system. This can be a subject of a further study.

5.2. Future work and perspectives

In this Thesis consideration was given to the dynamics of charged solid particles in viscous fluid. However, it was shown recently (Bunkin & Bunkin 2016) that small air bubbles in water or in other liquids usually have electric charges (such charged bubbles are called bubston) which support stability of bubbles. Therefore it becomes topical and important to investigate the dynamics of bubstones taking into account the buoyancy force, complete viscous drag forces (including the Hadamard–Rubzynski and MID forces), added mass effect and Bjerknes force. This work is currently underway, but it is not completed yet, therefore the preliminary results are not included in this Thesis.

Another important direction of the future research is the complex dynamics of bubbles under the action of acoustic radiation force (or even under the different types of forces, e.g., electric, magnetic, etc). In the Thesis, we have considered the simple models of impact of external forces onto one or two particles and bubbles. However, it is topical and important to study the dynamics of ensembles of particles or bubbles, including the interaction between them when their density is sufficiently high. This opens interesting and important perspectives for numerous applications such as mixing and steering liquids, quality control of food and beverages, and drug delivery to specific organs.

Appendix: The numerical code for the solution of dynamical equations for two charged particle moving in parallel to each other

```
      PROGRAM SDMID
C     Two solid particles in a viscous fluid with corrected viscosity coefficients
C     and corrected electrostatic force as derived by Saranin
      IMPLICIT DOUBLE PRECISION (A-H, O-Z)
      EXTERNAL FCT, OUTP, F1, F2
      DIMENSION PRMT(5), Y(4), DERY(4), AUX(8,4)
      DIMENSION YOUT1(200001), YOUT2(200001), YOUT3(200001),
     & YOUT4(200001), YOUT5(200001), YOUT6(200001),
     & YOUT7(200001),YSRVX(200001), YSRVZ(200001)
C     Check the dimensions of the arrays yout and ysrv, dim > or = N + 1
      COMMON/PAR/DT, EES, RS, G, SW, KJ, IS
      COMMON/DIM/YOUT1, YOUT2, YOUT3, YOUT4, YOUT5, YOUT6,
     &YOUT7, YSRVX, YSRVZ
      OPEN(1, FILE = 'OUTPUT.DAT')
      OPEN(2, FILE = 'MID-PAR1.DAT')
      OPEN(3, FILE = 'MID-PAR2.DAT')
C   Reading and displaying the parameters:
      READ(2,*) PRM, EES, RS, G, VIN, WIN, SW, ACCUR
      READ(3,*) DT, XIN, ZIN, KJ, N
      PRINT 11, PRM, EES, RS, G, VIN, WIN, SW, ACCUR
 11   FORMAT(/3X, 'PRM = ', E10.4, 3X, 'EES = ', E10.4, 3X, 'RS = ',
     &E10.4, 3X, 'G = ', E10.4/
     & 3X, 'VIN = ', E10.4, 3X, 'WIN = ', E10.4, 3X, 'SW = ', E10.4,
     & 3X, 'ACCUR = ', E10.4/)
```

```
      PRINT 12, DT, XIN, ZIN, KJ, N
 12   FORMAT(/ 'DT = ', E10.4, 2X, 'XIN = ', E10.4, 2X, 'ZIN = ', E10.4,
     & 2X, 'KJ = ', I4, 2X, 'N = ', I6 //)
C  DT is the step of integration
C  EES is the dimensionless coefficient of electric force
C  Initial data: XIN - initial position in X, VIN - initial velocity in X;
C  ZIN - initial position in Z, WIN - initial velocity in Z
C  N is the number of time steps from T = 0
      PRMT(1) = 0.D00
C  PRMT(1) is the lower bound of the integration interval
      PRMT(2) = DT
C  PRMT(2) is the upper bound of the integration interval
      PRMT(3) = DT*PRM
C  PRMT(3) is the initial increment of the independent variable
      PRMT(4) = ACCUR
C  PRMT(4) is the upper error bound
      Y(1) = XIN
      Y(2) = VIN
      Y(3) = ZIN
      Y(4) = WIN
C  Y is a vector of initial data: XIN, ZIN - positions,
C  VIN, WIN - velocity components
      DERY(1) = 0.25D00
      DERY(2) = 0.25D00
      DERY(3) = 0.25D00
      DERY(4) = 0.25D00
C  Dery is the input vector of the initial error weights
```

```
C   The sum of its components must be equal to 1
          NDIM = 4
C   NDIM is the number of equations in the system
CCCCCCC1CCCCCCC2CCCCCCC3CCCCCC4CCCCCC5CCCCCC6CCCCCC7
          SUM1 = 0.D00
          SUM2 = 0.D00
          DO 4 NI = 1,400
          SUM1 = SUM1 + (1.D0/DTANH(DLOG(0.5D0*XIN +
     &  DSQRT(0.25D0*XIN**2 - 1.D0))) - NI/DTANH(NI*DLOG(0.5D0*XIN +
     & DSQRT(0.25D0*XIN**2 - 1.D0))))*DSQRT(1.0D0 –
     & (DTANH(NI*DLOG(0.5D0*XIN + DSQRT(0.25D0*XIN**2 - 1.D0))))**2)/
     & DTANH(NI*DLOG(0.5D0*XIN + DSQRT(0.25D0*XIN**2 - 1.D0)))
          SUM2 = SUM2 + DSQRT(1.0D0 - (DTANH(NI*DLOG(0.5D0*XIN+
     & DSQRT(0.25D0*XIN**2 - 1.D0))))**2)/DTANH(NI*DLOG(0.5D0*XIN +
     & DSQRT(0.25D0*XIN**2 - 1.D0)))
   4      CONTINUE
          SUMSQ = SUM1/SUM2**2
CCCCCC1CCCCCC2CCCCCCC3CCCCCCC4CCCCCCC5CCCCCCC6CCCCCC7
          YOUT1(1) = PRMT(1)
          YOUT2(1) = Y(1)
          YOUT3(1) = Y(2)
          YOUT4(1) = (0.5D0*EES*SUMSQ/(0.25D0*XIN**2 - 1.D0) -
      & F1(0.5D0/XIN)*VIN)/(2.D0*RS + 1.D0)
C         YOUT4(1) = -(EES/XIN**2 + F1(0.5D00/XIN)*VIN)/(2.D00*RS + 1.D00)!
          Coulomb approximation
          YOUT5(1) = Y(3)
          YOUT6(1) = Y(4)
          YOUT7(1) = -(G*(RS - 1.D0) + F2(0.5D0/XIN)*WIN)/(2.D0*RS + 1.D0)
```

```
C       YOUT4(1) AND YOUT7(1) contain the initial forces (accelerations)
CCCCCC1CCCCCC2CCCCCC3CCCCCCC4CCCCCC5CCCCCCC6CCCCCCCC7
        DO 1 I = 1, N
        IS = I
        CALL RKGS(PRMT,Y,DERY,NDIM,IHLF,FCT,OUTP,AUX)
        YOUT1(I+1) = PRMT(2)
        YOUT2(I+1) = Y(1)
        YOUT3(I+1) = Y(2)
        YOUT4(I+1) = DERY(2)
        YOUT5(I+1) = Y(3)
        YOUT6(I+1) = Y(4)
        YOUT7(I+1) = DERY(4)
C       YOUT4(I), YOUT7(I) contain the forces acting on the bubble
        PRMT(1) = PRMT(2)
        PRMT(2) = PRMT(2) + DT
        PRINT 13, YOUT1(I), YOUT2(I), YOUT3(I), YOUT5(I), YOUT6(I)
C       WRITE(1,13) YOUT1(I), YOUT2(I)-XIN, YOUT3(I), YOUT5(I), YOUT6(I)
  1     CONTINUE
        KKK = KJ+1
        DO 3 J = 1, N+1
        IF(J-KKK) 3,2,3
  2     WRITE(1,13) YOUT1(J), YOUT2(J)-2.D0, YOUT3(J), YOUT5(J), YOUT6(J)
        KKK = KKK + KJ
  3     CONTINUE
  13    FORMAT(1X,5(E12.6,1X))
        STOP
        END
```

```
C
      SUBROUTINE FCT(T,Y,DERY)
      IMPLICIT DOUBLE PRECISION(A-H,O-Z)
      EXTERNAL F1, F2
      COMMON/PAR/DT, EES, RS, G, SW, KJ, IS
      COMMON/DIM/YOUT1, YOUT2, YOUT3, YOUT4, YOUT5, YOUT6, YOUT7,
     YSRVX, YSRVZ
      DIMENSION Y(4), DERY(4), YOUT1(200001), YOUT2(200001),
     & YOUT3(200001), YOUT4(200001), YOUT5(200001), YOUT6(200001),
     & YOUT7(200001),YSRVX(200001), YSRVZ(200001)
      PI=3.141592653589793D00
CALCULATION OF INTEGRALS BY NUMERICAL METHODS
      IF(IS.EQ.1) GO TO 1
C
      DO 4 K = 1, IS
      YSRVX(K) = 0.D00
      YSRVZ(K) = 0.D00
      IF(T - YOUT1(K).EQ.0) GO TO 4
      YSRVX(K) = YOUT4(K)/DSQRT(DABS(T - YOUT1(K)))
      YSRVZ(K) = YOUT7(K)/DSQRT(DABS(T - YOUT1(K)))
    4 CONTINUE
C
      IF(IS.GT.5) GO TO 9
      IF(IS.GT.2) GO TO 6
      RX = (YSRVX(1) + YSRVX(2))*DT*0.5D00
      RZ = (YSRVZ(1) + YSRVZ(2))*DT*0.5D00
      GO TO 2
    6 IF(IS.GT.3) GO TO 7
```

```
      RX = (9.D0*YSRVX(1) + 30.D0*YSRVX(2) + 9.D0*YSRVX(3))*DT/24.D0
      RZ = (9.D0*YSRVZ(1) + 30.D0*YSRVZ(2) + 9.D0*YSRVZ(3))*DT/24.D0
      GO TO 2
7     IF(IS.EQ.5) GO TO 8
      RX=(9.D00*YSRVX(1)+27.D00*YSRVX(2)+ 27.D00*YSRVX(3) +
     & 9.D00*YSRVX(4))*DT/24.D00
      RZ = (9.D00*YSRVZ(1)+27.D00*YSRVZ(2)+ 27.D00*YSRVZ(3) +
     & 9.D00*YSRVZ(4))*DT/24.D00
      GO TO 2
8     RX = (9.D00*YSRVX(1) + 28.D00*YSRVX(2) + 22.D00*YSRVX(3) +
     & 28.D00*YSRVX(4) + 9.D00*YSRVX(5))*DT/24.D00
      RZ=(9.D00*YSRVZ(1)+ 28.D00*YSRVZ(2) + 22.D00*YSRVZ(3) +
     & 28.D00*YSRVZ(4) + 9.D00*YSRVZ(5))*DT/24.D00
      GO TO 2
9     RX = (9.D00*YSRVX(1) + 28.D00*YSRVX(2) + 23.D00*YSRVX(3) +
     & 23.D00*YSRVX(4) + 28.D00*YSRVX(5) +
     & 9.D00*YSRVX(6))*DT/24.D00
      RZ=(9.D00*YSRVZ(1) + 28.D00*YSRVZ(2) + 23.D00*YSRVZ(3)+
     & 23.D00*YSRVZ(4) + 28.D00*YSRVZ(5) +
     & 9.D00*YSRVZ(6))*DT/24.D00
      DO 5 J = 4, IS-3
      RX = RX + DT*YSRVX(J)
      RZ = RZ + DT*YSRVZ(J)
5     CONTINUE
      GO TO 2
1     RX = 0.D00
      RZ = 0.D00
```

```
  2    DERY(1) = Y(2)
       ARGF = 5.D-1/YOUT2(IS)
CCCCCCC1CCCCCC2CCCCCCC3CCCCCC4CCCCCC5CCCCCCC6CCCCCCC7
       XIN = YOUT2(IS)
       SUM1 = 0.D00
       SUM2 = 0.D00
       DO 3 NI = 1,400
       SUM1 = SUM1 + (1.D0/DTANH(DLOG(0.5D0*XIN +
     & DSQRT(0.25D0*XIN**2 -
     & 1.D0))) - NI/DTANH(NI*DLOG(0.5D0*XIN + DSQRT(0.25D0*XIN**2 -
     & 1.D0))))*DSQRT(1.0D0 - (DTANH(NI*DLOG(0.5D0*XIN +
     & DSQRT(0.25D0*XIN**2 - 1.D0))))**2)/
     & DTANH(NI*DLOG(0.5D0*XIN + DSQRT(0.25D0*XIN**2 - 1.D0)))
       SUM2=SUM2+ DSQRT(1.0D0 - (DTANH(NI*DLOG(0.5D0*XIN +
     & DSQRT(0.25D0*XIN**2 - 1.D0))))**2)/
     & DTANH(NI*DLOG(0.5D0*XIN + DSQRT(0.25D0*XIN**2 - 1.D0)))
  3    CONTINUE
       SUMSQ = SUM1/SUM2**2
CCCCCC1CCCCCCC2CCCCCC3CCCCCCC4CCCCCCC5CCCCCCC6CCCCCC7
       DERY(2) = (0.5D0*EES*SUMSQ/(0.25D0*XIN**2 - 1.D0) -
     & F1(ARGF)*(YOUT3(IS) + SW*(3.D0/DSQRT(PI))*RX))/(2.D0*RS + 1.D0)
C      DERY(2) = -(EES/XIN**2 + F1(ARGF)*(YOUT3(IS) +
C    & SW*(3.D0/DSQRT(PI))*RX))/(2.D0*RS + 1.D0)!Coulomb approximation
       DERY(3) = Y(4)
       DERY(4) = -(G*(RS - 1.D00) + F2(ARGF)*(YOUT6(IS) +
     & SW*(3.D0/DSQRT(PI))*RZ))/(2.D0*RS + 1.D0)
       RETURN
```

```
      END
C
      SUBROUTINE OUTP(X,Y,DERY,IHLF,NDIM,PRMT)
      IMPLICIT DOUBLE PRECISION (A-H,O-Z)
      DIMENSION PRMT(5),Y(4),DERY(4)
      RETURN
      END
C
      FUNCTION F1(X)
      IMPLICIT DOUBLE PRECISION (A-H,O-Z)
      F1 = 1.D00 + 3.D00*X + 9.D00*X**2 + 19.D00*X**3 + 93.D00*X**4
     & + 387.D00*X**5 + 1197.D00*X**6 + 5331.D00*X**7
     & + 19821.D00*X**8 + 76115.D00*X**9 + (4.D00*X)**10/
     & (3.D00*(1.D00 - 4.D00*X))
      RETURN
      END
C
      FUNCTION F2(X)
      IMPLICIT DOUBLE PRECISION (A-H,O-Z)
      F2 = 1.D00 - 1.5D00*X + 2.25D00*X**2 - 59.D00*X**3/8.D00
     & + 273.D00*X**4/16.D00 - 1107.D00*X**5/32.D00 + (2.D00*X)**6/
     & (1.D00 + 2.D00*X)
      RETURN
      END
C
C     Subroutine RKGS (from the FORTRAN Library)          RKG00050
C                                                         RKG00060
```

```
C      Purpose                                                  RKG00070
C        To solve a system of first order ordinary differential RKG00080
C        equations with given initial values.                   RKG00090
C                                                               RKG00100
C      Usage                                                    RKG00110
Call RKGS (PRMT,Y,DERY,NDIM,IHLF,FCT,OUTP,AUX)                  RKG00120
C        parameters FCT and OUTP require an external statement. RKG00130
C                                                               RKG00140
C      Description of parameters                                RKG00150
C        PRMT - an input and output vector with dimension greater RKG00160
C          or equal to 5, which specifies the parameters of     RKG00170
C          the interval and of accuracy and which serves for    RKG00180
C          communication between output subroutine (furnished   RKG00190
C         by the user) and subroutine RKGS. Except PRMT(5)      RKG00200
C          the components are not destroyed by subroutine       RKG00210
C          RKGS and they are                                    RKG00220
C        PRMT(1)- lower bound of the interval (input),          RKG00230
C        PRMT(2)- upper bound of the interval (input),          RKG00240
C        PRMT(3)- initial increment of the independent variable RKG00250
C       (input),                                                RKG00260
C        PRMT(4)- upper error bound (input). If absolute error is RKG00270
C         greater than PRMT(4), increment gets halved.          RKG00280
C         If increment is less than PRMT(3) and absolute        RKG00290
C         error less than PRMT(4)/50, increment gets doubled.   RKG00300
C         the user may change PRMT(4) by means of his           RKG00310
C         output subroutine.                                    RKG00320
C        PRMT(5)- No input parameter. Subroutine RKGS initializes RKG00330
```

```
C       PRMT(5)=0. If the user wants to terminate                RKG00340
C       subroutine RKGS at any output point, he has to           RKG00350
C       change PRMT(5) to non-zero by means of subroutine        RKG00360
C       OUTP. Further components of vector PRMT are              RKG00370
C       feasible if its dimension is defined greater             RKG00380
C       than 5. However subroutine RKGS does not require         RKG00390
C       and change them. Nevertheless they may be useful         RKG00400
C       for handing result values to the main program            RKG00410
C       (calling RKGS) which are obtained by special             RKG00420
C       manipulations with output data in subroutine OUTP.       RKG00430
C       Y         - Input vector of initial values. (Destroyed)  RKG00440
C         Lateron Y is the resulting vector of dependent         RKG00450
C         variables computed at intermediate points X.           RKG00460
C       DERY  - Input vector of error weights. (destroyed)       RKG00470
C         the sum of its components must be equal to 1.          RKG00480
C         Lateron dery is the vector of derivatives, which       RKG00490
C         belong to function values Y at a point X.              RKG00500
C       NDIM  - An input value, which specifies the number of    RKG00510
C       equations in the system.                                 RKG00520
C       IHLF- An output value, which specifies the number of     RKG00530
C       bisections of the initial increment. If IHLF gets        RKG00540
C       greater than 10, subroutine RKGS returns with            RKG00550
C       error message IHLF=11 into main program. Error           RKG00560
C       message IHLF=12 or IHLF=13 appears in case               RKG00570
C       PRMT(3)=0 or in case SIGN(PRMT(3)).Ne.SIGN(PRMT(2)-RKG00580
C       PRMT(1)) respectively.                                   RKG00590
C       FCT- The name of an external subroutine used. This       RKG00600
```

```
C       subroutine computes the right hand sides DERY of                RKG00610
C       the system to given values X and Y. Its parameter               RKG00620
C       list must be X,Y,DERY. Subroutine FCT should                    RKG00630
C       not destroy X and Y.                                            RKG00640
C       OUTP  - The name of an external output subroutine used.         RKG00650
C       Its parameter list must be X,Y,DERY,IHLF,NDIM,PRMT.             RKG00660
C       None of these parameters (except, if necessary,                 RKG00670
C       PRMT(4),PRMT(5),...) should be changed by                       RKG00680
C       subroutine OUTP. If PRMT(5) is changed to non-zero,             RKG00690
C       subroutine RKGS is terminated.                                  RKG00700
C       AUX - An auxiliary storage array with 8 rows and NDIM           RKG00710
C       columns.                                                        RKG00720
C                                                                       RKG00730
C     Remarks                                                           RKG00740
C       The procedure terminates and returns to calling program, if     RKG00750
C       (1) More than 10 bisections of the initial increment are        RKG00760
C           necessary to get satisfactory accuracy (error message       RKG00770
C           IHLF=11),                                                   RKG00780
C       (2) Initial increment is equal to 0 or has wrong sign           RKG00790
C           (error messages IHLF=12 or IHLF=13),                        RKG00800
C       (3) The whole integration interval is worked through,           RKG00810
C       (4) Subroutine OUTP has changed PRMT(5) to non-zero.            RKG00820
C                                                                       RKG00830
C     Subroutines and function subprograms required                     RKG00840
C       the external subroutines FCT(X,Y,DERY) and                      RKG00850
C       OUTP(X,Y,DERY,IHLF,NDIM,PRMT) must be furnished by the user.
                                                                        RKG00860
C                                                                       RKG00870
```

```
C       Method                                                  RKG00880
C         Evaluation is done by means of fourth order Runge-Kutta RKG00890
C         formulae in the modification due to gill. Accuracy is RKG00900
C         tested comparing the results of the procedure with single RKG00910
C         and double increment.                                 RKG00920
C       Subroutine RKGS automatically adjusts the increment duringRKG00930
C         the whole computation by halving or doubling. If more than-RKG00940
C         10 bisections of the increment are necessary to get   RKG00950
C         satisfactory accuracy, the subroutine returns with    RKG00960
C         error message IHLF=11 into main program.              RKG00970
C         To get full flexibility in output, an output subroutine RKG00980
C         must be furnished by the user.                        RKG00990
C         For reference, see                                    RKG01000
C         Ralston/Wilf, Mathematical methods for digital computers, RKG01010
C         WILEY, NEW YORK/LONDON, 1960, PP.110-120.             RKG01020
C  SUBROUTINE RKGS(PRMT,Y,DERY,NDIM,IHLF,FCT,OUTP,AUX)
                                                                RKG01060
      IMPLICIT DOUBLE PRECISION (A-H,O-Z)
      DIMENSION Y(1),DERY(1),AUX(8,1),A(4),B(4),C(4),PRMT(1)
                                                                RKG01090
      DO 1 I=1,NDIM                                           RKG01100
    1 AUX(8,I)=.06666667*DERY(I)                              RKG01110
      X=PRMT(1)                                               RKG01120
      XEND=PRMT(2)                                            RKG01130
      H=PRMT(3)                                               RKG01140
      PRMT(5)=0.                                              RKG01150
      CALL FCT(X,Y,DERY)                                      RKG01160
```

```
C                                                              RKG01170
C     Error test                                               RKG01180
      IF(H*(XEND-X))38,37,2                                    RKG01190
C                                                              RKG01200
C     Preparations for Runge-Kutta method                      RKG01210
    2 A(1)=.5                                                  RKG01220
      A(2)=.2928932                                            RKG01230
      A(3)=1.707107                                            RKG01240
      A(4)=.1666667                                            RKG01250
      B(1)=2.                                                  RKG01260
      B(2)=1.                                                  RKG01270
      B(3)=1.                                                  RKG01280
      B(4)=2.                                                  RKG01290
      C(1)=.5                                                  RKG01300
      C(2)=.2928932                                            RKG01310
      C(3)=1.707107                                            RKG01320
      C(4)=.5                                                  RKG01330
C     Preparations of first Runge-Kutta step                   RKG01350
      DO 3 I=1,NDIM                                            RKG01360
      AUX(1,I)=Y(I)                                            RKG01370
      AUX(2,I)=DERY(I)                                         RKG01380
      AUX(3,I)=0.                                              RKG01390
    3 AUX(6,I)=0.                                              RKG01400
      IREC=0                                                   RKG01410
      H=H+H                                                    RKG01420
      IHLF=-1                                                  RKG01430
      ISTEP=0                                                  RKG01440
```

```
      IEND=0                                                    RKG01450
C     Start of a Runge-Kutta step                               RKG01480
    4 IF((X+H-XEND)*H)7,6,5                                     RKG01490
    5 H=XEND-X                                                  RKG01500
    6 IEND=1                                                    RKG01510
C                                                               RKG01520
C     Recording of initial values of this step                  RKG01530
    7 CALL OUTP(X,Y,DERY,IREC,NDIM,PRMT)                        RKG01540
      IF(PRMT(5))40,8,40                                        RKG01550
    8 ITEST=0                                                   RKG01560
    9 ISTEP=ISTEP+1                                             RKG01570
C                                                               RKG01580
C                                                               RKG01590
C     Start of innermost Runge-Kutta loop                       RKG01600
      J=1                                                       RKG01610
   10 AJ=A(J)                                                   RKG01620
      BJ=B(J)                                                   RKG01630
      CJ=C(J)                                                   RKG01640
      DO 11 I=1,NDIM                                            RKG01650
      R1=H*DERY(I)                                              RKG01660
      R2=AJ*(R1-BJ*AUX(6,I))                                    RKG01670
      Y(I)=Y(I)+R2                                              RKG01680
      R2=R2+R2+R2                                               RKG01690
   11 AUX(6,I)=AUX(6,I)+R2-CJ*R1                                RKG01700
      IF(J-4)12,15,15                                           RKG01710
   12 J=J+1                                                     RKG01720
      IF(J-3)13,14,13                                           RKG01730
```

```
   13  X=X+.5*H                                                    RKG01740
   14  CALL FCT(X,Y,DERY)                                          RKG01750
       GOTO 10                                                     RKG01760
C      End of innermost Runge-Kutta loop                           RKG01770
C                                                                  RKG01780
C                                                                  RKG01790
C      TEST OF ACCURACY                                            RKG01800
   15  IF(ITEST)16,16,20                                           RKG01810
C                                                                  RKG01820
C  In case ITEST=0 there is no possibility for testing of accuracy RKG01830
   16  DO 17 I=1,NDIM                                              RKG01840
   17  AUX(4,I)=Y(I)                                               RKG01850
       ITEST=1                                                     RKG01860
       ISTEP=ISTEP+ISTEP-2                                         RKG01870
   18  IHLF=IHLF+1                                                 RKG01880
       X=X-H                                                       RKG01890
       H=.5*H                                                      RKG01900
       DO 19 I=1,NDIM                                              RKG01910
       Y(I)=AUX(1,I)                                               RKG01920
       DERY(I)=AUX(2,I)                                            RKG01930
   19  AUX(6,I)=AUX(3,I)                                           RKG01940
       GOTO 9                                                      RKG01950
C                                                                  RKG01960
C      In case ITEST=1 testing of accuracy is possible             RKG01970
   20  IMOD=ISTEP/2                                                RKG01980
       IF(ISTEP-IMOD-IMOD)21,23,21                                 RKG01990
   21  CALL FCT(X,Y,DERY)                                          RKG02000
```

```
      DO 22 I=1,NDIM                                          RKG02010
      AUX(5,I)=Y(I)                                           RKG02020
   22 AUX(7,I)=DERY(I)                                        RKG02030
      GOTO 9                                                  RKG02040
C                                                             RKG02050
C     Computation of test value DELT                          RKG02060
   23 DELT=0.                                                 RKG02070
      DO 24 I=1,NDIM                                          RKG02080
   24 DELT=DELT+AUX(8,I)*ABS(AUX(4,I)-Y(I))                   RKG02090
      IF(DELT-PRMT(4))28,28,25                                RKG02100
C                                                             RKG02110
C     Error is too great                                      RKG02120
   25 IF(IHLF-10)26,36,36                                     RKG02130
   26 DO 27 I=1,NDIM                                          RKG02140
   27 AUX(4,I)=AUX(5,I)                                       RKG02150
      ISTEP=ISTEP+ISTEP-4                                     RKG02160
      X=X-H                                                   RKG02170
      IEND=0                                                  RKG02180
      GOTO 18                                                 RKG02190
C                                                             RKG02200
C     Result values are good                                  RKG02210
   28 CALL FCT(X,Y,DERY)                                      RKG02220
      DO 29 I=1,NDIM                                          RKG02230
      AUX(1,I)=Y(I)                                           RKG02240
      AUX(2,I)=DERY(I)                                        RKG02250
      AUX(3,I)=AUX(6,I)                                       RKG02260
      Y(I)=AUX(5,I)                                           RKG02270
```

```
   29 DERY(I)=AUX(7,I)                                    RKG02280
      CALL OUTP(X-H,Y,DERY,IHLF,NDIM,PRMT)                RKG02290
      IF(PRMT(5))40,30,40                                 RKG02300
   30 DO 31 I=1,NDIM                                      RKG02310
      Y(I)=AUX(1,I)                                       RKG02320
   31 DERY(I)=AUX(2,I)                                    RKG02330
      IREC=IHLF                                           RKG02340
      IF(IEND)32,32,39                                    RKG02350
C                                                         RKG02360
C     Increment gets doubled                              RKG02370
   32 IHLF=IHLF-1                                         RKG02380
      ISTEP=ISTEP/2                                       RKG02390
      H=H+H                                               RKG02400
      IF(IHLF)4,33,33                                     RKG02410
   33 IMOD=ISTEP/2                                        RKG02420
      IF(ISTEP-IMOD-IMOD)4,34,4                           RKG02430
   34 IF(DELT-.02*PRMT(4))35,35,4                         RKG02440
   35 IHLF=IHLF-1                                         RKG02450
      ISTEP=ISTEP/2                                       RKG02460
      H=H+H                                               RKG02470
      GOTO 4                                              RKG02480
C                                                         RKG02490
C                                                         RKG02500
C     Returns to calling program                          RKG02510
   36 IHLF=11                                             RKG02520
      CALL FCT(X,Y,DERY)                                  RKG02530
      GOTO 39                                             RKG02540
```

```
 37  IHLF=12                                                    RKG02550
     GOTO 39                                                    RKG02560
 38  IHLF=13                                                    RKG02570
 39  Call OUTP(X,Y,DERY,IHLF,NDIM,PRMT)                         RKG02580
 40  RETURN                                                     RKG02590
     END                                                        RKG02600
C
     SUBROUTINE ERROR(X,ERR) (From the FORTRAN Library)
C      ========================================
C     Purpose: Compute error function erf(x)
C     Input:   x   --- Argument of erf(x)
C     Output:  ERR --- erf(x)
C      ========================================
     IMPLICIT DOUBLE PRECISION (A-H,O-Z)
     EPS=1.0D-15
     PI=3.141592653589793D0
     X2=X*X
     IF (DABS(X).LT.3.5D0) THEN
       ER=1.0D0
       R=1.0D0
       DO 10 K=1,50
            R=R*X2/(K+0.5D0)
            ER=ER+R
            IF (DABS(R).LE.DABS(ER)*EPS) GO TO 15
10      CONTINUE
15      C0=2.0D0/DSQRT(PI)*X*DEXP(-X2)
       ERR=C0*ER
```

```
      ELSE
        ER=1.0D0
        R=1.0D0
        DO 20 K=1,12
              R=-R*(K-0.5D0)/X2
20            ER=ER+R
        C0=DEXP(-X2)/(DABS(X)*DSQRT(PI))
        ERR=1.0D0-C0*ER
        IF (X.LT.0.0) ERR=-ERR
      ENDIF
      RETURN
      END
```

References

1. Aksenov, A. V., Petrov, A. G., & Shunderyuk, M. M. (2011, July). The motion of solid particles in a fluid in a nonlinear ultrasonic standing wave. In *Doklady Physics* , 56(7), 379-384. SP MAIK Nauka/Interperiodica.
2. Ashkin, A. (1997). Optical trapping and manipulation of neutral particles using lasers. *Proceedings of the National Academy of Sciences*, 94(10), 4853-4860.
3. Batchelor, J. K. (1970). *An Introduction to Fluid Dynamics.* Cambridge University Press, Cambridge.
4. Bunkin, N. F., & Bunkin, F. V. E. (2016). Bubston structure of water and electrolyte aqueous solutions. *Physics-Uspekhi*, 59(9), 846.
5. Candelier, F., Angilella, J. R., & Souhar, M. (2004). On the effect of the Boussinesq–Basset force on the radial migration of a Stokes particle in a vortex. *Physics of Fluids*, 16(5), 1765-1776.
6. Candelier, F., Angilella, J. R., & Souhar, M. (2005). On the effect of inertia and history forces on the slow motion of a spherical solid or gaseous inclusion in a solid-body rotation flow. *Journal of Fluid Mechanics*, 545, 113-139.
7. Charalampous, G., & Hardalupas, Y. (2017). Collisions of droplets on spherical particles. *Physics of Fluids*, 29(10), 103305.
8. Ding, X., Shi, J., Lin, S. C. S., Yazdi, S., Kiraly, B., & Huang, T. J. (2012). Tunable patterning of microparticles and cells using standing surface acoustic waves. *Lab on a Chip*, 12(14), 2491-2497.
9. Gorodtsov, V. A. (1975). Creeping motion of a drop in a viscous fluid. J. Appl. Mech. Tech. Phys., 16, 865–868. (Engl. transl. from the Russian journal Zhurn. Prikl. Mekh. Tekh. Fiz., 6, 32–37 (1975)).
10. Gor'kov, L. P. (1962). On the forces acting on a small particle in an acoustical field in an ideal fluid. In *Sov. Phys. Dokl.* 6, 773-775.
11. Happel, J., & Brenner, H. (Eds.) (1983). *Low Reynolds Number Hydrodynamics.* Kluwer Academic, London.

12. Hassan, H. K., Ostrovsky, L. A., & Stepanyants, Y. A. (2017). Particle dynamics in a viscous fluid under the action of acoustic radiation force. *Interdisciplinary Journal of Discontinuity, Nonlinearity, and Complexity*, 6(3), 317-327.
13. Hidai, H., Yamazaki, T., Itoh, S., Hiromatsu, K., & Tokura, H. (2010). Metal particle manipulation by laser irradiation in borosilicate glass. *Optics Express*, 18(19), 20313-20320.
14. Kim, S., & Karrila, S. J. (2005). *Microhydrodynamics: Principles and Selected Applications*. Dover Publications Inc., Mineola, New York.
15. Klepper, D., & Kolenkow, R. (2014). *An Introduction to Mechanics.* Cambridge University Press.
16. Kobayashi, M. H., & Coimbra, C. F. (2005). On the stability of the Maxey-Riley equation in nonuniform linear flows. *Physics of Fluids*, 17(11), 113301.
17. Lamb, H. (1932). *Hydrodynamics*, 6th ed. Cambridge University Press, Cambridge.
18. Landau, L. D., & Lifshitz, E. M. (Eds.) (1988). *Hydrodynamics*. Nauka: Moscow [in Russian], English Translation: *Fluid Mechanics*. Pergamon Press: Oxford (1993).
19. Lovalenti, P. M., & Brady, J. F. (1993). The force on a bubble, drop, or particle in arbitrary time-dependent motion at small Reynolds number. *Physics of Fluids A: Fluid Dynamics*, 5(9), 2104-2116.
20. Madhav, N. S., & Kala, S. (2011). Review on microparticulate drug delivery system. *Int J PharmTech Res*, 3(3), 1242-4.
21. Michaelides, E. E. (2003). Hydrodynamic force and heat/mass transfer from particles, bubbles, and drops—the Freeman scholar lecture. *Journal of Fluids Engineering*, 125(2), 209-238.
22. Murthy, S. K. (2007). Nanoparticles in modern medicine: state of the art and future challenges. *International journal of nanomedicine*, 2(2), 129.
23. Nemtsov, B. E. (1983). Effects of radiation interaction of bubbles in a liquid. *Sov. Tech. Phys. Lett*, 9, 368-369.
24. Ostrovsky, L. (2015). Concentration of microparticles and bubbles in standing waves. *The Journal of the Acoustical Society of America*, 138(6), 3607-3612.
25. Ostrovsky, L., Priev, A., Ponomarev, V., & Barenholz, Y. (2011), Acoustic radiation force for rapid detection of particles in biological liquids, In *Proceedings*

of Meetings on Acoustics 162ASA, 14(1), 020002. (162 ASA Meeting, San Diego, CA, 2011).

26. Ostrovsky, L. A., & Stepanyants, Y. A. (2018). Dynamics of particles and bubbles under the action of acoustic radiation force. In *Chaotic, Fractional, and Complex Dynamics: New Insights and Perspectives* (pp. 205-230). Springer, Cham.
27. Pelekasis, N.A., & Tsamopoulos, J.A. (1993). Bjerknes forces between two bubbles. Part 1. Response to a step change in pressure, J. Fluid Mech., 254, 467–499. Part 2. Response to an oscillatory pressure field, J. Fluid Mech., 254, 501–527.
28. Priev, A., & Barenholz, Y. (2010). Ultrasonic food quality analyzer based on cylindrical standing waves. In *Proceedings of 20th International Congress on Acoustics, Sydney, Australia* (Vol. 4).
29. Priev, A., & Sarvazyan, A. (2009). Cylindrical standing wave resonator for liquid food quality control. *The Journal of the Acoustical Society of America*, 125(4), 2593-2593.
30. Saranin, V. A. (1999). On the interaction of two electrically charged conducting balls. *Physics-Uspekhi*, 42(4), 385–390.
31. Saranin, V. A., & Mayer, V. V. G. M. (2010). Interaction of two charged conducting balls: theory and experiment. *Physics-Uspekhi*, 53(10), 1067-1074.
32. Sarvazyan, A., & Ostrovsky, L. (2009). Stirring and mixing of liquids using acoustic radiation force. *The Journal of the Acoustical Society of America*, 125(6), 3548-3554.
33. Sazhin, S., Shakked, T., Sobolev, V., & Katoshevski, D. (2008). Particle grouping in oscillating flows. *European Journal of Mechanics-B/Fluids*, 27(2), 131-149.
34. Schmid, A.J., Dubbert, J., Rudov, A.A., Pedersen, J.S., Lindner, P., Karg, M., Potemkin, I.I., & Richtering, W. (2016), Multi-shell hollow nanogels with responsive shell permeability, *Scientific Reports*, 6, 22736.
35. Shoji, M. (2004). Studies of boiling chaos: a review. *International Journal of Heat and Mass Transfer*, 47(6-7), 1105-1128.
36. Siebert, W. M. (1986). *Circuits, signals, and systems* (Vol. 2). MIT press.
37. Stepanyants, Y. A., & Strunin, D. V. (2011, May). Dynamics of two charged particles in viscous fluid at small Reynolds numbers. *In Proceedings of the 2011*

International Conference on Mathematics and Computational Methods Applied to Nuclear Science and Engineering (MC 2011). American Nuclear Society.

38. Stepanyants, Y., & Yeoh, G. (2008). Interaction of gaseous bubbles under the action of radiation modified Bjerknes force. *In Proceedings of the International Congress of Theoretical and Applied Mechanics (ICTAM2008)*. University of Southern Queensland, Australia.
39. Stepanyants, Y. A., & Yeoh, G. H. (2009). Particle and bubble dynamics in a creeping flow. *European Journal of Mechanics-B/Fluids*, 28(5), 619-629.
40. Stepanyants, Y. A., & Yeoh, G. H. (2010). Nanoparticle dynamics in a viscous fluid at small Reynolds numbers. *In Proceedings of the 6th Australasian Congress on Applied Mechanics ACAM 6* (p. 868), Perth, Engineers Australia.
41. Svobodny, T. (1998) *Mathematical Modeling for Industry and Engineering*, Prentice-Hall International, London et al.
42. Thévoz, P., Adams, J. D., Shea, H., Bruus, H., & Soh, H. T. (2010). Acoustophoretic synchronization of mammalian cells in microchannels. *Analytical chemistry*, 82(7), 3094-3098.
43. Visitskii, Y. V., Petrov, A. G., & Shunderyuk, M. M. (2009). The motion of a particle in a viscous fluid under gravity, vibration and Basset's force. *Journal of Applied Mathematics and Mechanics*, 73(5), 548-557.
44. Weisstein, E. W. (2003). *In CRC Concise Encyclopedia of Mathematics*, 2 ed. Chapman & Hall/CRC, Boca Raton; see also: http://functions.wolfram.com/.
45. Xie, J. H., & Vanneste, J. (2014). Dynamics of a spherical particle in an acoustic field: A multiscale approach. *Physics of Fluids*, 26(10), 102001.
46. Yosioka, K., & Kawasima, Y. (1955). Acoustic radiation pressure on a compressible sphere. *Acta Acustica united with Acustica*, 5(3), 167-173.
47. Zhu, G., & Trung Nguyen, N. (2010). Particle sorting in microfluidic systems. *Micro and Nanosystems*, 2(3), 202-216.